Corrosion control of carbon steel by polyaniline/epoxy-(graphene)-based double-layered coatings and a caprylate/dodecyl-sulfate inhibitor

By

Ahmad Diraki

Department of Chemical Engineering

McGill University

Montréal, Québec, Canada

August 2022

A thesis submitted to McGill University in partial fulfillment of the requirement of the degree of Doctor of Philosophy

Abstract

Carbon steel (CS) is the preferred construction material in most industries due to its cost-effectiveness and unique mechanical properties. It is used in many applications, from structural components in civil engineering to pipes in heavy industries such as oil and gas. However, CS is susceptible to corrosion, and it thus requires the application of proper corrosion control measures to lengthen its service life. With regards to the oil and gas industry, the pipelines used to transport the oil and gas from the offshore production well are exposed to two main forms of the corrosive environment: the saltwater that surrounds the pipeline's outer wall, and the acidic corrosive environment that attacks the inner pipeline wall, especially during the oil and gas reservoir service such as the acidizing procedure for enhancing oil recovery (EOR). The most common method employed to protect the pipeline's outer wall is the application of protective coatings. However, many of the currently used coatings are not effective for extended periods of service since they are prone to the formation of scratches during pipeline assembly or during maintenance and the formation of cracks due to both chemical and mechanical impact. Therefore, there is a need to develop coatings with improved anti-corrosive properties, which could have an extended service life and, if damaged/compromised, could counterbalance the damage by acting as *smart* coatings. On the other side, for the pipeline inner-wall corrosion protection, the application of corrosion inhibitors is the most effective way; however, most currently used inhibitors are not environmentally friendly. Thus, there is a need for the application of molecules that are biodegradable and environmentally friendly, such as corrosion inhibitors.

To address the *outer-wall* corrosion of carbon steel pipelines exposed to a simulated sea environment (3.5wt.% NaCl), during the course of this Ph.D. research project, two types of coatings were developed and characterized: (*i*) a composite double-layered anti-corrosive coating based on the inner electrically-conductive polyaniline (PANI) layer doped with graphene oxide (GO) synthesized electrochemically directly on the CS surface, and on the outer commercial epoxy coating, and (*ii*) a *smart* double-layered coating based on the inner PANI layer electrochemically formed on the CS surface and doped with sodium caprylate (SC) and sodium dodecyl sulphonate (SDS) as a corrosion inhibitor mixture, and the outer commercial epoxy coating. On the other hand, to address the *inner-wall* corrosion of CS pipelines, the inhabitation efficiency of an

environmentally friendly corrosion inhibitor mixture containing SC and SDS was investigated in an acidic environment containing HCl and under various experimental conditions.

The use of the double-layer PANI/GO/epoxy coating resulted in significantly better long-term anti-corrosive properties in the protection of CS surface in 3.5 wt.% NaCl. The coating maintained its protection efficiency over two months of constant exposure to the corrosive electrolyte. It was found that the optimal GO concentration in the PANI layer is 0.01 wt.%. The excellent corrosion protection properties of the coating were prescribed solely to the presence of the underlying PANI/GO layer, which represents a high barrier for the transport of hydrated corrosive ions to the CS surface, through the combined action of charge (passive oxide film formation), surface energy (hydrophobicity), and blocking mechanisms.

The *smart* double-layered coating based on the inner PANI layer doped with SC+SDS and the outer epoxy layer yielded a hydrophobic surface and good adhesion to CS. When damaged to allow penetration of the corrosive electrolyte through it to reach the CS surface, it relatively quickly (within one day) recovered its anti-corrosive properties, as a consequence of the potential-driven release of SC+SDS from the PANI layer and its adsorption on the exposed CS surface, and it then continued to offer high corrosion protection during the remaining 29 days of exposure in aqueous 3.5 wt.% NaCl, in comparison with the undoped coating that failed rather quickly (within 4 hours).

For the control of inner wall corrosion of CS pipelines, the results showed that SC and its mixture with SDS as a green molecule, act as a good corrosion inhibitor for the protection of CS in an acidic environment. The addition of only 5 mM of SDS to the SC-containing electrolyte resulted in a significant increase in the inhibition efficiency: after 48 hours of immersion in 0.5M HCl and at 295K, the corrosion inhibition efficiency was ca. 89% for SC and ca. 98% for SC+SDS. The corrosion protection mechanism was associated with forming a barrier-type SC+SDS molecular layer on the CS surface. The Langmuir adsorption isotherm described the adsorption of the inhibitor molecules on the CS surface. The adsorption kinetics of the inhibitor was relatively quick, achieving a maximum inhibition efficiency after only ca. 60 min. XPS suggested that SC is adsorbed on the CS surface through the interaction of its carboxylate group with iron, while the SC+SDS mixture interacted with the CS surface through the SC's carboxylate group and through the thiophenic sulfur in SDS.

Résumé

L'acier au carbone est le matériau de construction préféré de la plupart des industries en raison de sa rentabilité et de ses propriétés mécaniques uniques. Il est utilisé dans de nombreuses applications, des composants structurels dans le génie civil aux tuyaux dans les industries lourdes telles que le pétrole et le gaz. Cependant, l'acier au carbone est sensible à la corrosion et nécessite donc l'application de mesures appropriées de contrôle de la corrosion pour prolonger sa durée de vie. En ce qui concerne l'industrie pétrolière et gazière, les pipelines utilisés pour transporter le pétrole et le gaz depuis les puits de production en mer sont exposés à deux formes principales d'environnement corrosif : l'eau salée qui entoure la paroi extérieure du pipeline et l'environnement corrosif acide qui attaque la paroi intérieure du pipeline, en particulier pendant l'entretien du réservoir de pétrole et de gaz, comme la procédure d'acidification pour améliorer la récupération du pétrole. La méthode la plus courante employée pour protéger la paroi extérieure du pipeline est l'application de revêtements de protection. Cependant, de nombreux revêtements actuellement utilisés ne sont pas efficaces pour des périodes de service prolongées, car ils sont sujets à la formation de rayures pendant l'assemblage du pipeline ou pendant l'entretien et à la formation de fissures dues à l'impact chimique et mécanique. Il est donc nécessaire de développer des revêtements avec des propriétés anticorrosives améliorées, qui pourraient avoir une durée de vie prolongée et, s'ils sont endommagés/compromis, pourraient compenser les dommages en agissant comme des revêtements intelligents. D'autre part, pour protéger contre la corrosion de la paroi interne des pipelines, l'application d'inhibiteurs de corrosion est le moyen le plus efficace ; cependant, la plupart des inhibiteurs utilisés actuellement ne sont pas respectueux de l'environnement. Il est donc nécessaire d'appliquer des molécules biodégradables et respectueuses de l'environnement, telles que les inhibiteurs de corrosion.

Pour traiter la corrosion de la paroi extérieure des pipelines en acier au carbone exposé à un environnement marin simulé (3,5 % en poids de NaCl), deux types de revêtements ont été développés et caractérisés au cours de ce projet de recherche de doctorat : (i) un revêtement composite anticorrosion à double couche basé sur la couche intérieure de polyaniline (PANI) électriquement conductrice dopée à l'oxyde de graphène (OG) synthétisée électro chimiquement directement sur la surface de l'acier au carbone, et sur le revêtement extérieur en époxy

commercial, et (ii) un revêtement intelligent à double couche basé sur la couche intérieure de PANI formée électro chimiquement sur la surface de l'acier au carbone et dopée avec du caprylate de sodium et du dodécylsulfonate de sodium comme mélange d'inhibiteurs de corrosion, et le revêtement époxy commercial extérieur. D'autre part, pour traiter la corrosion de la paroi interne des pipelines d'acier au carbone, l'efficacité d'habitation d'un mélange d'inhibiteurs de corrosion respectueux de l'environnement contenant du caprylate de sodium et du dodécylsulfonate de sodium a été étudiée dans un environnement acide contenant du HCl et dans diverses conditions expérimentales.

L'utilisation d'un revêtement double couche PANI/OG/époxy a permis d'obtenir des propriétés anticorrosives à long terme nettement meilleures pour la protection de la surface d'acier au carbone dans 3,5 % en poids de NaCl. Le revêtement a conservé son efficacité de protection pendant deux mois d'exposition constante à l'électrolyte corrosif. Il a été constaté que la concentration optimale de OG dans la couche de PANI est de 0,01 % en poids. Les excellentes propriétés de protection contre la corrosion du revêtement ont été attribuées uniquement à la présence de la couche sous-jacente de PANI/OG, qui représente une barrière élevée pour le transport des ions corrosifs hydratés vers la surface de l'acier au carbone, par l'action combinée de la charge (formation d'un film d'oxyde passif), de l'énergie de surface (hydrophobie) et des mécanismes de blocage. Le revêtement intelligent à double couche basé sur la couche intérieure de PANI dopée au caprylate de sodium + dodécylsulfonate de sodium et la couche extérieure d'époxy a donné une surface hydrophobe et une bonne adhésion à l'acier au carbone. Lorsqu'il a été endommagé pour permettre à l'électrolyte corrosif de pénétrer à travers lui et d'atteindre la surface de l'acier au carbone, il a retrouvé relativement rapidement (en un jour) ses propriétés anticorrosives, en raison de la libération par potentiel du caprylate de sodium + dodécylsulfonate de sodium de la couche PANI et de son adsorption sur la surface exposée de l'acier au carbone, et il a continué à offrir une protection anticorrosion élevée pendant les 29 jours d'exposition restants dans une solution aqueuse de NaCl à 3,5 % en poids, par rapport au revêtement non dopé qui a échoué assez rapidement (en 4 heures).

Pour le contrôle de la corrosion de la paroi interne des pipelines en acier au carbone, les résultats ont montré que le caprylate de sodium et son mélange avec le dodécylsulfonate de sodium comme molécule verte agissent comme un bon inhibiteur de corrosion pour la protection de l'acier au carbone dans un environnement acide. L'ajout de seulement 5 mM de dodécylsulfonate de sodium à l'électrolyte contenant du caprylate de sodium a entraîné une augmentation significative de l'efficacité d'inhibition : après 48 heures d'immersion dans 0,5 M HCl et à 295K, l'efficacité d'inhibition de la corrosion était d'environ 89% pour le caprylate de sodium et d'environ 98% pour le caprylate de sodium + dodécylsulfonate de sodium. Le mécanisme de protection contre la corrosion était associé à la formation d'une couche moléculaire de type barrière caprylate de sodium + dodécylsulfonate de sodium sur la surface de l'acier au carbone. L'isotherme d'adsorption de Langmuir a décrit l'adsorption des molécules d'inhibiteur sur la surface de l'acier au carbone. La cinétique d'adsorption de l'inhibiteur était relativement rapide, atteignant une efficacité d'inhibition maximale après seulement environ 60 minutes. La spectroscopie photo électronique par rayons-X a suggéré que le caprylate de sodium est adsorbé sur la surface de l'acier au carbone par l'interaction de son groupe carboxylate avec le fer, tandis que le mélange de caprylate de sodium + dodécylsulfonate de sodium interagissait avec la surface de l'acier au carbone par le groupe carboxylate du caprylate de sodium et par le soufre thiophénique du dodécylsulfonate de sodium.

I dedicated this thesis to my late father Samir and my mother Sousan, my brother Mohammad, my sister Saad, my lovely son Samir, and for the best person I met during my Ph.D. study Madam. Dorsaf, for their unconditional love and support throughout my study journey.

Acknowledgment

My sincere gratitude goes to Prof. Sasha Omanovic, my research advisor, for his continuous support and guidance throughout these years. I consider myself very lucky to have known him and worked with him. Without his inspiration, support, and patience throughout the period of this work, I may not be able to complete this thesis successfully.

During my Ph.D. journey, I was honoured to meet many esteemed people, namely, Mr. Tarek Allam (the first person I got to know in Canada on the third day after arrival), Mr. Rabih Kassab, and Mr. Bassam Moussa, Madam. Ibtissam Maalaoui, Madam. Dorsaf El Mekki, and their families. My colleagues in the electrochemistry and corrosion lab, namely, Xingge, Deepak, Kanghoon, Satria, Rihab, Raed, Zhouya, Yu Hao, and Kara. I would like to especially thank my officemate, Madam Elmira Pajootan, for assisting me in learning surface characterization techniques and for her continuous support. Special thanks go to supportive friends, Mr. Mahmoud Rammal, Mr. Aqeel Alrebh, and Adel Alamoudi, for all the great times we spent together in and out of the school.

I gratefully acknowledge the financial support from the Qatar National Research Fund (QNRF) for the provision of a Ph.D. study award grant under the Qatar Research Leadership Program (QRLP). I recognize that this research would not have been possible without their financial support.

Table of contents

List of Figures

Chapter 2

Chapter 3

Chapter 4

Chapter 5

List of Tables

Chapter 2

Chapter 3

Chapter 4

Chapter 5

Chapter 1

Introduction

1.1 Brief overview

Offshore pipelines transport the produced oil and gas from the upstream production well to the downstream hydrocarbon separation facilities. Although offshore oil and gas pipelines are the safest way of transporting the hydrocarbons due to low failure rates, in contrast to highway transportation, railroad, and ships, yet, failures do occur and often with catastrophic results, especially to the marine ecology and its environment. Most offshore operators ensure, already at the design stage, that the maximum safety provisions are implemented to minimize the failure rate for the life of the pipelines. However, in the unlikely case of pipeline failure, large volumes of oil and gas would be discharged into the sea. While gas and light liquid hydrocarbons would be dispersed, diluted by the wind, or evaporated into the atmosphere, oil would be raised from the seafloor to the sea surface preventing oxygen from reaching the sea life, resulting in substantial negative consequences. Therefore, pipeline integrity and health monitoring are crucial for safe pipeline operations.

Several reasons could cause pipeline failure, but corrosion is considered the main one. Corrosion can be simply defined as the deterioration or destruction of materials, predominantly due to the occurrence of electrochemical reactions with their environment [1]. The negative impacts of the corrosion phenomena have become a real problem of worldwide significance. A failure in the ability to prevent the corrosion process causes serious risks for both the society and the economy. The annual costs associated with corrosion and its inhibition have been assessed as a significant segment of the gross national product in the United States and other developed countries (up to 5% of GDP) [2]. In addition to the social and economic effects, corrosion can cause technological delays and structural failures in buildings, bridges, automobiles, aircraft, and oil and gas pipelines, which have dangerous consequences for humans, ecology and the surrounding environment [3, 4].

Carbon steel (CS) is the most used metal alloy in many industries and thus also as a construction material for pipelines due to its unique mechanical properties, availability, and cost-effectiveness, especially in the oil and gas industry [5]. Therefore, the protection of CS in terms of its corrosion inhibition is of great importance and has been a focus of intensive research. It involves investigating the strategies of reducing the corrosion kinetics through either changing the corrosion mechanism or slowing it down using barrier layers. The most common methods employed are cathodic or anodic protection [6, 7], corrosion inhibitors [8], and protective coatings [9]. These techniques are used in different industries, and thus also to protect oil and gas pipelines. A typical effective means to control and mitigate internal-wall corrosion of the oil and gas pipelines is the application of corrosion inhibitors [10]. The most effective inhibitors are mainly organic compounds that adsorb on the carbon steel's surface to form a molecular-level thin protective barrier layer and impart the metal substrate from the corrosive environment [11, 12]. However, most currently-used organic corrosion inhibitors are toxic, non-biodegradable, and have significant bioaccumulation [13]. To protect the pipeline's exterior (outer-wall corrosion), barrier coatings are commonly used, sometimes in combination with cathodic protection. These coatings will protect the material from corrosion and enhance the metal's surface properties, such as hydrophobicity and mechanical properties, to name a few [14]. Protective coatings can be applied to the metal substrate in many forms, such as for sacrificial coatings [15], oxide layers [16], varnishes [17], organic films [18], and polymeric layers [19], to name a few. Recently, non-conducting epoxy coatings combined with conducting polymers (CPs) have been used to protect metals from corrosion [20]. Epoxy coatings are often used for corrosion prevention because of their exceptional mechanical and chemical properties [21-23]. CP coatings have exhibited promising corrosion inhibition performance of metal substrates because they are environmentally stable, eco-friendly, non-toxic, and adhere firmly to the metal surface [24]. Recently, there has been an increased interest in developing and designing smart coatings with either self-healing abilities, or the ability to release a corrosion inhibitor upon damage, that extend the life of various materials in highly corrosive environments. For this purpose, conductive polymers (CPs) are useful materials for corrosion protection [25-31].

Smart coatings can detect changes in their environment and respond to the changes while maintaining coating compositional integrity. The changes may respond to different factors such as pH, light, polarity, pressure, temperature, biological factors, or changes in potential. Polyaniline, for example, acts as an anion reservoir which can release anions (e.g. inhibitors) doped during the synthesis in a smart way when damage is produced on the surface of the coating, forming a second physical barrier (inhibitor molecular layer adsorbed on the substrate surface) to avoid penetration of corrosive ions [32].

In addition to incorporating or releasing charged molecules to balance their charge (e.g. dopants - corrosion inhibitor) in response to the variation of the metal surface potential [33], DeBerry et al. [34] have shown that polyaniline stimulates the stabilization of the passive state of stainless steel in sulfuric acid solution. The key to their finding is that CPs can keep the surface potential of the metal in the passive state by forming a protective oxide film on the metal substrate. This process can be explained by reducing oxygen (needed for the cathodic corrosion reaction) within CP to refill the CP charge spent through metal oxidation [34], then preventing corrosion of the metal as the potential flips into the passive state.

Nonetheless, to satisfy the industrial requirement in terms of high corrosion protection efficiency of coatings and relatively low cost in contrast with increasing material life cycle, polymer-based nanocomposites have been studied more intensely since the processing applicability of composite coatings is less complicated than that for multi-layer coatings [35]. One of the approaches to improving the anti-corrosive properties of polymer-based coatings is to incorporate ‘fillers’ in their bulk structure. For example, zinc is commonly used as a ‘filler’ in primers, and its function is primarily to catholically protect the based material by its ‘sacrificial’ anodic dissolution. Graphene has emerged as one of the most interesting nano-fillers to produce composite coatings for corrosion protection. Graphene is a single-layer crystal lattice of a two-dimensional honeycomb formed through tightly packed double-bonded carbon atoms. Since 2004, the discovery year of graphene [36], an increasing number of research studies have concentrated on different graphene-based materials such as functionalized graphene, graphene nanoplatelets, reduced graphene oxide, and graphene nanocomposites in various polymer matrices to enhance their electric, thermal, and mechanical properties [37-46]. Graphene has a low density and high aspect ratio that give it superiority over other nano-fillers [47]. These significant properties fueled the interest in investigating graphene-based materials such as corrosion protection coatings and gas barriers [48-51].

1.2 Thesis Objectives

As stated above, Fe-based materials (e.g., carbon steels) are the most used industrial metals in many industries, especially in the oil and gas industry. However, their corrosion rate needs to be mitigated, particularly in high corrosive environments such as salty water and acidic environments. The impact of multiple experimental conditions, Fe alloy compositions, and electrolyte compositions on the corrosion protection behaviour of CPs and/or epoxy protective coating and different corrosion inhibitors has been investigated by scientists. Nevertheless, to the present date, less information is available concerning the integrity of protective anti-corrosive coatings over time and under mechanical rupture, the influence of filler, and the effect of the mix of molecules on the corrosion inhibitor's performance.

Therefore, the main objectives of this Ph.D. thesis focus on:

1. Developing *outer-wall* corrosion protection composite/multilayered coatings based on in-house synthesized polyaniline and commercial epoxy, for potential use for oil and gas pipelines constructed of CS and immersed in seawater, and
2. Investigating an environmentally friendly corrosion inhibitor mix for *inner-wall* corrosion inhibition of CS immersed in HCl.

To achieve the main objectives, the following set of specific objectives were accomplished:

- Two types of coatings were designed and investigated:
  - (i) a *double-layered* coating based on the inner electrically conductive polyaniline (PANI) layer doped with graphene oxide (GO) synthesized electrochemically directly on the CS surface, and the outer commercial epoxy coating, and
  - (ii) a *smart* double-layered coating based on the inner electrically conductive polyaniline (PANI) layer electrochemically formed on the CS surface and doped with sodium caprylate (SC) and sodium dodecyl sulphonate (SDS) as a corrosion inhibitor mixture, and the outer commercial epoxy coating.
- The possibility of using a mixture of SC and SDS as a corrosion inhibitor to regulate the inner-wall corrosion was investigated both from the fundamental and applied point of view.

1.3 Thesis organization

This thesis is manuscript-based and follows the guidelines outlined by the Faculty of Graduate and Postgraduate studies at McGill University, and it consists of seven chapters. Chapter 1 presents a brief introduction to the topic and outlines the main project objectives. Chapter 2 presents theoretical and fundamental aspects of corrosion and corrosion protection, it outlines specific methods employed in corrosion mitigation, and presents basic information on the development of anti-corrosive coatings and inhibitors, accompanied with the pertinent literature review. Then, it is followed by the presentation of three submitted/published peer-reviewed articles in Chapters 3, 4 and 5. Chapter 3 discusses the formation and characterization of a double-layered polyaniline/epoxy coating incorporating graphene oxide (PANI/GO/epoxy) and the investigation of its corrosion protection properties in artificial seawater. Chapter 4 discusses the synthesis and analysis of the corrosion protection performance of a smart PANI/epoxy coating doped with a 'green' corrosion inhibitor mixture (sodium caprylate and sodium dodecyl sulfonate) in artificial seawater. Chapter 4 presents the performance results of a mixture consisting of sodium caprylate and sodium dodecyl sulfonate as a corrosion inhibitor in an acidic environment and discusses the impact of a range of experimental parameters, including the adsorption mechanisms and thermodynamics, corrosion kinetics, and surface/inhibitor characterizations. Chapter 6 presents general conclusions drawn from the obtained results, and Chapter 7 presents the original contributions of the work and recommendations for future research.

Chapter 2

Background and literature review

2.1 Corrosion and its forms

Corrosion is the destruction of material, mostly referred to metals, through electrochemical chemical reactions between metals and species in the surrounded environment (however, it should be noted that there are other types of corrosion that do not involve solely electrochemical reactions, such as erosion/cavitation corrosion, chemical corrosion of metals and plastics, etc.). Corrosion of metals is classified in two main groups with respect to its extent: general/uniform corrosion, and localized corrosion. However, there are a few other types of corrosion, but the author of this thesis will summarize the general (uniform) corrosion, relevant to the Ph.D. work presented in this thesis. For the other types of corrosion, the reader is referred to the literature [52-54].

General (or uniform) corrosion affects the entire surface of metallic material that is in contact with a corrosive environment, and if the corrosion is spread consistently, it is referred to as uniform corrosion, otherwise, corrosion is considered as general but not uniform [53, 54]. In electrochemical reaction sense, the oxidation (anodic site) and reduction (cathodic site) reactions take place randomly over the metal surface. It is assumed that corrosion proceeds roughly at the same rate over the exposed metal surface. It is the most common corrosion type where we can see it everywhere around us attacking iron and steel when exposed to open atmosphere, soils, and water containing electrolytes, causing rusty appearance. It is a predictable type of corrosion, and it is considered as a design factor during the structure design stage over the desired lifetime service. Among a number of corrosion protection methods available, general corrosion can be mitigated through protective coatings or by the application of corrosion inhibitors to modify the metal surface through forming protective adsorbed inhibitor layer.

2.2 Corrosion in the oil and gas industry

During the oil production, the scale formation in the pipeline's inner wall is quite prominent, and it is caused by barium sulphate or calcium carbonate [55]. The presence of these scales reduces the oil recovery and can lead to corrosion issues under the deposited scales [56]. It is a common practice to solve the issue of the scales in the oil and gas pipelines by using mineral acids, like hydrochloric acid and/or hydrofluoric acid, to dissolve them [57]. These acids are very corrosive and can lead to severe corrosion underlying the carbon steel surface. An important method to protect the inner wall of a pipeline is the use of corrosion inhibitors. To mitigate such corrosion, organic inhibitors are a preferred choice due to the presence of heteroatoms (S, O, N) in the structure, heterocycles, π-bonds, functional groups [58, 59]. Currently, the most effective corrosion inhibitors in the acidic environment are quite toxic, non-biodegradable, and exhibit a high level of bioaccumulation [60].

2.3 Corrosion economic impact

Metals are the most-used material of construction in many industries. Nevertheless, the surface of metal corrodes quickly when in contact with the corrosive media. The corrosion of the metals causes a massive economic impact. According to the recent report by NACE, the total annual cost related to corrosion come to around 2.5 trillion US dollar, which is around 3.4% of the global GDP [61]. However, the estimated worldwide corrosion cost in the oil and gas industry is reported to be around 1372 billion US dollars [62].

2.4 The corrosive environment

Simply, the corrosive environment is categorized into three different categories based on the exposure type: atmospheric, immersion, and splash zone, Fig 2. 1 [63, 64]. However, the acidity/alkalinity. Other factors such as temperature, presence of biological organisms can also impact the corrosion behavior of the corrosive environment.

In the situation of immersed metals in water, which is the focus of this research, the aggressiveness is well defined due to a clear combination of pH, temperature, salinity, and dissolved gases, specifically oxygen. In addition, seawater has a high content of dissolved sodium chloride which is very aggressive toward the metal substrate [65].

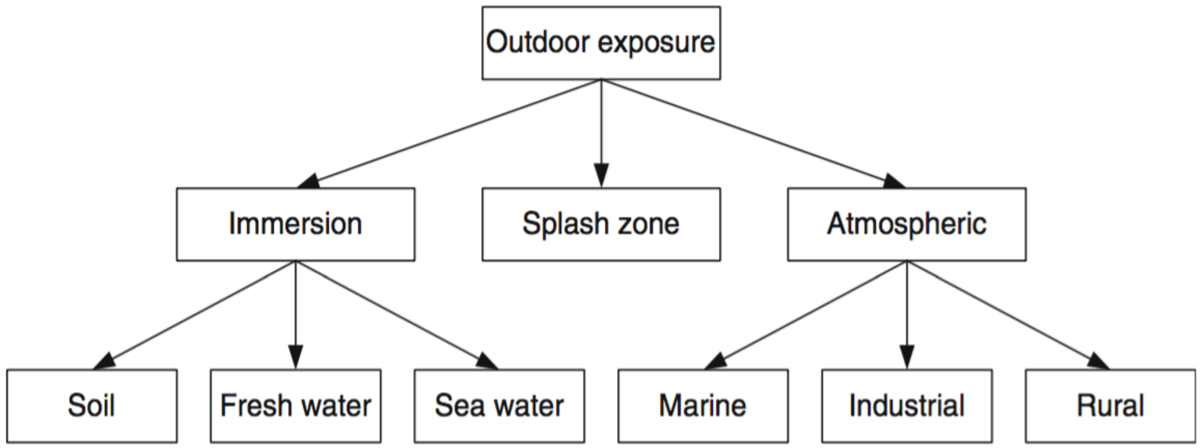

Fig 2. 1 Categories of different corrosive environments [64]

2.5 Basic corrosion reactions

Corrosion mainly occurs through electrochemical reactions between metals and their surrounding environment, especially electrolytes. This process happens when the area of higher surface potential (high surface energy) behaves as an anode, and the one of lower potential (low surface energy) behaves as a cathode, thus creating a corrosion cell [30, 66]. The anodic area of metal dissolves into the electrolyte, then the electrons go through the metal to the cathodic area where they are used in a cathodic reaction. This flow cycle of electrons from the anodic to the cathodic side generates the corrosion current. The equivalent amount of charge is carried through the electrolyte by ions. Thus, the corrosion rate is directly related to the corrosion current (through the Faraday law). For (electrochemical) corrosion to proceed, all four of the following conditions must be satisfied: anodic and cathodic reactions (i.e., the presence of anodic and cathodic areas on the metal surface), the presence of an electrolyte (for transport of charge by ions), and the presence of electrical connection between the anode and cathode areas (for transport of electrons). The absence of any of these four requirements results in the absence of a corrosion process.

The corrosion reactions can be, in a very simplified/generalized way, described as the following [27, 28, 30, 67]:

Anodic reaction: The metal (anode) releases electrons that migrate to the cathode

$M \leftrightarrow M^{z+} + ne$ (2. 1)

Cathodic reaction: The electrons released from the anodic side are consumed at the cathode, based on the environment. The major cathodic reactions which happen in corrosion are as follows:

Oxygen reduction (usually in aerobic conditions)

$O_2 + 4H^+ + 4e \leftrightarrow 2H_2O$ In acidic solution (2. 2)

$O_2 + 2H_2O + 4e \leftrightarrow 4OH^-$ In neutral or basic solution (2. 3)

Hydrogen evolution (usually in anaerobic conditions)

$2H^+ + 2e \leftrightarrow H_2$ In acidic solution (2. 4)

$2H_2O + 2e \leftrightarrow H_2 + 2OH^-$ In neutral or basic solution (2. 5)

Metal ion reduction

$M^{z+} + ne \leftrightarrow M^{(z-n)+}$ (2. 6)

The metal ion reduces its valence state by accepting an electron. This happens if there is a high concentration of M^{z+} ions.

Metal deposition

$M^{z+} + ne \leftrightarrow M$ (2. 7)

Metal may have reduced from an ionic to a neutral metallic state.

2.6 Wet corrosion mechanism on carbon steel

Corrosion damage is explained as effects that cause impairment of main function and the technical system. The creation of rust (ferrous oxides) is one of the main special effects of the corrosion process as steel and iron corrode [68]. Other examples of corrosion products are the white rust on zinc, and the green patina on copper [68]. As our focus in this study is carbon steel immersed in seawater, the process of steel corrosion in the presence of oxygen, water, and electrolytes is illustrated in Fig 2. 2, and explained below [68].

At the cathode, the reduction process occurs where the electrons produced by oxidation at the anode need to be consumed in the reduction reaction. It should be noticed that these anodes and cathodes could be two different metals or different sites on the heterogeneous surface of the same metal. In aerobic conditions, on the catalytically active surface of oxidized steel, oxygen is reduced to hydroxide ions (Reaction (3)), while other reactions may produce superoxide, peroxides, and radicals [69-71].

At the anode, metal (iron) dissolution (oxidation) takes place. Based on the corrosive environment, it could be deposited back on the bulk metal surface as corrosion products or transferred into the solution as metal ions. Numerous reactions happen and the general outcome is the production of ferrous ions and electrons [72]:

$Fe_{(s)} \rightarrow Fe^{2+}_{(aq)} + 2e^-$ (2. 8)

The initial stage of iron hydroxide oxidation into ferrous oxides is the production of green hydrated magnetite (note that the following set of reactions represent total corrosion reactions, where O_2 is reduced at the cathode) [68]:

$6Fe(OH)_{2(aq)} + O_{2(aq)} \rightarrow 4H_2O_{(1)} + 2FeO\ Fe_2O_3\ H_2O_{(s)}$ (2. 9)

Nevertheless, hydrated magnetite will decompose into black magnetite:

$FeO\ Fe_2O_3\ H_2O_{(s)} \rightarrow FeO\ Fe_2O_{3(s)} + H_2O_{(l)}$ (2. 10)

If oxygen is present in the process, black magnetite subsequently will oxidize to red-brown hydrated hematite, which is referred to as *rust* [68].

$2FeO\ Fe_2O_{3(s)} + \frac{1}{2} O_{2(aq)} + 3H_2O_{(1)} \rightarrow 3Fe_2O_3\ H_2O_{(s)}$ (2. 11)

Overall, the complete corrosion reaction is the following:

$4Fe_{(s)} + 3O_{2(aq)} + 3H_2O_{(1)} \rightarrow 2Fe_2O_3\ 3H_2O_{(s)}$ (2. 12)

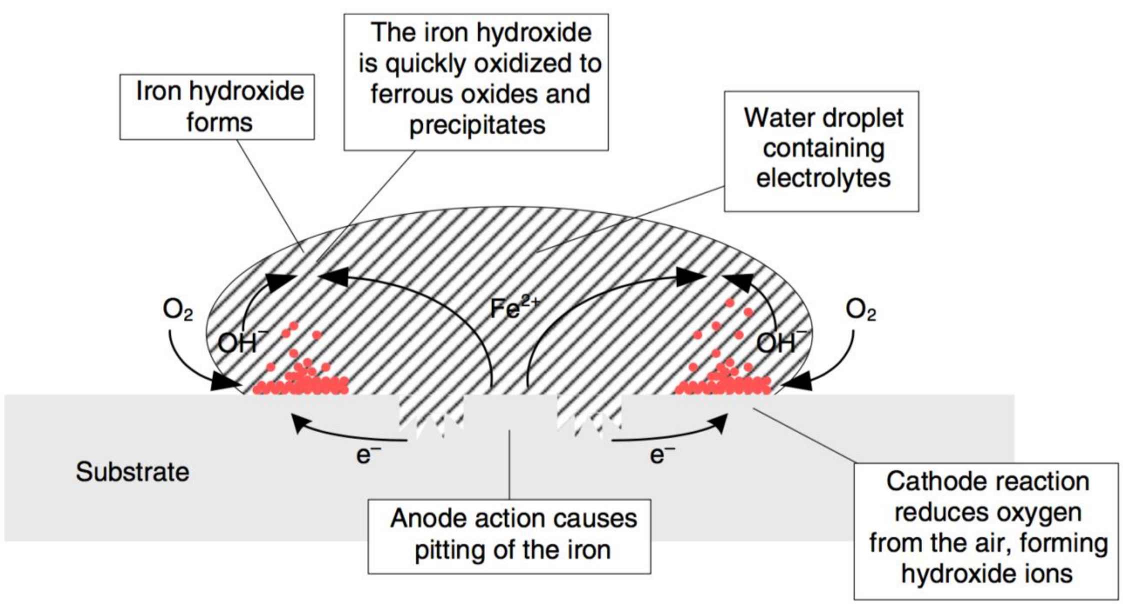

Fig 2. 2 The process of steel corrosion in the presence of oxygen, water, and electrolytes [68]

2.7 Corrosion thermodynamics

The driving force for steel corrosion is the difference in potential between anodic and cathodic sites. The electrochemical equilibrium potential (in volts, V) of a galvanic cell is the difference between the anodic and cathodic potentials of the corresponding half-cell reactions [68].

$$E_{Cell} = E_{Ox} + E_{Red} \tag{2. 13}$$

and each of the two reversible potentials in the equation can be expressed through the Nernst equation:

$$E = E^0 + \frac{RT}{nF} \ln\left(\frac{a_{Red}}{a_{Ox}}\right) \tag{2. 14}$$

where R is the gas constant which is equal to 8.314 J K^{-1} mol^{-1}, T is the temperature in Kelvins (K), n is the number of electrons involved in the reaction, a_{Red} and a_{Ox} are the chemical activities of the reduced and oxidized species, which are measured with respect to the standard state (1 atm for the gases, 1 $moldm^{-3}$ for solutes). In thermodynamics, the electrochemical reaction and electrochemical equilibrium are linked to the change in Gibbs free energy (ΔG), which means that corrosion is related to the Gibbs free energy:

$$\Delta G = -n \times F \times E_{Cell} \tag{2. 15}$$

where F is the Faraday constant (=96485 $Cmol^{-1}$). Referring to corrosion reactions outlined above (Reaction (2-5)), under standard conditions if the cathodic reaction is hydrogen evolution, the corresponding E_{cell} for the iron dissolution (Reaction (Fe^{2+} + 2e- ↔ Fe)) in the acidic and alkaline media is 0.409 V and -0.4187 V, respectively. If the cathodic reaction is oxygen reduction, the corresponding E_{cell} in the acidic and alkaline environments are 0.81 V and 1.638 V, respectively. Taking these values into account, and employing Eq.(15), one can calculate the corresponding standard Gibbs free energy for the corrosion processes as:

-78924.7, 80796.5, -156305.7, and -316084.9 $Jmol^{-1}$, respectively. One can see that three out of the four values are negative, demonstrating that corrosion is a highly spontaneous process under the specified conditions, with the exception of the second one for which the value is positive. However, if the value is positive, then the reaction is not spontaneous, as for the second case (anaerobic conditions in the alkaline media).

The extent of metal corrosion is dependent on its electrode potential and the pH of the solution. Fig 2. 3 illustrates the Pourbaix diagram of steel, which shows how steel can be prevented from corroding via:

- Increasing the pH by adding chemicals that make the electrolytes more alkaline (Fig 2. 3 from points A to 1)
- Applying external voltage for anodic protection to change the metal potential in a positive direction (Fig 2. 3 from points A to 2)
- Applying potential in the negative direction for cathodic protection. For example, employing a sacrificial zinc coating on the steel substrate or impressing cathodic current (Fig 2. 3 from points A to 3)

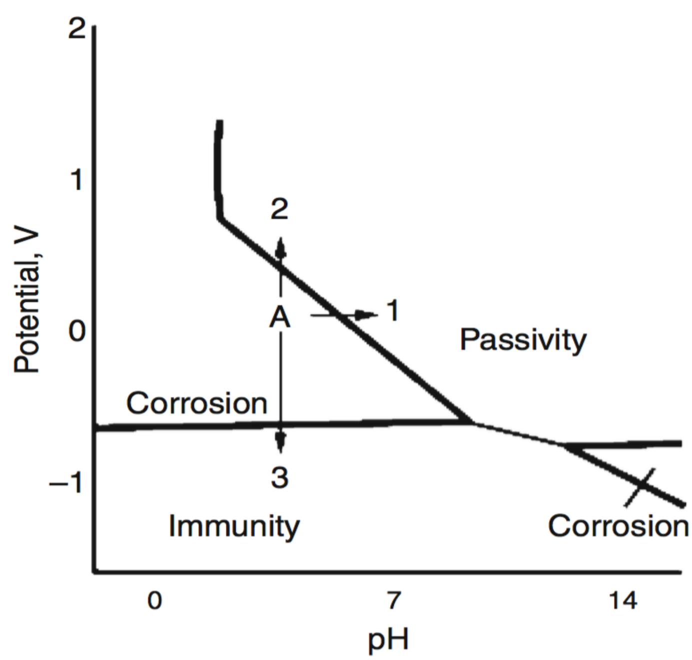

Fig 2. 3 Steel Pourbaix diagram [68]

2.8 Corrosion mitigation

Several methods could be used to control corrosion. The selection of the proper methods will be dependent on different parameters such as the local environment, type and location of the corrosion, type of metal structure to be protected, etc. The following sections summarize the current most-used approaches and methods to mitigate corrosion.

2.8.1 Proper material selection

The selection of metallic material is made at the design stage, and the choice will be made based on many factors such as the total cost, and mechanical, chemical, physical, and visual properties of the material. In the oil and gas industry, especially in production facilities such as production wells, pipelines, vessels and thanks, carbon steel is the most used metal due to its cost-effectiveness, good mechanical properties, and its availability [73].

2.8.2 Protective coatings

As mentioned before, if one of the four components of a corrosion system is absent (anode, cathode, electrolyte, electrical conductivity between the anode and cathode), an electrochemical corrosion reaction cannot proceed. This can be used for corrosion control. Thus, if the access of the corrosive electrolyte to the metal surface is prevented, the metal is protected from corrosion. This is the basis for the application of insulating corrosion protection coatings. However, other types of coatings could also be used, as mentioned below.

Corrosion protection by coating the metal generally consists of applying multiple layers of different coatings with different properties and for multiple purposes on the metal surface. A coating could be organic, inorganic, or metallic, the choice of which is based on the required properties of the coating method and the corrosive environment. There are three corrosion protection mechanisms: barrier protection, inhibitory effect through passivation of the substrate surface, and galvanic effect via sacrificial protection (cathodic protection) [74]. For highly corrosive environments like seawater, coatings usually contain an organic primer, one or many intermediate layers, and an organic top-coat layer, and their corrosion protection mechanism is based on the presence of barrier for transport of corrosive species from the electrolyte to the underlaying metal surface [74, 75].

There are almost limitless varieties of coatings that can be applied for steel corrosion control. Yet in this project, our focus is on using a double-layer coating containing epoxy and conducting polymers (CPs) incorporating graphene-based nanocomposites or a corrosion inhibitor (as a smart coating) for protection of the outer wall of oil and gas pipelines immersed in seawater.

2.8.2.1 Epoxy resins (ERs)

The term epoxy or ERs represents a special category of highly reactive pre-polymers or polymers that contain epoxide groups in their molecular structures [76]. Among different organic coatings, epoxy coatings are used for anticorrosion protection because of their excellent chemical and mechanical properties [77]. ERs have great adhesion to metal surfaces and consistent corrosion resistance, which makes them a perfect material for corrosion protection. However, the performance of ERs during long-term immersion in corrosive environments still has room for improvement. They are affected by the high crosslinking density of the epoxy network, and holes that might be generated in the coating with time, thus, reducing their corrosion protection performance. Also, the lower stability of the ERs to the ultraviolet rays limits their application to some extent [78]. However, these poor performances can be improved by various methods. Recently, attempts have been made to modify the pristine ERs to improve their properties by adding conductive polymers, siloxane and/or fluorinated compounds, or adding micro/nano-sized fillers, or hybrid nanocomposite coating [79-83]. Grgur et al. [84] synthesized PANI and PANI/epoxy coatings on the steel surface by electrochemical deposition using an aqueous solution containing sodium benzoate and aniline monomer (non-pigmented epoxy modified by amine and isocyanate). The corrosion measurements revealed that the PANI/epoxy coating on steel surfaces had lower pore resistance during initial time of exposure to a solution containing 3% NaCl. In contrast to the pure epoxy coating, the PANI/epoxy coating showed a stronger corrosion protection performance at long times of immersion. Hou et al. [85] evaluated the corrosion performance of epoxy incorporating a small amount of poly(3,4-ethylenedioxythiophene) and poly (styrenesulfonate), applied on a steel surface. The corrosion behavior of the studied sample was evaluated in seawater, and it was found that adding a small amount of the additive into the ERs substantially improve the corrosion resistance.

2.8.2.2 Polyaniline (PANI)

Fig 2. 4 shows the chemical structure of PANI (various bases), which is an interesting candidate coating for corrosion protection for several reasons. It can be simply synthesized either chemically or electrochemically, with high environmental stability and different redox states that make its properties easier to regulate [86]. The well-known insulating forms of PANI are leucoemeraldine base (LB), emeraldine salt (ES) and pernigraniline base (PB), Fig 2. 4 Polyaniline chemical structure [86]. These different forms of PANI are responsible for active corrosion protection [86].

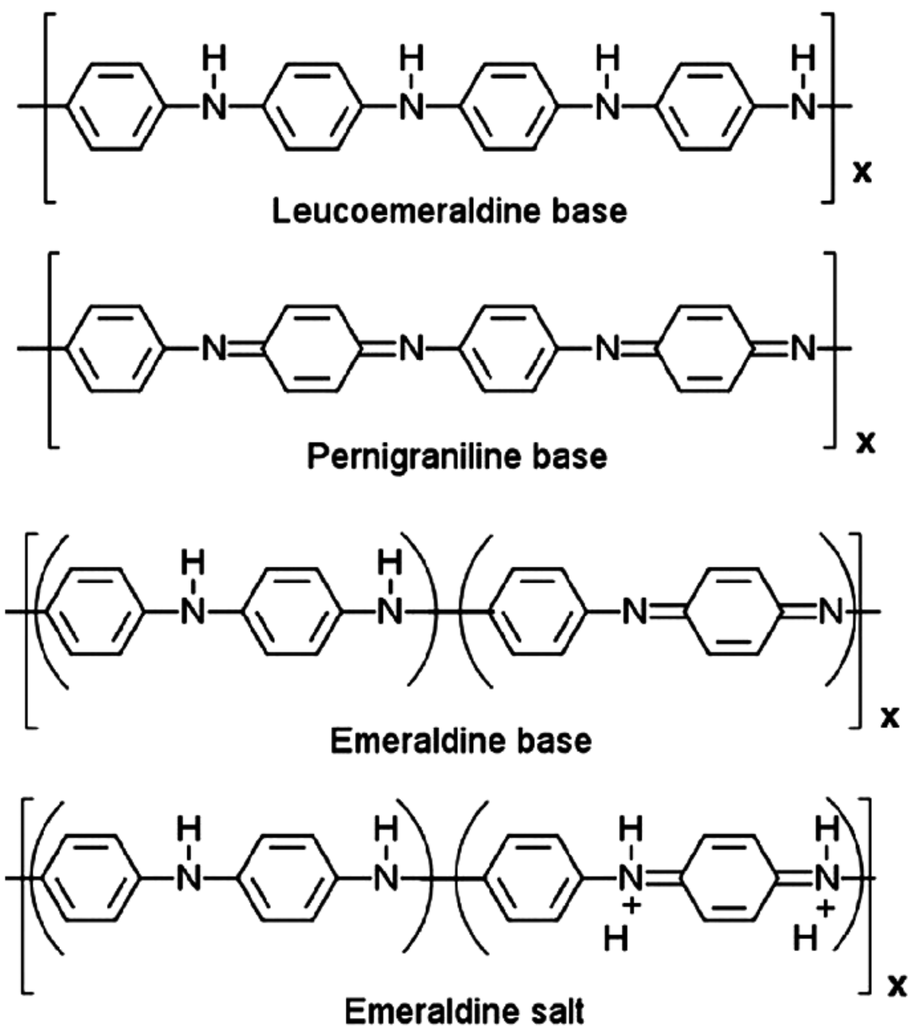

Fig 2. 4 Polyaniline chemical structure [86].

As an example of PANI application, Saravanan et al. [87] evaluated the epoxy primer incorporating PANI for steel bars corrosion protection. It was discovered that the steel bars re-passivate because of PANI's presence in the coating. The mixture of PANI and epoxy showed a good performance against chlorides: the uncoated bars reached the maximum current in 4 days, while for the coated ones, it took around 50 days.

Another study was conducted by Kalendova et al. [88] to evaluate the effects of different inorganic pigments such as zinc, zinc phosphate, and calcium borate along with PANI to protect against carbon steel corrosion. The results showed that the synergistic effect was very efficient for protecting the carbon steel compared to a single defense protection mechanism. Further, adding 2.5% w/w of PANI in the nano-particulate form in water-dispersible alkyds reflected a significant increase in corrosion protection performance [89]. Also, loading 1.5% w/w of chlorinated rubber (CR) binder system in PANI resulted in improved corrosion protection in the marine environment as compared to the same amount of zinc phosphate loading [90].

Riaz et al. [91] studied the impact of nanostructured particles on anti-corrosion properties of PANI/alkyd and compared it with poly(1-naphthylamine) (PNA)/alkyd. Comparisons between nanosized PANI and PNA dispersed soya oil-based alkyd composites applied on steel revealed that the (PNA)/alkyd had better anti-corrosion performance than PANI/alkyd coatings. It was noticeable that the best protective ability was for the smaller particle size of PNA. The smaller particle size had enhanced crosslinking between the PNA and alkyd matrix which provided improved barrier results.

Other nanomaterials like hybrid nanocomposites with PANI and ZnO as nano-particles mixed with poly(vinyl acetate), showed high improvement in barrier performance in contrast to a single component coating [92]. The dip-coated steel plates protected with these coatings showed excellent performance in corrosion resistance in high salinity water for long times (15 days). The high-performance protection results were explained based on these three mechanisms: high barrier effect, development of a p-n junction that eliminated easy charge movement, and high redox behaviour of PANI.

Nowadays, nano-casting was applied to synthesized PANI-based anti-corrosion coatings from a natural plant, Xanthosoma Sagittifolium, which is associated with biometric super-hydrophobic arrangement [93]. These materials reveal water-repelling properties and decent adhesion to cold-rolled steel. The estimated anti-corrosion performance of these materials showed improved protective capability in contrast with uncoated surface.

2.8.2.3 Polythiophene

There are fewer published research reports on polythiophene (PTh) as a coating for corrosion protection. Fig 2. 5 shows the chemical structure of PTh. It is possible to synthesize a range of derivatives of PTh. Some of the substitutes perform well in contrast to other conductive polymer derivatives, which depend upon the nature of the corrosive environment. Kousik et al. [94] used acetonitrile as a medium to produce PTh on steel as a surface coating. The AC impedance studies showed that the steel was protected via a passivation mechanism due to the redox activity of PTh. The delaminating area and water uptake studies confirmed the protection action of electropolymerized PTh.

Rammelt et al. [95] evaluated the impact of a special surface treatment of steel substrate using the 2(3-thienyl)ethylphosphono acids. After treating the steel surface, the polymethylthiophene films were well adherent homogeneously on the steel surface. These films were very thin (1 μm) and highly ordered, which saved the material and constituted better corrosion protection and significantly reduced the corrosion rate. Moreover, these films isolated oxygen from the electrochemical process in the surface region. Ocampo et al. [96] have investigated many anticorrosion marine paints based on PTh derivatives. It was concluded that the addition of 0.2 w/w of poly-(3-decylthiophene- 2.5-diyl) into an epoxy-based paint improved the corrosion resistance performance.

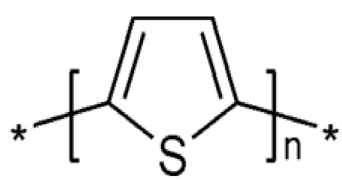

Fig 2. 5 Polythiophene chemical structure

2.8.2.4 Polypyrrole

Several studies have been done on corrosion protection using polypyrrole (PPy). Fig 2. 6 shows the chemical structure of PPy. CPs can be produced with various anions incorporated into the structure to balance the charge. A dopant anion is introduced upon oxidation into the conjugated polymer. When polymer undergoes a reduction state these dopant anions are released out of the coating, rendering them as “smart coatings”. Dopant ions have a large influence on the resultant PPy when they are used to synthesize PPy [97].

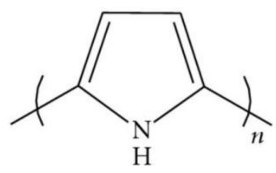

Fig 2. 6 Polypyrrole chemical structure

Kowalski et al. [97] evaluated the functionality of bi-layered PPy coatings on carbon steel. In this structure, the outer layer was doped with naphthalene disulfonate (NDS) ions, and the inner layer was doped with phosphate and molybdophosphate ions. The molybdophosphate ions incorporated in the inner layer stabilized the passive oxide film on the steel surface. The outer layer doped by the large size organic ions of NDS restricted decomposition and release of molybdophosphate ions in the inner layer, which resulted in a large enhancement in the corrosion protection performance.

Herrasti et al. [98] used electro-polymerized PPy on a copper surface. The main characteristic of the deposited layer was the homogenous surface with low porosity, which was the major result of the constant growth rate of the PPy film. The PPy deposited on the copper surface exhibited exceptional corrosion protection in a high salinity solution, 3wt. % sodium chloride. In addition, the authors advised a higher monomer concentration at 0.3 M to be used to achieve a decent barrier layer and redox properties.

Berekat et al. [99] evaluated the corrosion protection performance of electrochemically synthesized PPy on steel substrates. In addition, the effect of poly(5-amino-1-naphthol) topcoat formed on the PPy film was investigated using cyclic voltammetry. It was concluded that the deposition of more layers of this mixture improved the corrosion protection level. Another study used poly(N-methyl pyrrole) and electrodeposited PPy to synthesize coatings on a steel substrate from oxalate solutions. It was found that the synthesized coating passivated the steel substrate upon first deposit, and this led to enhanced corrosion protection [100].

Hosseini et al. [101] examined PPy, montmorillonite (MMT), and epoxy nanocomposite materials for protecting the aluminum substrate from corrosion. This mixture proved enhanced corrosion protection in contrast to epoxy-MMT and epoxy-PPy. On the other hand, alumina nanoparticles were used as PPy fillers in the presence of dihydroxybenzene [102]. It was concluded that the existence of dihydroxybenzene advanced the adhesion of the coating on the aluminum substrate. This study described the influence of coating voids on the coating aging and the penetration of the corrosive solution.

2.8.2.5 Corrosion protection mechanisms by conducting polymers

The exact mechanism of corrosion protection by conducting polymers is not yet well understood, and a few suggestions are presented below [103-106].

The controlled inhibitor release mechanism proposes that upon the creation of rupture in the CP coating formed on a metal substrate, there is a galvanic cell formed between the oxidizing metal surface and reducing CP, resulting in the release of the doped anions (inhibitors) [107]. Moreover, the oxygen reduction occurs at the same time on both the metal surface and the CP coating, causing the producing OH- and CP re-oxidation, which may lead to a self-healing process, depending on the nature of doped anions [107].

The anodic protection mechanism proposes that the CP coating may anodically polarize the metal surface to passive it, i.e. to form a metal oxide passive film on the metal surface; thus, the metal oxide layer works as a corrosion preventing layer [105, 108]. For example, steel passivation is possible to occur if its surface potential and the pH of a corrosive medium are sufficiently high (see Fig 2. 3). Because of the CP coating's redox nature, the coating could generate a passive metal state at the coating-steel interface that shifts the steel surface potential to the noble direction.

In the third mechanism, the adherent and low porosity film of CP coating creates a special type of defense that protects metal from the corrosive environment and prevents the oxidation of metal surface by simple isolation of the surface from the corrosive environment [109]. The lower the porosity of the CP coating, the better the isolation effects that leads to reduced transport of corrosive species, O2 and water through the polymer. This reduction in coating porosity is extremely significant for the long-term protection of the coating.

Lastly, it is understood that as metals get in electrochemical contact with an electrically conducting polymer (which is a doped semiconductor), an electric field is created, which would reduce the electrons flow between the metal and oxidizing species, thus preventing or limiting the corrosion rate [110].

2.8.3 Cathodic protection

Cathodic protection is one of the important corrosion mitigation techniques that is broadly applied to metal immersed in water or buried in moist soil. The method requires applying a potential difference between the protected metal structure (cathode) and an anode, where the metal is protected by making the metal structure more negative to the level at which the corrosion rate is drastically reduced [111].

A common way of cathodic protection is the use of a sacrificial anode, where the anode is made of a more active metal than steel, such as zinc or magnesium, rendering the steel as a cathode. While the sacrificial anodes corrode, the steel (cathodic structure) is being protected [112]. Similarly, the cathodic polarization of the steel structure can be done by applying a potential difference between the structure and an anode electrode, commonly referred to as the “impressed current protection”.

2.8.4 Corrosion inhibitors

Corrosion inhibitors are chemical compounds that once added in small quantities into the corrosive medium, will slow down the corrosion process of the metallic surface [113]. It is a very promising method to prevent metal surface corrosion, and it is the most used method for oil and gas pipeline's inner-wall protection [113]. The corrosion inhibitors are capable to protect the metal surface through retardation of the electrochemical reactions of the corrosion process [114].

There are different types of corrosion inhibitors: anodic, cathodic, and/or mixed-type inhibitors, which are based on the active inhibitor molecules that delay the corrosion reaction process. They could be obtained from organic or inorganic compounds, and/or the mix of both of them.

2.8.4.1 Anodic corrosion inhibitors

This inhibitor type operates by developing a protective oxide film on the surface of the protected metal or adsorbing on anodic sites on the surface. It builds a passive layer on the surface of the protected metal due to a large anodic shift that occurs, which reduces the corrosion rate and inhibits the anodic metal dissolution [115]. Moreover, the anodic inhibitor is also referred to as a passivation inhibitor, and there are numerous types available such as molybdate, nitrite, silicate, and chromate [116]. Nevertheless, chromate-based inhibitors (oxidizing anions that do not need oxygen to passivate the metal surface) are considered to be hazardous and harmful/toxic materials [116].

2.8.4.2 Cathodic corrosion inhibitors

This inhibitor decreases the rate of the cathodic corrosion reaction in a way of either reducing the diffusion rate of corrosive species to the metallic surface or adsorbing on the cathodic site and 'insulating' them from the environment. Cathodic poisons were mainly used as inhibitors, in which they inhabited the cathodic reduction reactions, and at the same time increased the vulnerability of the metal to hydrogen-induced cracking (as the metal can absorb hydrogen during cathodic charging) [117, 118]. For instance, sulphur is used as one of the cathodic inhibitors that forms hydrogen sulphide when it reacts with hydrogen, imposing a hazardous risk to the environment [119]. Other commonly used cathodic inhibitors such as polyphosphates, zinc salts, and cerium salts are considered acceptable to the environment [119].

2.8.4.3 Mixed corrosion inhibitors

This type of inhibitor is mutually reducing the kinetics of cathodic and the anodic reactions, where the most common used types are the organic compounds. They adsorbed on the metal surface and form a protective molecular-thick layer. Mixed type inhibitors offer the highest protection level since they impact mutually cathodic and the anodic reaction [120, 121]. However, the degree of protections is influenced by many factors like the inhibitor type, concentration, and the addition of different components (additives). Nevertheless, most of the currently-used organic inhibitors impose several hazardous impacts in terms of environmental health and safety [120, 121].

The mechanism of the interaction of a mixed-type (organic) corrosion inhibitor with the surface to be protected is mainly of an adsorptive type, and it is influenced by the chemical structure of the inhibitors and the metal surface electric charge. The interaction between the inhibitor molecules and the metal atoms result in formation of an inhibitor layer of a certain surface coverage at the electrolyte/metal interface, thus separating the metal from the corrosive environment, resulting in a decreased corrosion process rate [122, 123]. More fundamentally, organic inhibitors contain electron-donating groups or electrons in conjugated double bonds, heteroatoms, and electronegative groups, while the metal contains vacant electron orbitals of low energy, enabling the formation of a coordinated type of bond between the inhibitor molecule and the metal surface, and thus formation of a molecular inhibitor layer on the metal surface [124].

2.8.4.4 Environmentally friendly corrosion inhibitors

Novel types of organic corrosion inhibitors have been proposed, including natural (plant) extracts [125], ionic liquids [126], biopolymers [127], and pharmaceutical products [126]. The plant extracts contain phytochemicals having excellent aqueous solubility. Ionic liquids are widely established as environmentally friendly and used in diverse industrial applications, and they have been evaluated and considered as green corrosion inhibitors. Amino acids are biodegradable and considered as green corrosion inhibitors. Certain green pharmaceutical products have been demonstrated as efficient corrosion inhibitors [126]. Globally, there is a growing concern about the level of the discharged toxic effluents to the soil and aquatic life. Several guidelines have been proposed to test the toxicity, biodegradability, and bioaccumulation of chemicals [128, 129]. A number of green chemistry principles are in practice to develop safer environmentally friendly molecules to be used as corrosion inhibitors.

2.9 Current developments of nano-structured CPs

Many synthesis approaches have been developed to enhance the corrosion protection performance of CPs. Nanotechnology and its application in anticorrosion fields have caught the interest of a large number of scientists. CPs can be produced in the forms of nanoparticles, nanowires, nanofibers, nanotubes, and nanorods [130-132]. The nanostructured CPs have unique physio-chemical properties that were found to improve the functionality of CPs material in numerous applications [133]. These unique properties in comparison with other materials are stability, magnetic properties, catalytic properties, hydrophobicity, light absorption, and quantum tunnelling influence [134].

Yao et al. [133] evaluated the PANI nanofibers for their anticorrosion properties of carbon steel substrates in a 5 wt.% salinity corrosive solution. Experimental results proved that this material had superior corrosion protection in comparison to aggregated PANI. Raman spectroscopy results indicated that nanofibers enhanced the production of passive oxide layers on the surface of carbon steel substrate. This improved performance was attributed to the stability of well-dispersed PANI nanofibers.

Yang et al. [135] used different polymerization techniques to produce a one-dimensional PANI nanostructure through a direct mix reaction and conventional and interfacial polymerization. They used the PANI material to coat mild steel surfaces. Then, they investigated the anticorrosion properties of the nanostructured material in 3.5wt.% sodium chloride aqueous solution. They concluded that the nanofibers synthesized employing a direct mixed reaction technique had the best uniform morphology as well as enhanced corrosion protection in contrast to the other PANI synthesis methods.

2.10 CPs nanocomposites

Several scientists have explored the possibility of studying the anticorrosion performance of coatings formed by mixing a nanostructured/nanosized material with CPs. Generally, composites yield many beneficial material properties to achieve better corrosion protection for metals. Various materials can be encapsulated within different CPs matrices to form CP-based nanocomposite materials, such as different graphene-based materials, carbon nanotubes, nanoparticles and some other metal oxide nanoparticles [136].

Silica nanoparticles is one of the promising materials for anti-corrosion coatings. The result of applying a PANI-silica nanocomposite layer on steel surfaces showed higher protection efficiency in comparison with pure PANI [137]. This composite coating had a dual protection mechanism: by the creation of a layer of passive oxide film on the steel surface and simultaneously by acting as a physical barrier to prevent the chloride ions to penetrate and reach the underlaying metal surface. Moreover, the passive oxide layer also acted as a barrier between metal surface and the corrosive environment. Additionally, the silica nanoparticle enhanced the reinforcement of PANI and thus lowered its degradation rate [137].

Another study was conducted using PPy incorporating single-wall carbon nanotubes, CNT, which acted as a dopant in the composite[138]. The coating was applied on carbon steel which was immersed in 3.5wt.% saline solution. The results were compared with pure PPy: the PPy-CNT-composite showed lower corrosion current.

A composited produced by multi-walled carbon nanotubes, MWCNT, incorporated into a PANI matrix was used as paint to protect carbon steel from corrosion[138]. This composite coating considerably reduced the corrosion of carbon steel in a high salinity solution.

Zinc oxide nanoparticles incorporated into a PPy coating were investigated for their corrosion prevention properties in 3.5wt.% saline electrolyte. The experimental results indicated a better anti-corrosion performance in comparison to a pure PPy coating [139].

2.11 Graphene

Since various forms of graphene will be used in this work to produce PANI/graphene composite coatings, the following section presents basic information on graphene.

Graphene is a thin layer of two-dimensional (2-D) sheets of sp2 carbon atoms in a honeycomb structure network, as presented in Fig 2. 7. Graphene is the base for all graphitic shapes which can be wrapped in different dimensions such as bucky-ball (0-D), nanotube (1-D), and stacked graphite (3-D). Graphene, since its discovery, has attracted the attention of many scientists due to its unique ductility and strength, among many other unique properties [140].

One of the potential applications of graphene is in corrosion protection, due to its impermeability to gases and liquids, as well as its incredible chemical inertness, even to HF [141]. The primary criteria for corrosion protection by surface coatings are an effective barrier for penetration of corrosive fluids, resistance to degradation in a corrosive environment, and mechanical reliability for the required lifetime of the coated component. Based on these main requirements, a thin layer of graphene has been testified to have chemical toughness, inertness, and impermeability, as well as being reported to be the thinnest corrosion-resistant coating [48].

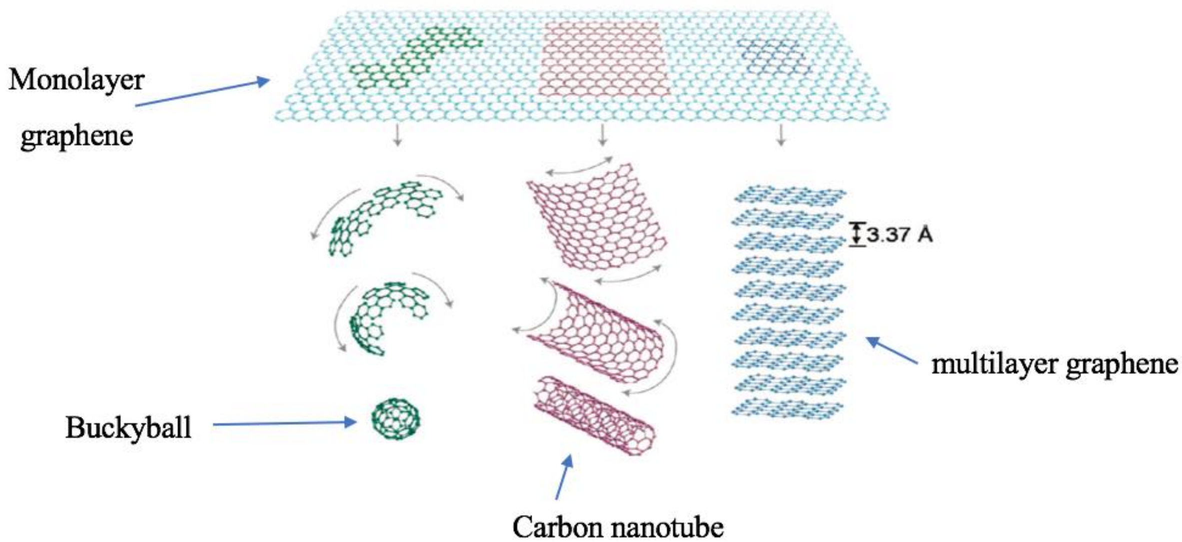

Fig 2. 7 Graphene and all graphitic forms structures [142]

2.12 Pure graphene as anti-corrosion coatings

The greatest remarkable discovery in this research field was reported by Parsai et al. [48]. They studied the corrosion protection using graphene coating on Ni through two routes. They found that the graphene coating produced via the chemical vapour deposition (CVD) technique was 20 times more efficient than the one produced by the mechanical-transferring technique. They explained that this was due to the combined mechanism during the CVD process: first, the carbon solution solubility in Ni at high temperature and second, at low temperature the formation of a thin layer of graphene [48]. The high performance in corrosion protection of Ni by graphene was also reported for commercial graphene coatings, the results varied from low corrosion protection by graphene to higher corrosion protection, with more than seven times the improvements in performance for the copper films coated with CVD-grown graphene [143]. Cu corrosion protection using graphene coatings has been evaluated in different studies [48, 143, 144].

However, scientists have found that pure graphene is not efficient as corrosion protection for long period of time for many reasons ,such as low adhesion on the metal surface [145], the graphene coating surface prepared by CVD has wrinkles, defects, and cracks which were found to be more susceptible to oxidation under increased temperatures [146]. Another issue related to the pure graphene coatings is local oxidation, these local oxidation accumulate oxygen at coating defects and boundaries, which and affects the mechanical properties of the coatings and its reliability [147].

2.13 Composite graphene based anti-corrosive coatings

The modification of corrosion-protective coatings by adding nano-fillers such as graphene, carbon nanotubes (CNTs), metallic particles, and fullerenes is becoming an interesting route to functionalize coatings in terms of their electroactivity. Recently, researchers have reported the application of graphene-based nanocomposite coatings for metal corrosion protection.

For example, Cahng et al. [51] developed an epoxy/graphene composite coating through nano-casting and found that it helps with corrosion protection by rendering the coating surface hydrophobic: the contact angle of water droplet increased up to ~127o and the coating appeared to ensure excellent corrosion protection of cold-rolled steel. Qi et al. [148] synthesized a new type of solution-processable polymer-grafted graphene oxide (GO) nanocomposite by grafting polymethylmethacrylate (PMMA) brushes on GO via surface-initiated atom-transfer radical polymerization. This study established that the PMMA/GO coating can prevent charge transfer at the metal electrolyte interface inhibiting corrosion of the copper in high salinity conditions. In another study conducted by Zeng et al. [149], they synthesized a novel poly(urea-formaldehyde)/GO composite (GUF/GO) by anchoring a prepolymer of urea-formaldehyde (UF) onto GO sheets with epoxy resin (EP) via in-situ polycondensation. They concluded that the barrier corrosion protection performance of modified GO sheets in the epoxy coating was prominently superior in contrast to unmodified GO sheets.

Chang et al. [19] evaluated the performance of polyaniline/graphene composite (PAGCs) for corrosion protection of carbon steel substrates. The subsequent chemical oxidation polymerization of aniline monomers with different amounts of 4-aminobenzoyl group-functionalized graphene sheets was done in ammonium persulfate and hydrochloric acid. The coatings showed effective corrosion protection for steel substrate in comparison with the PANI/clay composite. Mooss et al. [150] synthesized a series of PANI/GO composite coatings through altering the graphene oxide content, and the produced PANI/GO composite coating showed good corrosion resistance in 3.5 wt.% NaCl solution for 96 h, and excellent GO dispersion within the PANI matrix. Zadeh et al. [151] produced PANI/GO with high conductivity and crystallinity, and investigated the impact of GO and PANI/GO on the corrosion protection mechanism of zinc-rich coatings (ZRC). The addition of PANI/GO into ZRC enhanced the barrier resistance performance of ZRC, extended the cathodic protection time and improved the electrical contact between the zinc particles and the steel substrate. Table 2. 1 summarizes the corrosion protection performance of Graphene-based composite anti-corrosive coatings on different metals and various coating methods.

Table 2. 1 Corrosion protection performance of graphene-based coatings

Metals	Graphene coating	Corrosive environment	Corrosion protection performance	Ref
Steel	Silica nanoparticles-graphene oxide/epoxy	3.5wt.% NaCl	SiO2-GO nanohybrids coating significantly reduced the cathodic delamination rate of epoxy coating	[152]
Steel	Graphene oxide/epoxy	3.5 wt.% NaCl, pH = 10	The GO/epoxy coating improves the adhesion strength, reduces the cathodic delamination of the epoxy coating, and increases the corrosion protection properties	[153]
Stainless steel	Ceramic/CVD grown reduced graphene oxide	3.5 wt.% NaCl	High corrosion protection through increasing the impedance of the interface and the pitting potential	[154]
Steel	Polyaniline/graphene oxide composite	3.5 wt.% NaCl	Results showed that the inclusion of GO enhanced the barrier properties of the coating, and better improvement leading to longer protection service life	[151]
Steel	Functionalized graphene oxide/epoxy	3.5 wt.% NaCl	Report data showed incorporation of fGO nanosheets into the epoxy significantly enhances the corrosion protection performance, and reduced the cathodic delamination	[155]
Mild steel	3-(Aminopropyl) triethoxysilane /Graphene nano platelets	3.5 wt.% NaCl	The incorporation of graphene increased the activation energy peak for the water diffusion process	[156]
Mild steel	Epoxy/GO-amino-silane	3.5 wt.% NaCl	Coatings can provide superior corrosion protection performance and maximum corrosion resistance is achieved via adding 0.1 wt.% amino-silane -GO	[157]
Iron substrates	graphene nano-platelets/polyvinylbutyral	3.5 wt.% NaCl	Coatings are shown to exhibit exceptional resistance to important corrosion is driven failure process, namely cathodic delamination	[158]
Copper	Polyaniline–graphene nanocomposite	0.5 wt.% NaCl	PANI/G exhibit excellent corrosion resistance in very aggressive environments	[159]
Carbon steel	graphene oxide–poly-(urea–formaldehyde) composites	3.5 wt.% NaCl	Results revealed that the modified GO sheets significantly reinforced the corrosion protection property of epoxy coatings	[149]

Chapter 3

Anti-corrosive Properties of the Double-layer PANI/graphene-oxide/epoxy Coating in Protecting Carbon Steel in Salt Water

3.1 Preface

This chapter presents an article submitted to the journal of Coatings Technology and Research.

Ahmad Diraki, Sasha Omanovic: Anti-corrosive Properties of the Double-layer PANI/graphene-oxide/epoxy Coating in Protecting Carbon Steel in Salt Water

Ahmad Diraki (Ph.D. candidate) conceived the idea, planned and executed the experiments, analyzed the data, and drafted the manuscript. Prof. S. Omanovic supervised the work and reviewed and edited the manuscript.

This paper reports and discusses results on the electrochemical synthesis of a polyaniline/graphene-oxide layer on the surface of carbon steel subsequently coated by a top-layer of neat epoxy, with the aim of investigating the double-layer coating's potential use for the long-term corrosion protection of oil and gas carbon steel pipelines' outer-wall, immersed in seawater. The double-layer coating of PANI-GO/epoxy showed excellent long-term corrosion protection performance, compared to the single-layer commercial epoxy coating.

Highlights

- An anti-corrosive coating composed of inner PANI and outer epoxy layer was formed
- The thin inner PANI layer significantly improved the coating corrosion resistance
- Graphene oxide (GO) incorporated into the PANI layer provided additional protection
- The PANI/GO/epoxy coating provided excellent long-term (60 days) protection

Abstract

The work reports result in improving the anti-corrosive properties of a commercial epoxy coating by forming a double-layer coating structure. First, a thin (ca. 5 μm) electrically conductive polyaniline (PANI) coating was formed directly on the carbon steel (CS) surface, on top of which a thicker (ca. 20 μm) epoxy coating was applied. The inner PANI layer was also loaded with graphene oxide (GO). The resulting anti-corrosive properties of the coatings were investigated in 3.5 wt.% NaCl employing electrochemical techniques, while the surface and cross-sectional morphology of the coatings was examined by scanning electron microscopy (SEM). The results showed that the commercial epoxy coating started gradually failing several days after its exposure to the electrolyte, while it took 37 days for larger pores to appear in the PANI/epoxy coating, which then gradually continued to fail. On the other hand, the PANI/GO/epoxy coating maintained its high corrosion resistance, without the formation of impedance-detectable pores, over the entire testing period (two months). The excellent corrosion protection properties of the PANI/GO/epoxy coating were prescribed solely to the presence of the underlying PANI/GO layer, which represents a better barrier for the transport of hydrated corrosive ions to the CS surface, through the combined action of charge (repulsion of hydrated corrosive anions and iron oxide film formation), surface energy (hydrophobicity), and blocking mechanisms.

Keywords: Corrosion, Polyaniline, Graphene, Epoxy, Coatings

3.2 Introduction

Carbon steel (CS) is one of the most used metals in numerous industrial applications, including infrastructure, transport, and energy. The yearly production of different types of steel exceeds 1.6 billion tons. Although CS offers unique properties such as strength, hardness, electrical conductivity, and cost-effectiveness, it is sensitive to corrosion [160], a severe economic and industrial structure threat [161]. Economically, the annual direct cost of metal corrosion in the USA is more than $200 billion, around $2.2 billion worldwide, and about 4% of the GDP of an industrialized country [162-164].

Many techniques have been implemented to control corrosion, including corrosion inhibitors, protective coatings, cathodic protection, etc.[165, 166]. Protective coatings can be applied on the metal substrate in many forms of sacrificial coatings [15], oxide layers [16], varnishes [17], organic films [18], polymeric layers [19], to name a few. Recently, non-conducting epoxy coatings combined with conducting polymers (CPs) have been used to protect metals from corrosion [20]. Epoxy coatings are often used for corrosion prevention because of their exceptional mechanical and chemical properties [21-23]. CPs coatings have exhibited promising corrosion inhibition performance of metal substrates because they are environmentally stable, eco-friendly, non-toxic, and adhere firmly to the metal surface [24]. CPs such as polyaniline, polypyrrole, polythiophene, and polyacetylene varied in corrosion protection efficiency depending on their oxidation degree [26]. It has been reported that polyaniline stabilizes steel's passive state and provides anodic protection during electrochemical deposition [20, 27]. However, CPs for corrosion protection are often limited due to the matrix's intrinsic microstructure porosity, which fails to prevent the entry of corrosive species [167, 168]. Therefore, incorporating a filler with unique mechanical properties to form a composite with a CPs-based coating would overcome the porosity issue related to CPs [169, 170].

Many inorganic materials with different characteristics and structures have been studied as fillers incorporated into CPs to enhance the tortuosity of the coatings [171-176]. Among efficient fillers, graphene demonstrated exceptional capabilities due to its outstanding mechanical properties, high specific surface area, and corrosion protection performance [177-180]. In addition, graphene promotes charge transfer in CPs, allowing better corrosion protection [181]. Graphene is a two-dimensional honeycomb lattice nanostructure, and it is chemically inert. Thus, it may limit matrix/nanofiller interactions and cause more extensive nanofiller aggregation [182]. Conversely, the oxygen functional groups in the hydrophilic graphene oxide (GO) render better matrix/nanofiller interactions [19, 183]. Yeh et al.[19] produced GO reinforced polyaniline membranes with higher corrosion protection and gas barrier. A single-layer graphene sheet showed in the reported literature better corrosion protection than the multilayered graphene sheets. This is attributed to better dispersion of the filler and stronger adhesion [184-188]. Although CPs/GO composite coatings showed superior corrosion prevention efficiency, many have not emerged in industrial applications; this is mainly due to the composite coating's high cost and pure adhesion to the metal surface, not enabling longer-term corrosion protection [107].

In the present work, we developed and applied a double-layer coating on G1117 carbon steel (CS) to overcome the limitation of CP/graphene composites during an extended emersion time in the corrosive environment. We first electrochemically synthesized polyaniline (PANI) coating incorporating a single-layer-GO directly on the carbon steel substrate (inner layer), which was then followed by the application of a second (outer/top) layer of commercial pure epoxy resin. The corrosion resistance studies revealed that the two-layer composite PANI/GO/epoxy coating offered a significantly better long-term protection towards corrosion of the CS surface than the GO-free two-layer PANI/epoxy and, especially, than the single-layer commercial epoxy coating.

3.3 Experimental

3.3.1 Materials

All reagents were AR grade and used as received from the suppliers. The aqueous solutions were prepared with ultrapure water (18 MΩ cm). The single-layer graphene oxide (GO) was purchased from Advanced Chemicals Supplier Material, ACS Material. (Massachusetts, USA) with a flake diameter of 0.4-5 µm and thickness between 0.6 and 1.2 nm, which was synthesized by thermal exfoliation reduction plus hydrogen reduction. The aniline monomer ($C_6H_5NH_2$, ACS reagent grade, ≥99.5%) was bought from Sigma-Aldrich (Missouri, USA). Oxalic acid (98%, anhydrous) used in the electrolyte preparation was purchased from Acros organics (USA). Sodium dodecyl sulphate (SDS), sodium chloride (certified ACS), denatured ethanol (95% EA), and acetone (Certified ACS) were purchased from Fisher Scientific (USA). HELOXY™ Modifier 48 epoxy resin (epoxide equivalent weight = 138-154 g/eq), and EPIKURE™ curing agent 3388 (amine value as KOH 260-285 mg/g) were purchased from Hexion Inc. (Ohio, USA). G1117 low carbon steel, acquired from McMaster-Carr (USA) with a chemical composition of 0.14-0.20 wt.% carbon and 1.00-1.30 wt.% manganese, was used as a metal substrate for corrosion testing.

3.3.2 Instrumentation

An AUTOLAB Potentiostat/Galvanostat/FRA PGSTAT 30 was used for electropolymerization and corrosion tests. This system was interfaced with a computer to control the experiments, and the data were acquired and analyzed using NOVA 2.1 software. A conventional three-electrode electrochemical cell consisted of a conductive graphite rod as the counter electrode, a saturated calomel electrode as reference electrode (SCE), and a coated/uncoated carbon steel sample as the working electrode. A programable dip coater (1-200 mm/min)-PTL-MM02 was used to apply epoxy coatings on the carbon steel sample. Morphology of materials was observed using a field-emission scanning electron microscope (Hitachi FE-SEM SU3500). Fourier transform infrared spectroscopy (FTIR-ATR) was performed using a Nicolet iS50 ATR Thermo Scientific spectrophotometer. Coating's mechanical properties were determined with an adhesion test (ASTM D 3359). Profilometer Dektak XT-Bruker was used to determine the coatings film thickness. Goniometer (FSA OCA 15EC)-Data-Physics was employed to evaluate the material surface wettability. Polishing machine MetaServ-3000 and Branson-1510 ultrasonic water bath was used for sample preparation.

3.3.3 Sample preparation

A carbon steel metal rod was machined to a diameter of 1.59 cm and cut into coins with a thickness of 3.3 mm. A Teflon holder was used to hold the sample when immersed in the electrolyte, leaving a metal area of 1.039 cm^2 exposed to the electrolyte (one side of the sample). Before undergoing the coating-application process, the samples were adequately pre-treated to improve and favour the adhesion with the coating. Namely, the carbon steel surface was wet-polished using a 600-silicon carbide grit paper for 2 minutes on the rotation speed of 200 rpm. Then, the sample was ultrasonicated in ethanol for 5 minutes to remove the polishing residue. Finally, the substrate was rinsed with acetone to degrease its surface and dried with an argon stream.

3.3.4 Preparation of the coatings

In this study, three different coatings were formed on the CS surface: (1) a single-layer neat epoxy (EP) coating, (2) a double-layer PANI/epoxy coating, and (3) a double-layer PANI/GO/epoxy coating containing different amounts of graphene oxide.

3.3.4.1 Polyaniline (PANI)

PANI coatings were electrochemically synthesized on carbon steel (CS) samples in a stirred 100 ml aqueous solution containing 0.1 M aniline monomer and 0.2 M oxalic acid. The electrochemical synthesis was carried out by cyclic voltammetry (CV) at a scan rate of 10 mV s^{-1} over 10 cycles. The experimental conditions were chosen based on published literature [189, 190]. Multiple experiments were performed with different potential regions to optimize the electropolymerization potential range while keeping other parameters constant. The optimum potential range was determined to be from -0.6 and 1.6 V. Upon completing the electropolymerization process. The electrode was removed from the electrolyte solution, rinsed with deionized water, dried with argon gas, then kept at room temperature (cured) for 72 hours before performing corrosion tests.

3.3.4.2 Polyaniline/Graphene oxide composite

PANI/GO nanocomposites were synthesized following the same procedure outlined above for pure polyaniline coatings. Different loadings of GO into the PANI layer were investigated (Fig. 3-S. 1 in the supplemental document), and it was determined that the PANI coating with the 0.01 wt.% of GO in 100 ml aqueous solution containing 0.1 M aniline monomer and 0.2 M oxalic acid gave the best results. Therefore, only these results are presented in the manuscript. The GO loading was utterly dispersed in the aniline-monomer-containing solution used in 2.4.1 under magnetic stirring for 1 hour with brief ultrasonication to accelerate the dispersion. 1 mM of SDS was added as a surfactant to disperse the GO in the aqueous solution and minimize its aggregation [191]. At the used GO loading, the smaller particles constitute a more significant proportion of suspended solids, and these high solid loading dispersions allow for the preparation of PANI/GO with yield pinhole-free film [44-46].

3.3.4.3 Epoxy coatings

Commercially available epoxy resin was a HELOXY^{TM} Modifier 48, and the curing agent was EPIKURE^{TM} 3388. Both compounds were clear, transparent, and contained no additional additives. For the preparation of epoxy coatings, the curing agent and epoxy resin ratio were 1:1, and the calculated amount was mixed for 5 minutes, then sonicated for 1 minute. The coatings were deposited on the CS substrate by a dip-coater to ensure the uniform layer thickness and reproducibility, with a withdrawal speed of 4 mm/s. The sample was then placed for curing at 22±1^{o}C for 7 days. The epoxy/ curing agent ratio, curing time and temperature were followed as the manufacturer's recommendation for optimum adhesion and mechanical properties.

3.3.5 Corrosion measurements

Electrochemical/corrosion measurements were carried out in an aqueous 3.5 wt.% NaCl. Electrochemical impedance spectroscopy (EIS) and Tafel polarization were used to investigate the corrosion resistance of the coated and uncoated samples. Before each Tafel and EIS run, the samples were conditioned at open-circuit potential (OCP) for 1 hour, except in long-term experiments. EIS measurements were performed at OCP in the frequency range between 10 mHz and 50 kHz applying a ±10 mV alternating voltage amplitude. Tafel polarization curves were recorded by anodically polarizing the samples from -200 mV to +200 mV vs. OCP at a scan rate of 1 mV s^{-1}. All potentials in this paper are referred to SCE. All the measurements were performed at 22±1ºC.

3.3.6 Surface characterization

Coatings' surface morphology was studied by field-emission scanning electron microscopy. To confirm the chemical composition of the PANI/GO coating, Fourier transform infrared spectroscopy (FTIR-ATR) was recorded in the region between 4000 and 400 cm^{-1} wavenumbers, employing 64 scans at a resolution of 2 cm^{-1}. The thickness mapping of different coatings was evaluated and analyzed by a profilometer, and the technical characteristics of the profilometer are presented in Table 3. 1. A step between the CS surface and the coatings was produced by masking portions of the substrate during coating deposition. Water contact angle measurements examined the surface wettability with a drop shape analyzer, in which the image analysis software determined the contact angle (Θ). The contact angles were generated between the surfaces and deionized water drops with a dosing rate of 0.5 µL/s and a dosing volume of 5 µm. The coatings' adhesions on the CS substrates were determined following the ASTM D 3359 standard tape adhesion test [192].

Table 3. 1 Technical characteristics of the profilometer.

Variable stylus force	**0.098 mN to 147 mN**
Vertical resolution	0.1 µm
Maximum scan length	50000 µm
Automation	Yes

3.4 Results and discussion

3.4.1 Physical characterization of the coatings

The scanning electron microscopy (SEM) of the uncoated and coated carbon steel surfaces are presented in (Fig 3. 1). The freshly prepared CS surface (Fig 3. 1(a)) is characterized by the appearance of scratches produced by mechanical polishing. On the other hand, the PANI-coated CS surface (Fig 3. 1(b)) is nonhomogeneous and is characterized by the presence of clews comprised of the interconnected network of fibrils. Surprisingly, when 0.01 wt.% GO was incorporated into the PANI layer, the coating's structure and morphology drastically changed, Fig 3. 1(c), resulting in a homogeneously corrugated structure surface [193]. (Fig 3. 1(d)) shows (under high magnification) the morphology of GO sheets in the PANI coating, where the corrugated structure of GO is still maintained. Fig 3. 1(e) presents the morphology of the neat epoxy coatings deposited on top of the PANI/GO coating; the surface of the epoxy coating is characterized by a smooth finish, without visible pores under the 110X magnification. These results indicate good dispersion of GO and compatibility with the PANI matrix and confirm the successful synthesis of the PANI and PANI/GO composite [194, 195]. The cross-section images presented in Fig 3. 1(f) PANI/GO, (g) epoxy, and (h) PANI/GO/epoxy show the thickness of the layers, 5 μm for PANI/GO, 20 μm for epoxy, and 25 μm for the double layer PANI/GO/epoxy. Profilometry measurements also revealed that the thickness of the PANI and PANI/GO coatings was 4.84±0.12 μm, while the epoxy coating was substantially thicker, 20.6±0.2 μm, and the thickness of the double layer PANI/epoxy and PANI/GO/epoxy coatings was 24.9±0.1 μm. However, as it will be shown later, the existence of the thin PANI/GO coating layer underneath outer the epoxy coating contributed to a substantial increase in the long-term corrosion protection efficiency of the composite coating, with respect to that of the thicker epoxy coating when deposited without the inner PANI/GO coating.

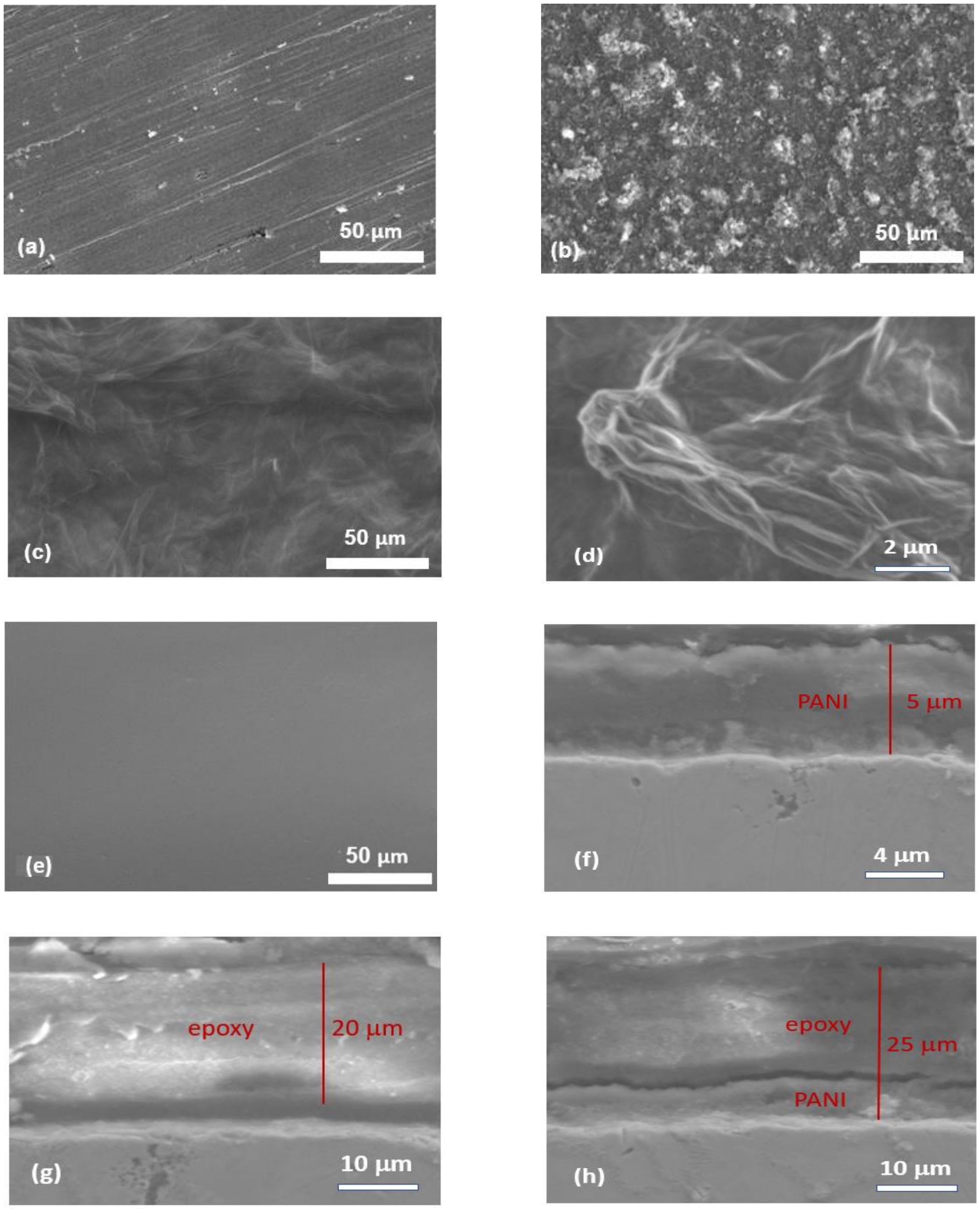

Fig 3. 1 SEM micrographs of the (*a*) freshly polished uncoated CS surface; (*b*) PANI-coated CS surface ;(c) PANI/GO-coated CS surface; (d) PANI/GO-coated CS surface under the 12k X magnification; (e) neat epoxy resin coating formed on the PANI/GO coating; (f) cross-sectional image of a PANI/GO-coated CS surface (under the 10k X magnification); (g) cross-sectional image of a neat epoxy-coated CS surface; (h) cross-sectional image of a PANI/GO/epoxy-coated CS surface.

Fig 3. 2 presents the FTIR-ATR spectra of pristine PANI, and PANI/GO coatings deposited on a CS surface. The broadband around 3246-3257 cm^{-1} on the PANI spectrum shown in Fig 3. 2 (curve *a*) is attributed to the N-H stretching vibration of the PANI due to the protonation of nitrogen [196-198]. The C=C stretching vibrations of quinoid and benzenoid rings are confirmed by the bands at 1581 cm^{-1} and 1497 cm^{-1} [196, 197], respectively. The band at 1300 cm^{-1} can be assigned to the π-electron delocalization induced in the polymer through protonation, while the band at 1248 cm^{-1} corresponds to the C-N stretching vibration of secondary aromatic amine [199]. The band at 1146 cm^{-1} is assigned to the plane bending vibration of C-H which is formed during the protonation, and it is described as the electronic-like band and considered to be a measure of the degree of delocalization of electrons of PANI [135, 197, 198]. The band at 817 cm^{-1} is assigned to a C-H out-of-plane bending vibration of aromatic rings [200]. The presence of these distinct vibrations on the recorded spectrum is characteristic of the emeraldine salt form of polyaniline [197-199, 201].

On the other hand, the FTIR spectrum of the PANI/GO nanocomposite, presented in Fig 3. 2 (curve *b*) shows a marked alteration in the characteristic peaks, confirming the formation of new chemical bonds between PANI and graphene oxide (GO). Thus, a more pronounced and wide vibration at 3420 cm^{-1} appears; this vibration can be related to the tensile vibration of the O-H bond group in the GO, and to the hydrogen bond between NH from PANI and oxygenated groups from the GO [193, 202, 203]. The band at 1715 cm^{-1} is attributed to the C=O vibration of carboxyl groups on the GO, while the band at 1359 cm^{-1} can be prescribed to the O–H deformation of the C–OH group on the GO [193, 202, 203]. Correspondingly, the FTIR spectrum in Fig 3. 2 (curve *b*) evidences the successful incorporation of GO into the PANI coating.

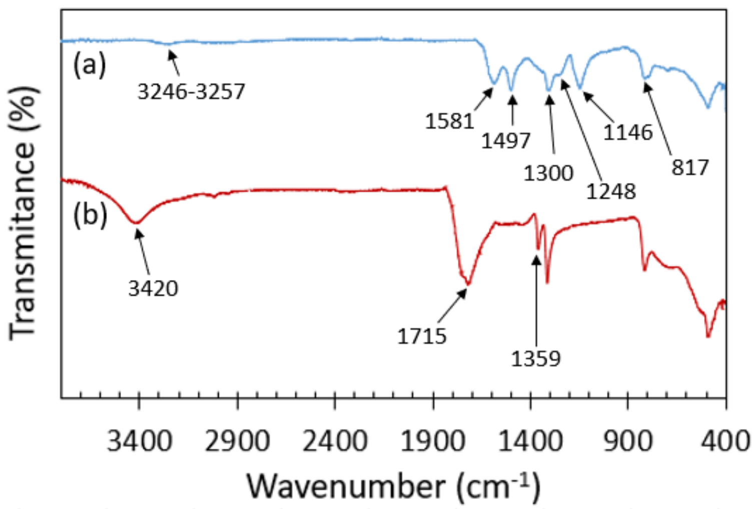

Fig 3. 2 FTIR-ATR spectra of (a) a pristine PANI coating, and (b) of a PANI/GO coating formed on the CS surface.

One of the desired features of anti-corrosive coatings is their increased surface hydrophobicity. Since the epoxy coating was the top coating employed in this research, its hydrophobicity was compared to that of the bare CS surface, Fig 3. 3. The contact angle value sharply increased from 49.7±0.2° for the uncoated CS surface (Fig 3. 3(a)) to 81.9±0.5° for the epoxy-coated CS sample Fig 3. 3(b), thus confirming the higher hydrophobicity of the epoxy-coated surface. Hydrophobicity can also enhance corrosion resistance due to the decreased water/surface interactions [204]. Although the PANI and PANI/GO layers are sandwiched between the CS surface and the epoxy layer, it is essential also to examine their interaction with water; this is because the damaged epoxy coating will allow water to penetrate and reach the PANI (or PANI/GO) layer, and it would be of interest for this layer to also repel water. Indeed, Fig 3. 3(c) shows that the PANI coating is even more hydrophobic than the epoxy coating, offering the contact of 96.2±0.3° (Fig 3. 3 (c)). However, once GO was incorporated into the PANI layer, the contact angle further increased to 113.2±0.1° (Fig 3. 3(d)), thus rendering this coating potentially highly water repellent, which is of importance for good corrosion protection [205].

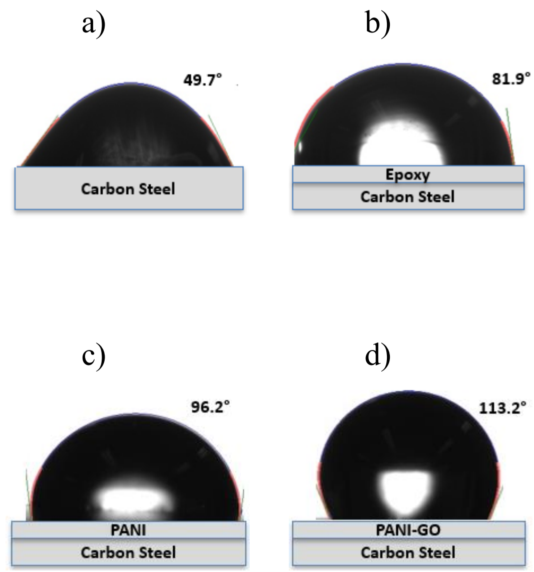

Fig 3. 3 The contact angles between the deionized water drop and the (*a*) freshly polished uncoated CS surface, (*b*) the neat epoxy resin coating formed on the CS surface, (*c*) the PANI coating deposited directly on the CS surface, and (*d*) the PANI/GO coating deposited directly on the CS surface.

Adhesion of coatings to the substrate is an essential factor influencing the long-term performance of the coatings [206, 207]. To examine the adhesion of PANI, PANI/GO, PANI/epoxy and PANI/GO/epoxy coatings on the CS substrate, the ASTM D 3359 standard tape test was performed. It was determined that all the coatings adhered to the substrate well, yielding the adhesion remaining (AR%) values between 94% to 97% (percentage of non-failed regions). Thus, it can be concluded that the presence of GO in the inner PANI layer, or the presence of the top epoxy layer neither influences the adhesion of the PANI layer to the CS surface nor the adhesion of the epoxy layer to the underlying PANI and PANI/GO layer. The pull-off adhesion test confirmed low adhesion loss in coatings even after a long immersion in the corrosive environment.

3.4.2 Anti-corrosive properties of the coatings – electrochemical measurements

Proportional corrosion studies were conducted for the uncoated (control 1) and epoxy-coated CS samples (control 2). The CS samples were coated with the double-layer coatings of PANI/epoxy and PANI/GO/epoxy. CS samples coated with only PANI, or PANI/GO could not be instigated using Tafel and EIS techniques due to the samples' relatively good electrical conductivity.

3.4.2.1 Potentiodynamic polarization studies (Tafel)

Initial information on the corrosion protection of the coatings was obtained from Tafel polarization measurements, presented in Fig 3. 4. All the curves display a similar shape, characterized by the cathodic Tafel branch corresponding to the oxygen reduction reaction and the anodic Tafel branch corresponding to the metal dissolution. As can be seen, a drastic change in the response of the CS sample was recorded when its surface was modified by the coatings. Most notably, the corrosion potential shifted to more positive values, and the Tafel curves decreased to lower currents. When the epoxy coating coated the CS surface, the decrease in the Tafel curve was by ca. 2 orders of magnitude, which was expected due to the barrier properties of the coating. However, the currents further decreased when the CS surface was coated first by a thin PANI and then by the epoxy coating (double-layer coating). Incorporating GO into the PANI coating yielded even a further decrease in the currents. This demonstrates a significant increase in barrier properties of the PANI-containing coatings versus the epoxy coating. To quantify the actual protection degree of the coatings, corrosion currents (I_{corr}) were determined from the Tafel plots employing the standard extrapolation method [208], and their values are listed in Table 3. 2. As it can be seen, the application of the epoxy coating resulted in a corrosion current decrease by almost two orders of magnitude, while the addition of the thin PANI inner layer contributed to the further decline by ca. two orders of magnitude. Considering that the PANI sub-layer is electrically semi-conductive and that Tafel measurements were done, the decrease in corrosion current by incorporating this inner layer to form a double-layer coating cannot only be related to its barrier properties. In fact, the literature has shown that CPs, once directly electropolymerized on the metal surface with proper dopant molecules, may lead to a conductive and electroactive film that possesses inherently reversible redox reactions with the metal surface [24, 209]. The redox reactions based on the conductivity of CPs include introducing/releasing dopant ions, providing a unique corrosion inhibition method [210]. Moreover, several other mechanisms have been suggested, including shifting the electrochemical interface, anodic protection, formation of an ennobled CPs/metal interface, and facilitation of protective oxide [211]. PANI coatings possess superior corrosion protection performance in comparison with other CPs [19]. In addition to the above mechanism, PANI increases the corrosion potential and its redox catalytic ability in forming the passive metal oxide layer [212].

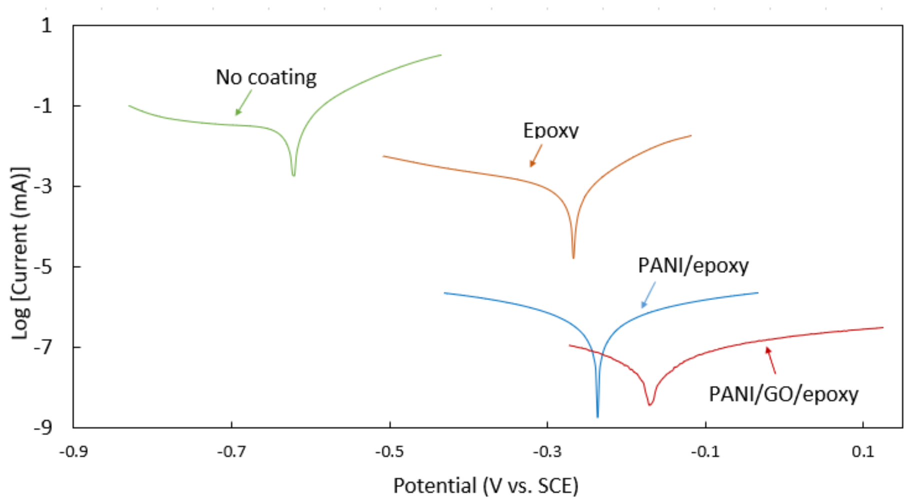

Fig 3. 4 Tafel polarization plots of the uncoated and coated CS, recorded in 3.5 wt.% NaCl at a scan rate of 1 mVs^{-1}.

A surprising finding was that the incorporation of just 0.01 wt.% of GO into the PANI matrix resulted in a further significant decrease in the corrosion current of almost two orders of magnitude (Table 3. 2); it should, thus, be noted that the application of the PANI/GO/epoxy coating results in a decrease of corrosion current of four orders of magnitude relative to the commercial epoxy coating, and a staggering six orders of magnitude with respect to the naked (unprotected) surface, thus demonstrating excellent barrier / anti-corrosive properties. The two-decade decrease in corrosion current upon the incorporation of GO into the PANI matrix can be explained based on the schematics shown in Fig 3. 8 (to be discussed later in detail).

Table 3. 2 Corrosion current determined from Tafel measurements recorded on the naked (unprotected) CS surface and the CS surface protected by the three coatings.

Sample	I_{corr} (A cm^{-2})
Carbon steel	(2.7±0.3) x10^{-5}
Epoxy	(5.5±0.2) x10^{-7}
PANI/epoxy	(1.5±0.2) x10^{-9}
PANI/GO/epoxy	(5.1±0.1) x10^{-11}

3.4.2.2 Electrochemical impedance spectroscopy (EIS)

EIS was used as a powerful tool to characterize the electrode-solution interface and estimate the corrosion protection efficiency of the coatings on the CS surface. Nyquist plots of selected results of the coated and uncoated CS samples are presented in Fig 3. 5 Nyquist plots of the uncoated and CS surface coated by epoxy, double layer of PANI/epoxy and PANI/GO/epoxy coatings recorded at OCP in 3.5 wt.% NaCl. Symbols represent the experimental spectra, while the solid curves represent the modelled spectra.. A larger diameter of the semicircle indicates higher corrosion resistance. The spectra do not include a diffusion (Warburg impedance) behavior at lower frequencies, indicating that the CS corrosion process is primarily a charge transfer controlled process [213]. Most notably, the epoxy-coated sample showed a larger arc radius than the uncoated CS sample, implying an increase in the corrosion resistance, which is due to the barrier properties of the surface. The EIS spectra of the double-layer coatings of PANI/epoxy and PANI/GO/epoxy exhibited a remarkably larger diameter, indicating a substantial increase in corrosion resistance compared to the uncoated carbon steel sample.

These EIS spectra presented in Fig 3. 5 were modelled employing the one-time-constant electrochemical equivalent circuit (EECs) shown in Figs. 5a and 5b. In this EEC, R_{el} represents the solution resistance between the reference electrode and the CS working electrode, R_1 is the polarization resistance linked to the overall kinetics of the CS corrosion reactions occurring at OCP, CPE_1 is the constant phase element related either to the capacitance of the electric double-layer at the uncoated electrode/electrolyte interface (Fig 3. 6a), or the coating pseudocapacitance for the coated surfaces (Fig 3. 6b) [214]. An excellent agreement between the experimental (symbols) and modelled data (lines) in spectra. Confirms the applicability of the EEC in Fig 3. 6 and 6b in describing the EIS behavior of the studied systems. The values of the EEC parameters are summarized in Table 3. 3.

The values in Table 3. 3 show that when the epoxy coating was formed on the CS surface, the corrosion resistance value increased by ca. four orders of magnitude. The formation of the PANI and PANI/GO layers underneath the epoxy coating resulted in a further increase in corrosion resistance by ca. two orders of magnitude. The trend in CPE values also demonstrates the excellent barrier properties of the coatings. Namely, when the epoxy coating was formed on the CS surface, the CPE drastically decreased, followed by a further decrease upon incorporating the inner PANI and PANI/GO layers. The decrease in the CPE exponent “n” shows the transition from the more capacitive behaviour of the naked CS surface (higher values) to the pseudo-capacitive behaviour for the coated surfaces (lower values).

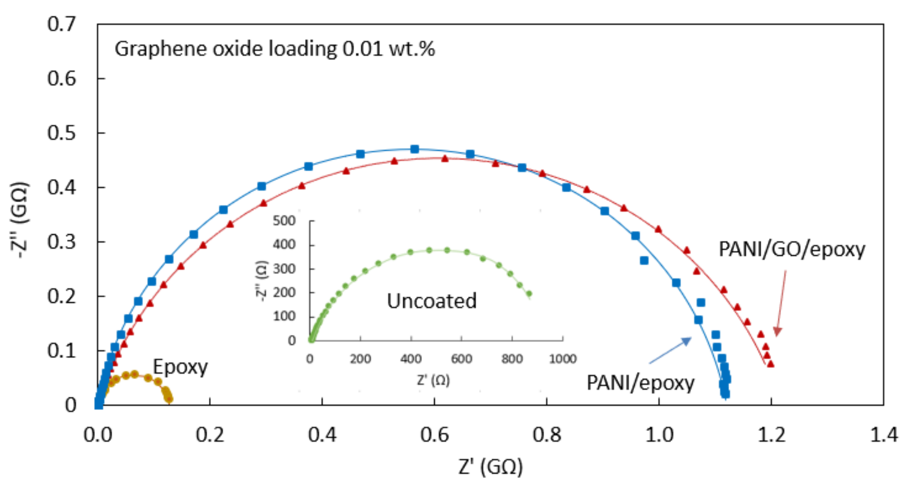

Fig 3. 5 Nyquist plots of the uncoated and CS surface coated by epoxy, double layer of PANI/epoxy and PANI/GO/epoxy coatings recorded at OCP in 3.5 wt.% NaCl. Symbols represent the experimental spectra, while the solid curves represent the modelled spectra.

Table 3. 3 EEC parameter values obtained by modelling the EIS spectra presented in Fig 3. 4.

Sample	R_{corr} (Ω cm^2)	CPE_1 (Ω^{-1} cm^{-1} s^n) x 10^6	n
Carbon steel	(9.00 ±0.04) x10^2	695±0	0.89±0.04
Epoxy	(1.26±0.01) x10^7	9.1±0.4	0.83±0.02
PANI/epoxy	(1.11±0.06) x10^9	3.8±0.2	0.77±0.01
PANI/GO/epoxy	(1.28±0.04) x10^9	0.1±0.1	0.71±0.01

(a) (b) (c)

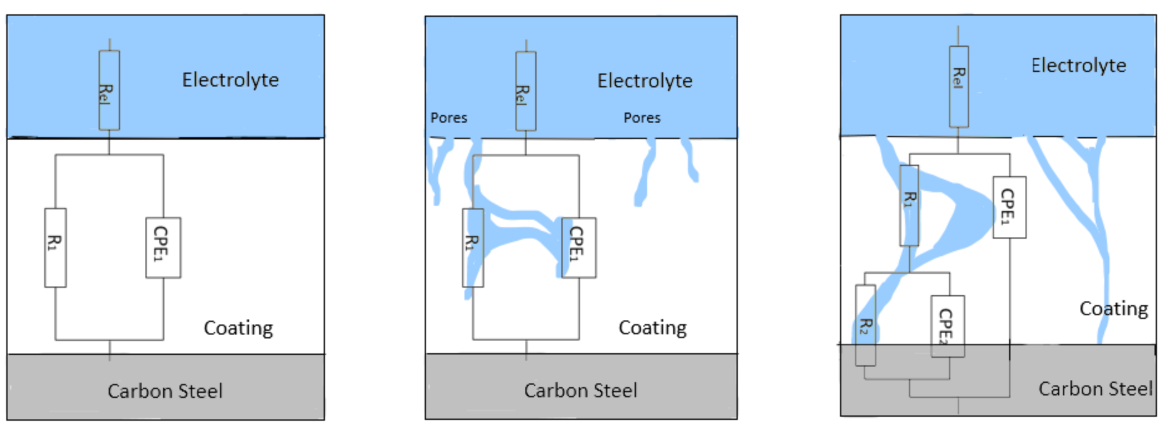

Fig 3. 6 EEC models used to fit EIS spectra of the (*a*) uncoated and (*b*) pore-free coated CS surface, and (*c*) the CS surface coated by coatings that developed pores that penetrate to the CS/coating interface.

3.4.3 Long-term corrosion study

Long-term corrosion protection is crucial in determining the coatings' potential industrial applicability and evaluating how well the coatings hold up with time. The above-presented short-term Tafel and EIS measurements showed that incorporating the inner PANI, especially PANI/GO layer underneath the epoxy coating, provides a significant increase in the corrosion resistance of the CS surface. However, the information on their long-term performance is of major importance, which was also investigated.

The influence of time on the coatings' corrosion protection performance was quantified using the EIS technique over 60 days of constant immersion in a 3.5 wt.% NaCl solution, by recording the EIS spectra every 6 hours. Each spectrum was then modelled using the EECs presented in Fig 3. 6, and the corresponding corrosion resistance was determined – Fig 3. 7 shows its trend with time for the three different coatings. As it can be seen, the protecting properties of the commercial epoxy (yellow circles) are the poorest among the three coatings. Shortly after the immersion, the corrosion resistance of this coating decreased. Only after two days of exposure to the electrolyte, the EIS modelling of the recorded spectra show the presence of the second time constant related to the formation of pores in the coating, enabling the penetration of the corrosive electrolyte; accordingly, the EEC presented in Fig 3. 6c was used in describing the behaviour of this coating. In this EEC, the outer CPE_1-R_1 time constant represents the response of these pores, while the inner CPE_2-R_2 time constant represents the response of the double layer and charge-transfer resistance, respectively [215]. Consequently, the sum of the two resistances represents the total resistance to corrosion, R_{corr}. Fig 3. 7 shows that after 24 days of constant immersion, the corrosion resistance of the epoxy-coated CS surface significantly decreased, although it was still high (9.24±0.05) x10^6 MΩcm^2.

On the other hand, when the epoxy was applied on top of the PANI coating, the corresponding corrosion resistance significantly increased (Fig 3. 7, blue squares) in comparison to the CS surface coated by only the epoxy coating (yellow circles). Further, unlike the appearance of the pores in the latter coating, the pores in the PANI/epoxy coating appeared only after 38 days of immersion; however, once they appeared, the corrosion resistance of the coating continued to gradually deteriorate, albeit still being significantly higher than that offered by the sole epoxy coating.

Although the short-term Tafel and EIS results demonstrated the superior protection properties of the PANI/GO/epoxy coating, the results of its long-term behaviour shown in Fig 3. 7(red triangles) are surprising; even after 60 days of constant immersion, no larger pores that could have been detected by EIS appeared. A slight decrease in its corrosion resistance was recorded. However, at the end of the testing period, its barrier properties were still superior to those offered by the other two coatings.

Consequently, the results in Fig 3. 7 demonstrate that the formation of the double-layer PANI/epoxy coating and especially the incorporation of GO into the inner PANI coating results in a significant increase in protective properties of the coatings, not only during the short-term immersion but also during prolonged exposure of the coating to the corrosive electrolyte.

The corrosion protection mechanism of the PANI/GO/epoxy coating can be explained by considering the following points and referring to the schematics in Fig 3. 8.

During the electrochemical synthesis of PANI on the CS surface, an interfacial passive Fe_2O_3 oxide layer is formed through the mediation of PANI [216, 217]:

$$PANI^{m+} + \frac{m}{3} Fe \rightarrow PANI^{0} + \frac{m}{3} Fe^{+3} \quad (3.\ 1)$$

$$4PANI^{0} + mO_2 + 2mH_2O \rightarrow 4PANI^{+m} + 4mOH^{-} \quad (3.\ 2)$$

$$2Fe^{+3} + 6OH^{-} \rightarrow Fe_2O_3 + 3H_2O \quad (3.\ 3)$$

$PANI^{m+}$ oxidizes Fe/Fe^{2+} to Fe^{3+}, while being itself reduced to $PANI^{0}$ (Equation 1). After the reaction with oxygen, $PANI^{0}$ gets oxidized back to $PANI^{m+}$ (Equation 2). Then, Fe^{3+} reacts with OH^{-} ions to form a hard, insoluble Fe_2O_3 oxide layer on the top of the CS surface. This oxide layer partially contributes to the corrosion protection of the underlying CS surface. This process occurs in a cyclic order for an entire period where the PANI layer remains active [216, 217]. On top of this partial corrosion protection offered by the iron oxide layer, the PANI layer itself also represents a barrier for penetration of corrosive ions to the CS surface, albeit to a smaller degree given its porous structure[169, 170]. However, this drawback can be improved by incorporating GO sheets into the PANI matrix to form “the labyrinth effect” [218], leading to better corrosion protection due to the improved compactness of the coating [191]. The impermeable graphene can retard the penetration of corrosive species by providing a tortuous diffusion path [219]. The addition of graphene also increases the electrical conductivity of the PANI layer by several orders of magnitude [220], enabling it to become charged; in the current case, the GO is negatively charged due to the presence of negatively-charged carboxylic groups on its surface, thus offering resistance to penetration of corrosive anions through the PANI coating to reach the CS surface[221]. Further, since the PANI and PANI/GO sub-layers are hydrophobic (Figure 2), additional barrier towards penetration of hydrated corrosive ions is enabled [222].

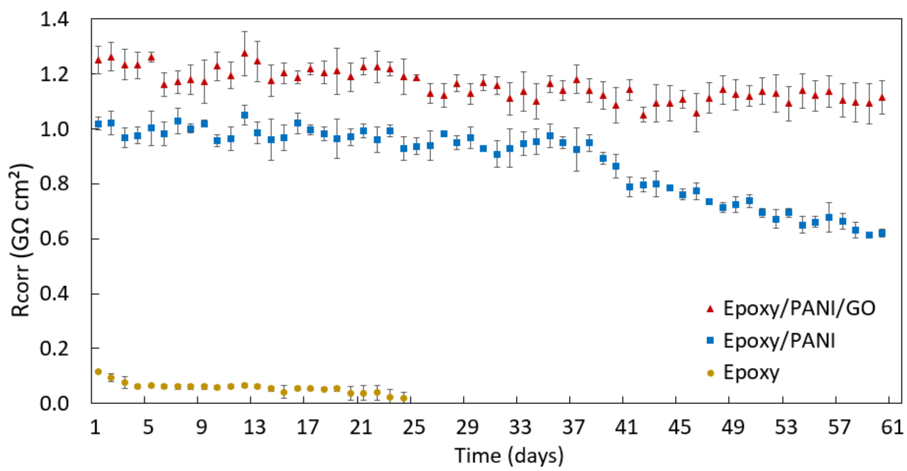

Fig 3. 7 Dependence of corrosion resistance on immersion time recorded at OCP by EIS and in 3.5 wt.% NaCl, for CS, coated with epoxy, and by the double-layer coatings of PANI/epoxy and PANI/GO/epoxy. The arrows indicate the appearance of the second time constant in the EEC (Fig 3. 6c) due to the formation of pores in the coating, which extend from the electrolyte to the CS/coating interface.

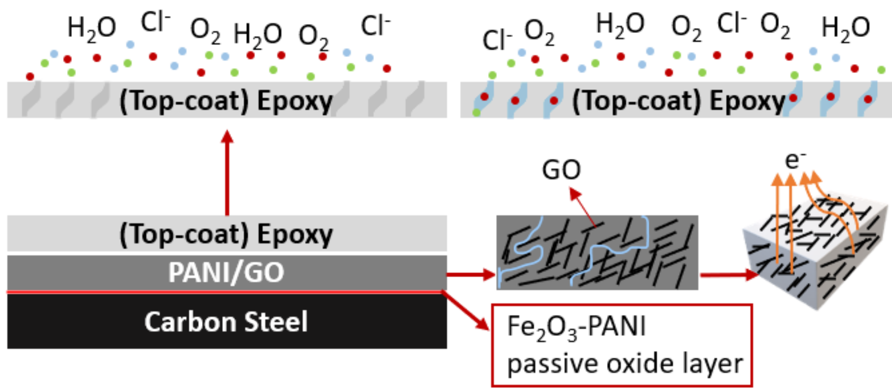

Fig 3. 8 Schematic depicting the corrosion protection mechanisms of the double-layer PANI/GO/epoxy coating formed on a CS surface.

3.5 Conclusions

Results on the development of a double-layer coating based on the inner PANI or PANI/GO layer and outer epoxy layer for long-term corrosion protection of CS surface 3.5 wt.% NaCl are presented. The PANI and PANI/GO composites were formed on the CS surface by *in-situ* electrochemical polymerization of aniline monomer. The neat epoxy resin was then applied on the top of the PANI and PANI/GO layer using an automated dip coater. The optimal GO concentration in the PANI layer was found to be 0.01 wt.%. Compared to the single-layer commercial epoxy coating, the double-layer PANI/GO/epoxy coating offered significantly better long-term anti-corrosive properties, maintaining its structural integrity over two months of constant exposure to the corrosive electrolyte. The excellent corrosion protection properties of the double-layer coating were prescribed solely to the presence of the underlying PANI/GO layer, which represents a high barrier for the transport of hydrated corrosive ions to the CS surface, through the combined action of charge (repulsion and iron oxide film formation), surface energy (hydrophobicity), and blocking mechanisms.

Acknowledgements

The authors would like to convey their gratitude to the Qatar National Research Fund (QNRF) under the QRLP postgraduate award granted to Mr. Ahmad Diraki, to the Natural Science and Engineering Council of Canada (NSERC), and to the Chemical Engineering Department at McGill University.

Funding

This work was supported by Qatar National Research Fund (QNRF) under QRLP postgraduate award and by the Natural Science and Engineering Council of Canada (NSERC).

3.6 Supplementary Information

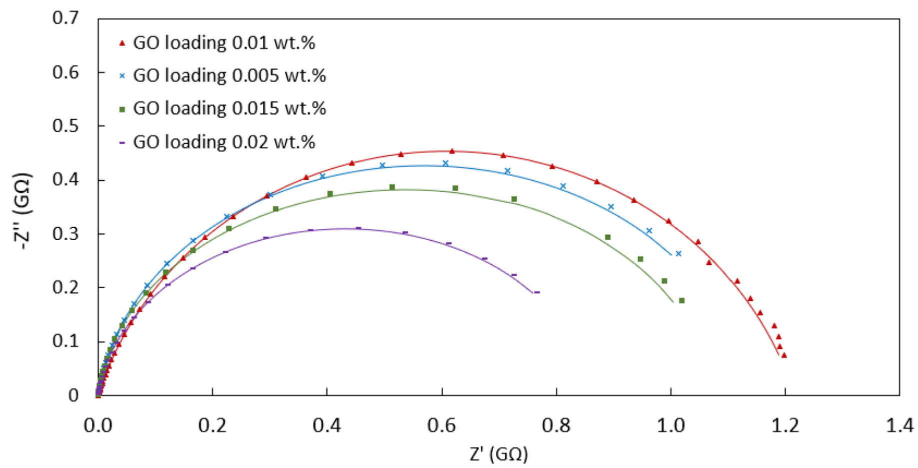

Fig. 3-S. 1 Nyquist plots of the CS surface coated by a double-layered PANI/GO/epoxy coating with a different loading of GO, recorded at OCP in 3.5 wt.% NaCl. Symbols represent the experimental spectra, while the solid curves represent the modelled spectra.

Chapter 4

Smart PANI/epoxy Anti-corrosive Coating for Protection of Carbon Steel in Sea Water

4.1 Preface

This chapter presents an article published in the journal *Progress in Organic Coatings*:

Ahmad Diraki, and Sasha Omanovic: Smart PANI/epoxy anti-corrosive coating for protection of carbon steel in sea water, *Progress in Organic Coatings* 168 (2022) 106835.

Ahmad Diraki (Ph.D. candidate) conceived the idea, planned and executed the experiments, analyzed the data, and drafted the manuscript. Prof. S. Omanovic supervised the work and reviewed and edited the manuscript.

Coated oil and gas pipelines are exposed to mechanical damages (scratches that could penetrate to the underlaying steel surface) during installation or maintenance. It is, thus, essential to address this issue by developing coatings of improved properties, which could respond in a way to alleviate the damage. In the first article (Chapter 3), the double-layer PANI-GO/epoxy coating showed excellent long-term corrosion protection performance, compared to the single-layer commercial epoxy coating. Nevertheless, the long-term corrosion protection performance will not be efficient once the coating is damaged, and the scratch reaches the metal surface. Therefore, it is of interest to further improve the properties of this coating by rendering it *smart*.

Consequently, the paper presented in this chapter reports and discusses the results of the electrochemical synthesis of a double-layer coating consisting of the inner electrochemically formed polyaniline layer on the surface of carbon steel, incorporating sodium caprylate (SC) and sodium dodecyl sulfate (SDS), followed by a top (outer) layer of neat epoxy. This *smart* coating was investigated in a saline solution for its ability to continue protecting the underlying CS surface after a scratch (damage) penetrating through the coating down to the CS surface was induced. Their hypothesis was that SC+SDS would be released into the scratch and adsorb on the exposed CS surface, thus continuing to protect it. Indeed, this double-layer PANI-SC+SDS/epoxy coating showed a quick smart response upon getting damaged and excellent long-term corrosion protection performance, approaching one of the undamaged coatings. In contrast, the anti-corrosive properties of the damaged *undoped* coating deteriorated very quickly (within hours) and continued to deteriorate with time.

Highlights

- A smart anti-corrosive double-layered polyaniline/epoxy coating was formed
- The PANI layer was doped with a caprylate anion and sodium dodecyl sulfonate
- Potential-driven SC-SDS release from PANI occurred upon inducing the scratch
- The coating restored its corrosion resistance within a day of inducing a scratch in it
- The restored corrosion resistance of the damaged coating was maintained for 29 days

Abstract

A double-layer coating composed of an inner polyaniline (PANI) and outer epoxy layer, was investigated as a potential “smart” coating for corrosion protection of carbon steel (CS) in an aqueous 3.5 wt.% NaCl. The PANI coating, incorporating an anion of sodium caprylate (SC) and sodium dodecyl sulfonate (SDS), was electrochemically synthesized directly on the CS surface. A layer of commercial epoxy was then applied on top of this PANI coating. It was determined that the SC-SDS-doped coating was able to almost completely recover its anti-corrosive properties, within one day upon creating the CS-surface-reaching damage (scratch) in it, sustaining the high level of corrosion protection for the remaining 29 days of constant exposure to the corrosive solution. On the other hand, the anti-corrosive properties of the damaged undoped coating deteriorated very quickly (within hours) and continued to deteriorate with time. The mechanism of “smart” protection of the doped coating was postulated to be through the release of the dopant (SC-SDS) from the PANI layer at the damaged coating site, driven by a potential difference between the reducing PANI layer and oxidizing (corroding) CS surface. This was followed by the adsorption of SC-SDS on the CS surface exposed to the electrolyte and its protection through the formation of a molecular SC-SDS layer offering a barrier for transport of corrosive species to the CS surface.

Keywords: Corrosion inhibitor, Smart Coatings, Polyaniline, Epoxy, Sodium caprylate, Sodium dodecyl sulfonate

4.2 Introduction

Corrosion is a global issue causing significant financial and sometimes even human losses. Aggressive corrosive environments limit the service life of various metal structures, causing a negative impact on a country's economy. In the petrochemical industry, where carbon steel is the most used metal, corrosion has been declared the primary mechanism for pipelines' failure, which causes safety, environmental, and economic problems. Generally, organic coatings are applied on the metal surface to form a barrier and isolate the surface from its surrounding corrosive environment. During the service, when the protective barrier coating is at risk of undetectable microcrack, the corrosive species can easily penetrate through the coating, reaching the substrate surface and causing degradation (corrosion) of the metallic parts [223].

To partially overcome this issue, anti-corrosion inhibitors can be incorporated into the coating to offer additional protection of the metal substrate when microcracks are formed in the coating [224-226]. In general, inhibitors form a molecular(s)-layer thick barrier film on the metal substrate, producing an efficient anti-corrosion performance [227]. In the last century, metal-based corrosion inhibitors were added to coatings to enhance their anti-corrosion performance [228]. However, these heavy metals would be released into the surrounding environment over time, causing severe environmental toxic pollution [229]. To overcome these issues, alternative approaches to creating new coating materials and incorporating inhibitors have become attractive. One such technique is using electrically conductive polymers (CPs) as possible anti-corrosive coatings; CPs are not toxic, they have good stability, surface adhesion, and corrosion-resistant properties [230-232].

Polyaniline (PANI) is a CP formed by the repeated connection of aniline monomers [233]. PANI has different oxidation and reduced states. These states can switch under specific conditions when there is a change in local potential on the metal surface due to corrosion or other mechanical factors. This, in turn, could enable PANI to release dopants incorporated in its bulk structure during its synthesis. These dopants could be corrosion inhibitors, thus enabling a PANI-based anti-corrosive coating to act as a "smart" coating by releasing an inhibitor molecule at the damaged site (crack in the coating) to inhibit the corrosion of the exposed part of the metal surface [234-238]. This inhibitor release can be triggered by several factors (potential, pH, temperature, etc.). For example, Wang et al. [239] grafted PANI onto the surface of mesoporous silica spheres loaded with doxorubicin. A pH-responsive release of doxorubicin was reported to the presence of PANI. This exceptional feature of PANI has made it a promising material applied to smart coatings.

In our previous report [240], we showed that by applying a commercial epoxy anti-corrosive coating onto a thin (5 μm) PANI coating formed directly on the carbon still surface, a significant increase in the anti-corrosive properties of the double-layer coating can be achieved over long-term exposure to the corrosive electrolyte, in comparison when the epoxy was deposited directly onto the carbon steel surface. During the two-month exposure period, no pores/cracks in the double-layer coating containing 0.01wt.% graphene oxide in the PANI layer was recorded. However, in real applications, the exposure time should be significantly longer, possibly resulting in chemical degradation of the produced double-layer coatings and their possible mechanical damage, enabling the penetration of the aggressive electrolyte through the damaged coating, ultimately resulting in corrosion of the underlying carbon steel structure. To address this, at least to a certain extent, we have attempted to design a "smart" PANI/epoxy coating by incorporating a corrosion inhibitor, sodium caprylate (SC) and also sodium dodecyl sulfonate (SDS) into the PANI layer during its synthesis. The corrosion resistance of the doped coatings (as produced and "damaged") was evaluated by electrochemical impedance spectroscopy (EIS). Long-term immersion tests were performed to study the release of the corrosion inhibitor over 30 days when a scratch (penetrating the carbon steel substrate) in the coating was induced. All corrosion tests were conducted in 3.5 wt.% NaCl aqueous solution at room temperature.

4.3 Experimental

4.3.1 Materials

All reagents were of the AR grade and used as received from the suppliers. The aqueous solutions were prepared with ultrapure water (18 MΩ cm). The aniline monomer ($C_6H_5NH_2$, ACS reagent grade, ≥99.5%) was bought from Sigma-Aldrich (Missouri, USA). Sodium caprylate (98%) was used as a corrosion inhibitor, and oxalic acid (98%, anhydrous) used in the electrolyte preparation was purchased from Acros organics (USA). Sodium dodecyl sulphate (SDS), sodium chloride (certified ACS), denatured ethanol (95% EA), and acetone (Certified ACS) were purchased from Fisher Scientific (USA). HELOXY™ Modifier 48 epoxy resin (epoxide equivalent weight = 138-154 g/eq), and EPIKURE™ curing agent 3388 (amine value as KOH 260-285 mg/g) were purchased from Hexion Inc. (Ohio, USA). G1117 low carbon steel (CS) acquired from McMaster-Carr (USA) with a chemical composition presented in Table 4. 1 was used as a substrate for corrosion testing.

Table 4. 1 The chemical composition of low-grade carbon steel G1117.

Carbon steel G11117 compositions	
Element	**Wt.%**
C	0.14 – 0.20
Mn	1.00 – 1.30
P	0.00 – 0.04
S	0.08 – 0.13
Fe	Balance

4.3.2 Instrumentation

An AUTOLAB Potentiostat/Galvanostat/FRA PGSTAT 30 was used for electropolymerization and corrosion tests. This system was interfaced with a computer to control the experiments, and the data were acquired and analyzed using NOVA 2.1 software. A conventional three-electrode electrochemical cell consisted of a conductive graphite rod as the counter electrode, a saturated calomel electrode as reference electrode (SCE), and a coated/uncoated carbon steel sample as the working electrode was used in all measurements. A programable dip coater (1-200 mm/min)-PTL-MM02 was used to apply epoxy coatings on the carbon steel sample. The surface morphology of the samples was observed using a field-emission scanning electron microscope (Hitachi FE-SEM SU3500). Fourier transform infrared spectroscopy (FTIR)-(ATR) was performed using a Nicolet iS50 ATR Thermo Scientific spectrophotometer. Adhesion of the coatings to the CS surface was evaluated employing the ASTM D3359 test. Profilometer Dektak XT-Bruker was used to determine the coatings film thickness. Goniometer (FSA OCA 15EC)-Data-Physics was employed to evaluate the material surface wettability. Polishing machine MetaServ-3000 and Branson-1510 ultrasonic water bath was used for sample preparation.

4.3.3 Sample preparation

A carbon steel (CS) metal rod was machined to a diameter of 1.59 cm and cut into coins with a thickness of 3.3 mm. A Teflon holder was used to hold the sample when immersed in the electrolyte, leaving a metal area of 1.039 cm^2 exposed to the electrolyte (one side of the sample). Before undergoing the coating-application process, the samples were adequately pre-treated. Namely, the CS surface was wet-polished using a 600-silicon carbide grit paper for 2 minutes on the rotation speed of 200 rpm. Then, the sample was ultrasonicated in ethanol for 5 minutes to remove the polishing residue. Finally, the substrate was rinsed with acetone to degrease its surface and dried with an argon stream.

4.3.4 Preparation of the coatings

In this study, two different coatings were formed on the CS surface: (1) a double-layer PANI and epoxy coating, and (2) a double-layer PANI/epoxy coating with corrosion inhibitor (SC-SDS) incorporated into the PANI layer.

4.3.4.1 Polyaniline (PANI)

PANI coatings were electrochemically synthesized on carbon steel (CS) samples in a 100 ml aqueous solution containing 0.1 M aniline monomer and 0.2 M oxalic acid. The electrochemical synthesis was carried out by cyclic voltammetry (CV) at a scan rate of 10 mV s^{-1} over 10 cycles. The experimental conditions were chosen based on published literature [189, 190]. Multiple experiments were performed within different potential regions to optimize the electropolymerization potential range while keeping other parameters constant. The optimum potential range was determined to be from -0.6 and 1.6 V. Upon completing the electropolymerization process. The electrode was removed from the electrolyte solution, rinsed with deionized water, dried with argon gas, then kept at room temperature (cured) for 72 hours before performing corrosion tests or further depositing epoxy on top of this PANI coating.

4.3.4.2 Polyaniline doped with corrosion inhibitor

Sodium caprylate (SC) was used as a corrosion inhibitor for carbon steel (CS) in this work [241]. However, our other study (publication in preparation) showed that corrosion inhibition efficiency could be increased when SC is mixed with a small amount of sodium dodecyl sulphate (SDS). Therefore, the PANI coating used in the current work was also doped with a mixture of SC and SDS. PANI doped with SC-SDS was synthesized following the same procedure outlined above for the pure polyaniline coating. The concentration of SC and SDS in the solution containing the aniline monomer was 40 mM and 5 mM, respectively. Before forming the PANI coating, the aniline-SC-SDS solution was stirred for 1 hour with brief ultrasonication to improve the homogeneous composition of the electrolyte.

4.3.4.3 Epoxy coatings

Commercially available epoxy resin was a HELOXY™ Modifier 48, and the curing agent was EPIKURE™ 3388. Both compounds were clear, transparent, and contained no additional additives. For the preparation of epoxy coatings, the epoxy resin and curing agent volume ratio was 1:2, and the calculated amount was mixed for 5 minutes, then sonicated for 1 minute. The coatings were deposited on the CS substrate by a dip-coater to ensure the coating uniformity and reproducibility, with a withdrawal speed of 4 mms^{-1}. The sample was then placed for curing at 22±1°C for 7 days. The curing time and temperature were applied following the manufacturer's recommendation for optimum adhesion and mechanical properties. Although the manufacturer recommends the epoxy/curing agent ratio to be 1:1 for the optimum corrosion barrier protection, we decided to double the balance of the curing agent over the epoxy resin to increase the number of defects and cracks within the epoxy-coated layer, which will reduce the epoxy coating corrosion resistance [242, 243]. This allowed us to more conveniently evaluate the corrosion inhibitor release and the “smart” properties of the coating.

4.3.5 Corrosion measurements

Electrochemical/corrosion measurements were carried out in an aqueous 3.5 wt.% NaCl. Electrochemical impedance spectroscopy (EIS) was used to investigate the corrosion resistance of the damaged and undamaged samples. Before each EIS run, the samples were conditioned at open-circuit potential (OCP) for 1 hour. EIS measurements were performed at OCP in the frequency range between 10 mHz and 50 kHz, applying a ±10 mV alternating voltage amplitude. All potentials in this paper are referred to SCE. All the measurements were performed at 22±1ºC.

4.3.6 Surface characterization

Coatings' surface morphology was studied by field-emission scanning electron microscopy. To confirm the chemical composition of the PANI/SC-SDS coating, Fourier transform infrared spectroscopy (FTIR)-ATR was recorded in the region between 4000 and 400 cm^{-1} wavenumbers, employing 64 scans at a resolution of 2 cm^{-1}. The thickness mapping of different coatings was evaluated and analyzed by a profilometer. A step between the CS surface and the coatings was produced by masking portions of the substrate during coating deposition. Water contact angle measurements examined the surface wettability with a drop shape analyzer, in which the image analysis software reported the contact angle (Θ). The contact angles were generated between the coated/uncoated surface and deionized water drops with a dosing rate of 0.5 µL/s and a dosing volume of 5 µm. The coatings' adhesions on the CS substrates were determined following the ASTM D3359 standard tape adhesion test [192].

4.4 Results and discussion

4.4.1 Physical characterization of the coatings

The scanning electron microscopy (SEM) of the uncoated and coated carbon steel surfaces are presented in Fig 4. 1. The freshly prepared CS surface Fig 4. 1(a) is characterized by the appearance of scratches produced by mechanical polishing. On the other hand, the PANI-coated CS surface Fig 4. 1(b) is nonhomogeneous and is characterized by clews comprised of the interconnected network of fibrils. Surprisingly, a less smooth surface of the PANI coating was obtained when SC and SDS were incorporated into the coating Fig 4. 1(c). The fibers are inlaid and interlaced with each other. However, the doped coating still shows uniformly distributed surface structures, indicating that SC-SDS has good dispersion and compatibility with the PANI matrix [244]. Fig 4. 1(d) presents the morphology of the neat epoxy coatings deposited on the CS substrate, and the coating is characterized by a smooth surface without visible pores under 110X magnification. Fig 4. 1(e) presents the blade scratch made in the doped PANI/epoxy coating to simulate the formation of pores/cracks in the coating by its long-term exposure to the corrosive environment (chemical degradation and change in physiochemical properties) and/or physically induced damage.

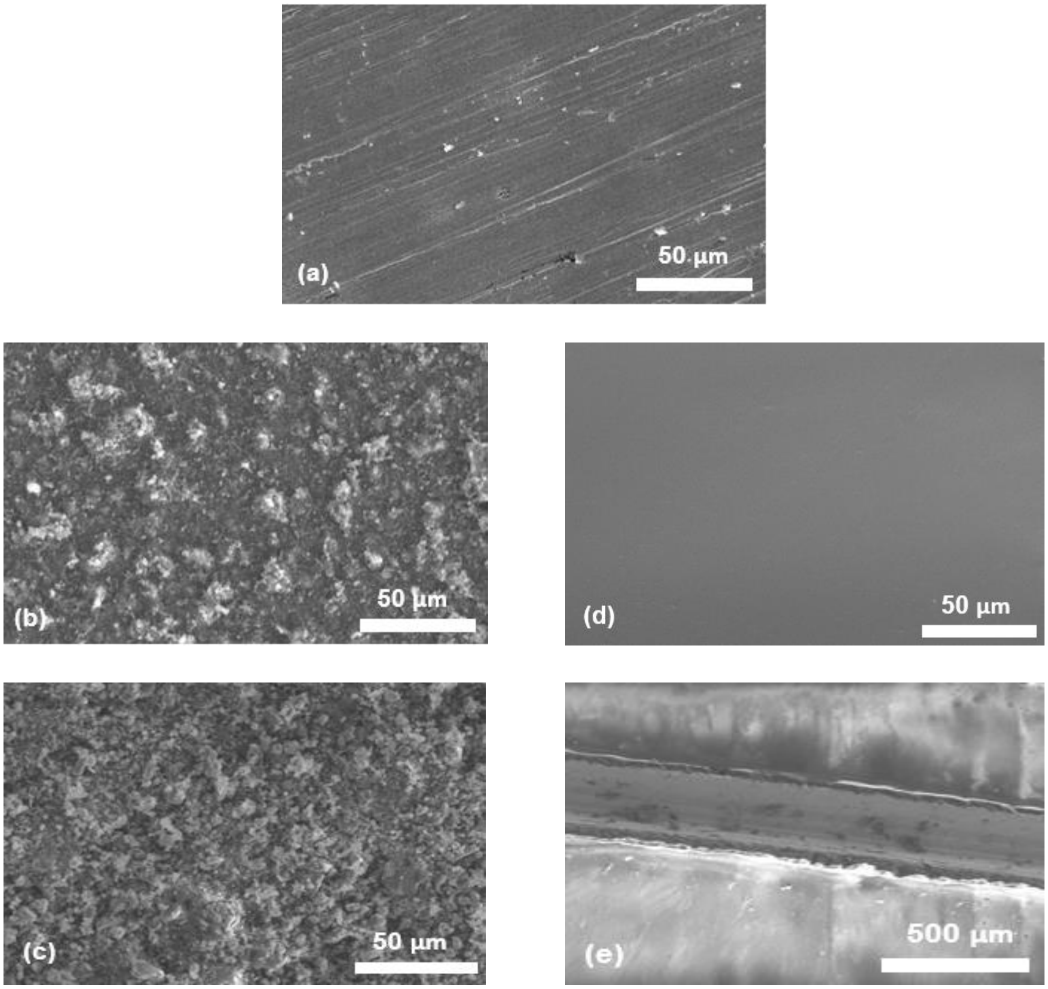

Fig 4. 1 SEM micrographs obtained on coated and uncoated CS surface: (a) freshly polished uncoated carbon steel sample; (b) synthesized PANI on CS surface ;(c) PANI doped with CS-SDS; (d) neat epoxy resin coatings; (e) damaged coating.

Fig 4. 2 presents the FT-IR (ATR) spectra of a pristine PANI film, and a PANI/SC-SDS coating deposited on a CS surface. The broadband between around ~3246 cm^{-1} and 3257 cm^{-1} on the PANI spectrum shown in Fig 4. 2 (curve *a*) is attributed to the N-H stretching vibration due to the protonation of nitrogen [196-198]. The C=C stretching vibrations of quinoid and benzenoid rings are confirmed by the bands at ~1581 cm^{-1} and ~1497 cm^{-1} [196, 197], respectively. The band at ~1300 cm^{-1} can be assigned to the π-electron delocalization induced in the polymer through protonation, while the band at ~1248 cm^{-1} corresponds to the C-N stretching vibration of secondary aromatic amine [199]. The band at ~1146 cm^{-1} is assigned to the plane bending vibration of C-H which is formed during the protonation, and it is described as the electronic-like band and considered to be a measure of the degree of delocalization of electrons of PANI [135, 197, 198]. The band at ~817 cm^{-1} is assigned to a C-H out-of-plane bending vibration of aromatic rings [200]. The presence of these distinct vibrations on the recorded spectrum is characteristic of the emeraldine salt form of polyaniline [197-199, 201].

On the other hand, the FT-IR spectrum of the PANI doped with SC-SDS, presented in Fig 4. 2 (curve *b*) shows alteration in the characteristic vibrations and appearance of the vibrations due to the incorporation of SC and SDS into the PANI coating. Thus, the vibrations at ~1062 cm^{-1} and ~737 cm^{-1} can be assigned to the S=O and S-O stretching vibrations of the SDS sulphonate group, respectively, indicating that SDS is incorporated into the PANI coating [245, 246]. The intensity of this vibration, relative to those of the PANI, is small due to the relatively low amount of SDS in the PANI coating. The vibration at 1690 cm^{-1} is characteristic of the -C=O group in the SC [247-250], thus confirming the SC is also successfully incorporated into the PANI coating. The differences in intensities of vibrations between PANI and PANI/SC-SDS and the shift of peaks after the formation of PANI/SC-SDS (compare curves *a* and *b* in Figure 2) is potentially due to the differences in the protonation level and oxidation level or to the change in stability of the conjugated system due to the interaction between the PANI and SC-SDS [251].

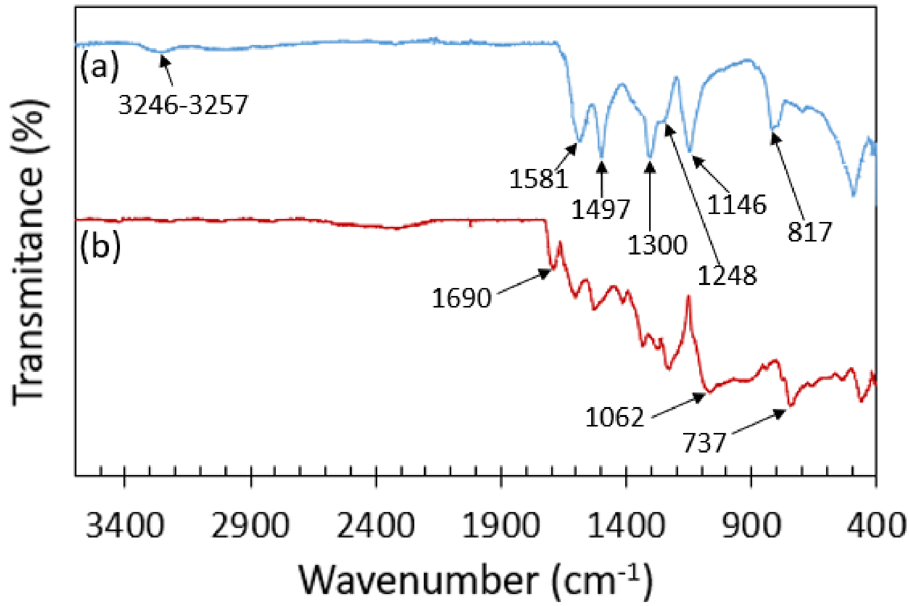

Fig 4. 2 FT-IR (ATR) spectra of (a) a pristine PANI coating formed on the CS surface; and (b) of a PANI coating doped with CS-SDS, on the CS surface.

Profilometry measurements revealed that the thickness of the PANI and PANI/SC-SDS coatings was 5.4±0.1 µm, while the epoxy coating was substantially thicker, 25.2±0.5 µm, and the double layers coating thickness was 30.6±0.15 µm. These values agree with the values obtained by examining the cross-sectional SEM images of the coatings presented in our other paper [240].

One of the desired features of anti-corrosive coatings is their increased surface hydrophobicity [204]. Since the epoxy coating was the top coating employed in this research, its hydrophobicity was compared to that of the bare CS surface. The influence of the presence of a scratch in the coating was studied for the doped and undoped coating, and the results are presented in Fig 4. 3. The contact angle value sharply increased from 49.7±0.2º for the uncoated CS surface, Fig 4. 3(a), to 66.0±0.4º for the CS surface coated by the undoped coating, Fig 4. 3(b), which was to expect given a certain degree of hydrophobicity of epoxy. However, when the undoped coating was scratched, the contact angle decreased significantly Fig 4. 3(c). On the other hand, the contact angle of the doped coating is 88.9±0.5º, Fig 4. 3(d), and when the coating was damaged, the contact angle decreased to 76±1º, Fig 4. 3(e).

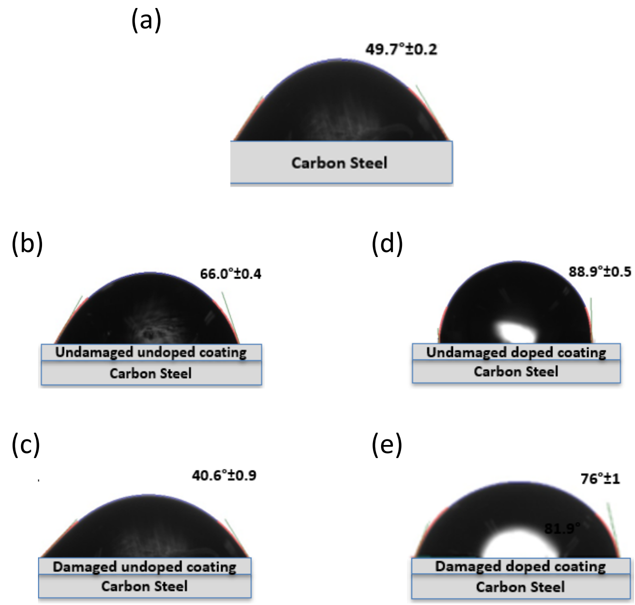

Fig 4. 3 The contact angle between the deionized water drops and the surface of; (a) the as-polished CS; (b) the freshly prepared undamaged PANI/epoxy coating; (c) the damaged (scratched) undoped coating; (d) the freshly prepared undamaged SC-SDS-doped PANI/epoxy coating; (e) the surface of the SC-SDS-doped PANI/epoxy coating.

Adhesion of coatings to the substrate is an essential factor influencing the long-term performance of coatings [206, 207]. To examine the adhesion of PANI, PANI-epoxy, and PANI/SC-SDS/epoxy coatings on the CS substrate, the ASTM D3359 standard tape test was performed. It was determined that all the coatings adhered to the substrate well, yielding the adhesion remaining (AR%) values between 95% to 98% (percentage of non-failed regions). Thus, it can be concluded that the presence of SC-SDS in the inner PANI layer or the presence of the top epoxy layer does not influence the adhesion of the PANI layer to the SC surface.

4.4.2 Anti-corrosive properties of the coatings – electrochemical measurements

Proportional corrosion studies were conducted for the damaged undoped PANI/epoxy coating (control 1), and for the CS samples coated with the SC-SDS-doped PANI/epoxy coating. Because of the PANI's relatively good electrical conductivity, CS samples coated with only the doped and undoped PANI layer could not be instigated using the EIS technique.

4.4.2.1 Short-term experiments

EIS is an effective electrochemical method to investigate the protective ability of anti-corrosive coatings. To examine the influence of SC-SDS inhibitor incorporated into the PANI layer in the double-layer PANI/epoxy coating applied on a CS surface, the coating was scratched (all the way to the CS surface, Fig 4. 1(e) and EIS measurements in the presence and absence of SC-SDS in the coating were performed, initially over a short period of exposure of the samples to the corrosive electrolyte, and then during long-term exposure.

Fig 4. 4(a) shows the Nyquist spectra of the undamaged undoped PANI/epoxy coating. The spectra is characterized by the presence of one time constant, indicating the absence of pores in the coating (which would require a two-time-constant EEC to be used) [252]. Consequently, the equivalent electrical circuit (EEC) presented in Fig 4. 5(a) was used to model the spectra. In this EEC, R_{el} represents the solution resistance between the reference electrode and the working CS electrode, and the CPE_1 and R_1 represent the pseudo-capacitive and barrier/resistance response of the coating, respectively. In this case, the resistance also represents the resistance of the coated CS surface to corrosion, R_{corr}. The corresponding EEC parameter values are listed in Table 4. 2, and the schematic of the system is presented in Fig 4. 5(a') (note that there is no SC-SDS incorporated in the PANI layer for the undoped coating, as shown in the schematics). Instead of pure capacitance, a constant-phase-element (CPE) was used, which is due to the heterogeneity (in terms of surface charge distribution and morphology) of the surface studied [253]. The excellent agreement between the EEC model (lines) and the experimental data (symbols) in Fig 4. 5(a) indicates the applicability of the proposed EEC model. However, when the coating was damaged, the EIS response of the system significantly changed, as seen in Fig 4. 4(b). First, the spectra indicate the presence of two-time constants and, second, the diameter of the semicircles decreased significantly with respect to that one in Fig 4. 4(a). Taking that the diameter of the semicircle can be related to the overall corrosion resistance, the trend in Fig 4. 4(b) shows that upon damaging the coating, the corrosion resistance significantly decreased (as expected). The result in Fig 4. 4(b) also shows that a further decrease in corrosion resistance occurred with an increase in immersion time, indicating acceleration of the CS corrosion due to the presence of scratch in the coating. This control experiment, performed over a short exposure time, demonstrates that the damaged PANI/epoxy coating is not capable of 'self-healing.' In fact, the decrease in corrosion resistance with time indicates progressive deterioration of protective properties of the coating (long-term experiments presented later in the paper also confirmed this).

To quantitatively evaluate the behaviour in Fig 4. 4(b), the EIS spectra were modelled using the electrochemical equivalent circuit (EECs) presented in Fig 4. 5(b). In this EEC, the outer CPE_1-R_1 time constant represents the response of the pores in the coating (macropores and the induced scratch) in terms of their pseudo-capacitance (CPE_1) and resistance (R_1), the inner CPE_2-R_2 time constant represents the response of the double layer and charge-transfer resistance at the electrolyte/CS surface (the exposed part of the surface), respectively, while the inductivity, L, can be related to the impedance response of corrosion intermediates formed on the exposed part of the CS surface [215]. The sum of the two resistances, $R_1 + R_2$, represents the total resistance to corrosion, R_{corr}. Fig 4. 4(b) shows that the agreement between the employed EEC model (solid line) and the experimental data (symbols) is very good, thus validating the use of the EEC in Fig 4. 5(b) in describing the impedance response of the system studied. The EEC parameter values obtained by fitting the spectra in Fig 4. 4(b) are presented in Table 4. 2. It is seen that only after 15 minutes of exposure to the corrosive electrolyte, the corrosion resistance of the damaged coating dropped by ca. 91% relative to the resistance of the undamaged coating. Prolonged exposure of the damaged coating to the electrolyte induced further deterioration of the performance, and after 2 hours of exposure, the corrosion resistance dropped by ca. 96% relative to that one measured after 15 min of exposure (or by 99.6% relative to the corrosion resistance of the undamaged coating), evidencing the fast acceleration in corrosion of the CS surface. At the same time, CPE values increased. Both trends point towards the increase in surface area of CS exposed to the electrolyte, probably due to the penetration of the electrolyte under the coating (between the CS surface and the coating) at the point of its damage, as illustrated by the schematics in Fig 4. 5(b').

The incorporation of SC-SDS into the PANI layer resulted in a significant change in the PANI/epoxy coating impedance behaviour. The impedance of the undamaged coating (Fig 4. 6, red triangles) significantly increased relative to that one recorded for the undamaged coating that was not doped with SC-SDS (Fig 4. 4(a)). However, the incorporation of the inhibitor into the PANI layer did not result in the appearance of new time constants; consequently, the EEC in Fig 4. 5(a) was used to model the EIS spectra of the undamaged doped PANI/epoxy coating, the schematics of which is presented in Fig 4. 5(a'). The excellent agreement between the EEC model (lines) and the experimental data (red triangles) in Fig 4. 6 indicates the applicability of the proposed EEC model. The corresponding EEC parameter values are listed in Table 4. 3. By comparing the values for the undamaged doped (Table 4. 3) and undoped (Table 4. 2) coatings, it can be seen that a significant increase (by a factor of ca. 37) in corrosion resistance of the coating was achieved as the result of the presence of SC-SDS in the PANI layer. This is in agreement with the results in Fig 4. 3, which show that the doped coating is significantly more hydrophobic, thus representing a more efficient barrier for the transport of hydrated corrosive species.

However, Fig 4. 6 shows that after scratching the doped coating, the impedance first decreased, but then gradually started to recover (increase). The one-time constant EEC in Fig 4. 5(a) could not fit the EIS spectra of the damaged coating well, and the two-time-constant EEC model, presented in Fig 4. 5(c), was used. In this EEC, the outer CPE_1-R_1 time constant represents the EIS response of the scratched part of the coating, while the inner CPE_2-R_2 time constant represents the response of the CS surface exposed to the electrolyte, i.e. double layer and charge-transfer resistance, respectively [215]. The agreement between the model (lines) and experimental data (symbols) in Fig 4. 6 indicates the applicability of the EEC proposed in modelling the EIS response of the damaged coating, and the EEC parameter values are listed in Table 4. 3. The table shows that upon exposing the damaged coating to the corrosive electrolyte, the corrosion resistance dropped by ca. 63%, and the values of CPEs increased significantly, relative to the response of the undamaged coating, both indicating the exposure of the underlying CS surface to the electrolyte and acceleration of corrosion of the surface (Fig 4. 5(c')). However, unlike with the undoped coating (Fig 4. 4, Table 4. 2), the corrosion resistance of the damaged SC-SDS-doped coating increased over time (Fig 4. 6, Table 4. 3), while the CPE values decreased. This indicates a gradual improvement in corrosion resistance. Indeed, after four hours of immersion, the corrosion resistance of the damaged coating almost completely recovered, reaching a value very close to that of the undamaged coating (Table 4. 3). On the other hand, the CPE values, although decreased with time, did not reach those for the undamaged coating, which can be explained based on the difference in corrosion protection of the undamaged coating (pure blocking of the corrosive species penetration) and the damaged coating (protection of the exposed CS surface by adsorbed SC-SDS). Indeed, the results in Fig 4. 6 and Table 4. 3 indicate that CS-SDS were released with time from the PANI layer to protect the scratch-exposed CS surface (see the schematics in Fig 4. 5(c'), indicating that the designed coating can act as a smart coating [226, 237, 238, 254].

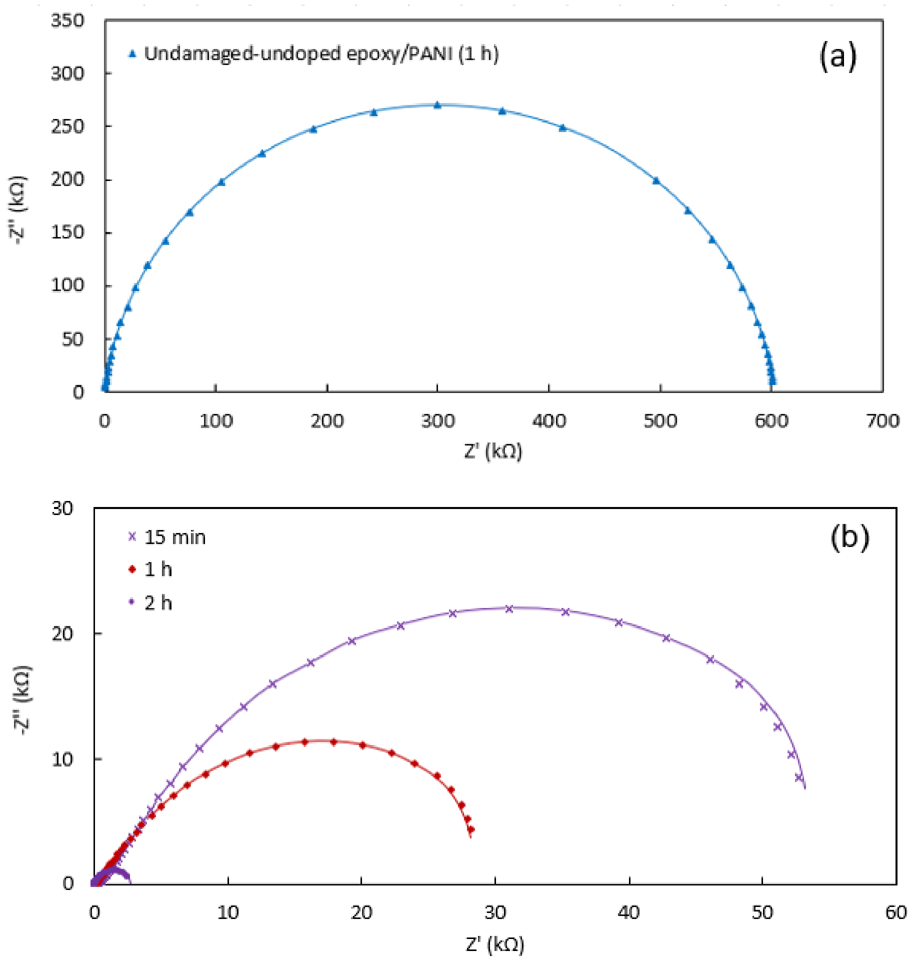

Fig 4. 4 EIS spectra of (a) the undoped undamaged epoxy/PANI coating recorded after 1h, and (b) the undoped damaged coating recorded after 15 minutes, 1h, and 2h of immersion in 3.5 wt.% NaCl at OCP. Symbols represent the experimental values, while the solid curves represent modelled spectra.

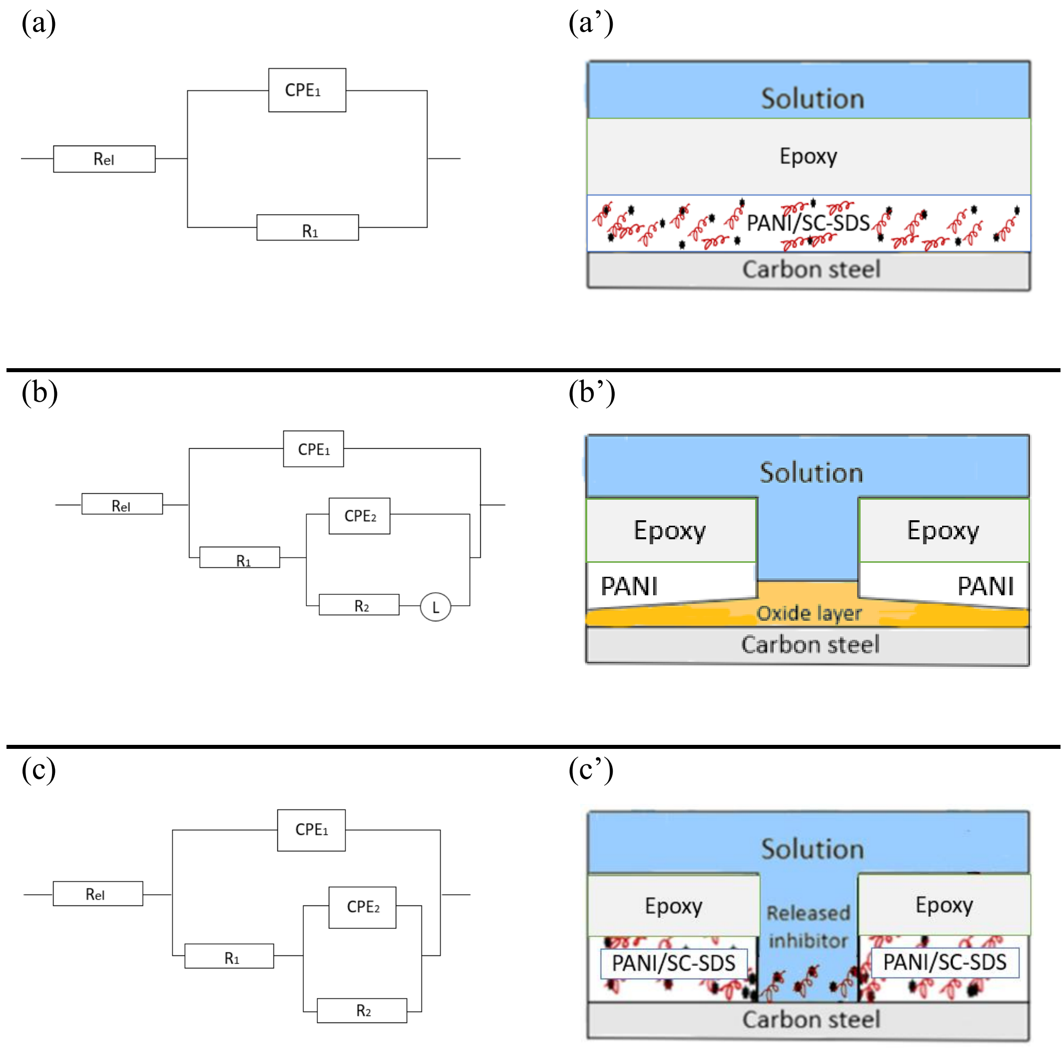

Fig 4. 5 EEC models and the corresponding schematics of the coating/CS interface, used to fit EIS of (a, a') the undamaged coatings (both doped and undoped); (b, b') damaged undoped coating; (c, c') damaged SC-SDS- doped coating.

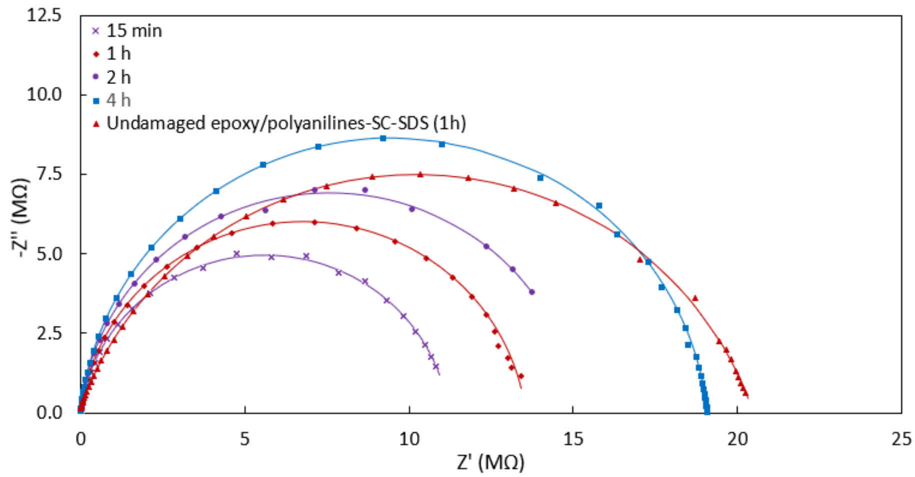

Fig 4. 6 EIS spectra of the undamaged doped coatings with SC-SDS recorded after 1h. The spectra of the damaged coating recorded after 15 minutes, 1h, 2h, and 4h of immersion in 3.5 wt.% NaCl, at OCP. Symbols represent the experimental values, while the solid curves represent the modelled spectra.

Table 4. 2 EEC parameter values were obtained by modelling the EIS spectra recorded on the damaged undoped coating.

Immersion time	R_{el} (Ω cm^2)	R_{corr} (Ω cm^2)	L (H)	CPE_1 (Ω^{-1} cm^{-1} s^n) x 10^6	CPE_2 (Ω^{-1} cm^{-1} s^n) x 10^6
Undamaged-undoped epoxy/PANI	432±31	(6.1±0.3) x10^5		7.9±0.3 (n=0.95±0.02)	
15 minutes	285±64	(54.7±0.9) x10^3	4.8±0.3	8.8±0.9 (n=0.81±0.04)	6.2±0.8 (n=0.85±0.03)
1 h	99±19	(27.2±0.7) x10^3	2.1±0.1	9.1±0.3 (n=0.89±0.03)	8.9±0.5 (n=0.88±0.08)
2 h	14±7	(2.3±0.3) x10^3	0.1±0.1	12.3±0.3 (n=0.92±0.01)	11.8±0.6 (n=0.93±0.03)

Table 4. 3 EEC parameter values were obtained by modelling the EIS spectra recorded on damaged doped coating with SC-SDS.

Immersion time	R_{el} (Ω cm^2)	R_{corr} (Ω cm^2)	CPE_1 (Ω^{-1} cm^{-1} s^n) x 10^6	CPE_2 (Ω^{-1} cm^{-1} s^n) x 10^6
Undamaged epoxy/PANI/SC-SDS	3940±40	(22.5±0.2) x10^6	0.5±0.3 (n=0.91±0.04)	
15 minutes	2275±83	(8.4±3.9) x10^6	7.6±0.9 (n=0.79±0.09)	6.3±0.8 (n=0.77±0.08)
1 h	3157±49	(13.5±2.9) x10^6	4.9±0.7 (n=0.80±0.07)	3.2±0.7 (n=0.82±0.05)
2 h	3641±51	(14.8±3.2) x10^6	1.5±0.4 (n=0.81±0.04)	1.3±0.5 (n=0.84±0.03)
4 h	3769±31	(19.2±1. 5) x10^6	1.8±0.2 (n=0.82±0.03)	0.9±0.1 (n=0.85±0.02)

4.4.2.2 Long-term corrosion study

The results in Fig 4. 7 demonstrate that the SC-SDS-doped PANI/epoxy coating can act like a ‘smart’ coating over a short period (four hours). However, its long-term corrosion protection would be crucial for potential practical use. Namely, the above results showed that SC-SDS can be released relatively quickly to ‘re-seal’ the damaged (CS-exposed) site, but given the finite amount of SC-SDS in the PANI layer and a possibility of SC-SDS to desorb from the ‘naked’ SC surface and diffuse through the crack in the coating into the bulk corrosive electrolyte, the protection of the damaged coating could decline over time. To investigate this, the influence of immersion time of the damaged coating on its corrosion protection performance was quantified using the EIS technique over 30 days of constant immersion in 3.5 wt.% NaCl solution, which was replaced with a fresh one every 24 hours. The EIS spectra were recorded every 4 hours in the entire frequency region specified previously in the paper and were then modelled using the EECs in Fig 4. 5. The variation of corrosion resistance obtained by modelling is presented in Fig 4. 7.

If we first analyze the behaviour of the damaged undoped PANI/epoxy coating (inset to Fig 4. 7, we can see that the corrosion resistance of the coating quickly decreased with time. Thus, after four days of immersion, the corrosion resistance fell from 610kΩcm^2 (the undamaged coating) to only 0.723kΩcm^2. On the other hand, when the SC-SDS-doped coating was damaged, the corrosion resistance also decreased, from 22.5 to 8.4 MΩcm^2 after 15 minutes of immersion, but it then gradually increased. After one day of immersion, it reached a value close to that one recorded for the undamaged coating (Fig 4. 7, red line). Surprisingly, the corrosion resistance then remained constant over the remaining 29 days of immersion. The trend in Fig 4. 7, thus, evidences that once the SC-SDS was released from the PANI layer to 're-seal' the damaged site (most likely by adsorbing on the naked SC surface), it remained on the SC surface for the remaining period of exposure, indicating that it chemisorbed, rather than physiosorbed, on the CS surface; the latter would result in desorption of SC-SDS and its diffusion into the bulk of the electrolyte through the scratch in the coating. Given the finite amount of SC-SDS in the PANI layer, the constant desorption of SC-SDS from the CS surface and its replenishment by the fresh SC-SDS released from the PANI layer would diminish with time, and thus also the coating's corrosion resistance, which is not seen in Fig 4. 7 during the first one month of testing. This indicates that the coating can perform as a 'smart' coating for an even more extended time; however, more measurements under different conditions (variable sheer fluid stress, pH and temperature changes, to name a few) should be performed to validate this assumption.

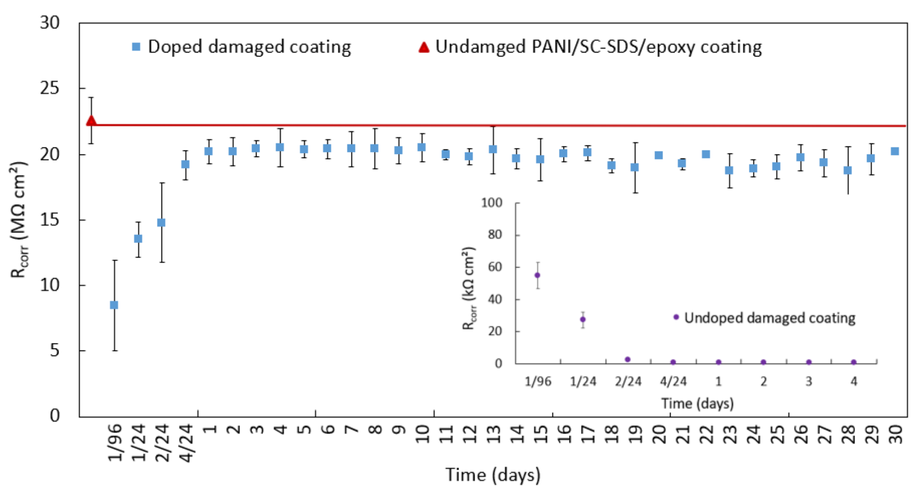

Fig 4. 7 The trend of corrosion resistance values with time during the immersion of the damaged SC-SDS-doped (main plot) and undoped (inset) PANI/epoxy coating in 3.5 wt.% NaCl The red triangle symbol and the red horizontal line represent the corrosion resistance of the undamaged SC-SDS-doped PANI/epoxy coating. The values were obtained from EIS measurements recorded at open circuit potential.

The mechanism of the PANI/epoxy "smart-coating" action can be explained in the following way. During the electrochemical synthesis of the PANI layer [88, 255-258], the sodium caprylate anion and SDS get incorporated into the PANI layer as dopants, and the PANI layer is in its oxidized state [88, 255-258]. When cracks appear in the PANI/epoxy layer, protruding to the coating/CS interface, the corrosive electrolyte penetrates through the crack to the CS surface, which starts corroding. This anodic (corrosion) process is accompanied by the cathodic reduction of PANI (which acts as a cathode) [88, 255-258]. During the reduction of PANI, the change in its charge is compensated by the release of the negatively-charged SC-SDS into the surrounding electrolyte that penetrated into the crack. The released SD-SDS adsorbs on the CS surface and 'insulates' it from the corrosive electrolyte, thus decreasing its corrosion rate [258-260]. Due to the decrease in corrosion rate, the reduction of PANI also decreases, and thus also the release of SC-SDS, rendering the behaviour of the coating as "smart and controlled inhibitor release".

4.5 Conclusions

The corrosion protection performance of a thin (30.6±0.15 µm) double-layered coating based on the inner PANI layer doped with SC-SDS and the outer epoxy layer, was studied for a short and long period in aqueous 3.5 wt.% NaCl. The PANI was formed directly on the carbon steel (CS) surface by *in-situ* electrochemical polymerization of aniline monomer, and SC-SDS was incorporated into this layer during its formation. The neat epoxy resin was then applied on the top of the SC-SDS-doped PANI layer using an automated dip coater. The doped coating yielded a hydrophobic surface and good adhesion to CS. When damaged to allow penetration of the corrosive electrolyte through it to reach the CS surface, it relatively quickly (within one day) recovered its anti-corrosive properties, as a consequence of the potential-driven release of SC-SDS from the PANI layer and its adsorption on the exposed CS surface, and continued to offer high corrosion protection during the remaining 29 days of exposure to the corrosive electrolyte. On the other hand, when damaged, the undoped double-layered PANI/epoxy coating was not capable of offering the sustained protection of SC surface towards corrosion, but its protection rather rapidly degraded.

Acknowledgements

The authors would like to convey their gratitude to the Qatar National Research Fund (QNRF) under the QRLP postgraduate award granted to Mr. Ahmad Diraki, to the Natural Science and Engineering Council of Canada (NSERC), and to the Chemical Engineering Department at McGill University.

Funding

This work was supported by Qatar National Research Fund (QNRF) under QRLP postgraduate award and by the Natural Science and Engineering Council of Canada (NSERC). 0

Chapter 5

The influence of the addition of sodium dodecyl sulfonate to sodium caprylate on the corrosion inhibition of carbon steel in aqueous HCl

5.1 Preface

This chapter presents an article submitted to the *Journal of Applied Electrochemistry*.

Ahmad Diraki, Sasha Omanovic: The influence of the addition of sodium dodecyl sulfonate to sodium caprylate on the corrosion inhibition of carbon steel in aqueous HCl

Ahmad Diraki (Ph.D. candidate) conceived the idea, planned and executed the experiments, analyzed the data, and drafted the manuscript. Prof. S. Omanovic supervised the work and reviewed and edited the manuscript.

Because the inner wall of the oil and gas pipeline is exposed to corrosion in an acidic environment during the oil and gas reservoir acidizing and cleaning process, but since most currently used corrosion inhibitors are toxic and environmentally unfavorable, it is essential to investigate the performance and efficiency of environmentally-friendly molecules as possible corrosion inhibitors. In the second article (Chapter 4), sodium caprylate (SC) and sodium dodecyl sulfate (SDS) were incorporated into the inner PANI layer of the smart double-layered PANI/epoxy coating, and the coating showed the ability to release the incorporated SC+SDS into the scratch and adsorb on the exposed CS surface, thus continuing to protect the underlaying CS surface. Based on these results, it was hypothesized that the SC+SDS mixture dissolved in a corrosive electrolyte could, by itself, inhibit corrosion of CS that is in contact with the corrosive electrolyte. Therefore, this mixture was deemed to be of interest to investigate in terms of its interaction with the CS surface under various experimental conditions, to potentially propose it as an environmentally friendly corrosion inhibitor for mitigation of inner-wall corrosion in oil and gas pipelines.

The paper presented in this section, thus, reports and discusses results on the potential use of a mixture of molecules containing sodium caprylate (SC) and sodium dodecyl sulfate (SDS) as a corrosion inhibitor of carbon steel in the acidic environment containing HCl, with the aim of potentially using it for control of inner-wall corrosion of pipelines employed in the oil and gas industry. Fundamental and applied aspects of the adsorptive interaction of the two molecules with the CS surface were investigated. SC and SC+SDS were found to act as good corrosion inhibitors for CS immersed in aqueous HCl under different experimental conditions, with SC+SDS offering a maximum corrosion protection efficiency of 98%, thus rendering this molecular mixture as a potential inhibitor for practical use in the oil and gas industry.

Highlights

- Na-caprylate (SC)+Na-dodecyl sulfonate (SDS) inhibits carbon steel (CS) corrosion.
- A synergistic corrosion-inhibition effect between SC and SDS is demonstrated.
- SC+SDS acts as a mixed-type inhibitor, forming an adsorbed layer on CS.
- The (SC+SDS)-CS adsorptive bond is strong.

Abstract

Sodium caprylate (SC) and a SC + sodium dodecyl sulfonate (SC+SDS) mixture was studied as corrosion inhibitors for carbon steel (CS) in aqueous HCl at different inhibitor concentrations, temperatures, HCl concentrations, and immersion times. The maximum corrosion inhibition efficiency of 87.9% for SC was achieved within 1 hour of CS immersion in 40 mM SC, while adding only 5 mM to SC boosted the inhibition efficiency up to 94.2%. After 48 hours of immersion, the corrosion inhibition efficiency was maintained, slightly increasing to ca. 89% for SC and ca. 98% for SC+SDS. The high inhibition performance was maintained even at higher temperatures. The Tafel polarization curves suggested that both SC and SC-SDS act as mixed-type inhibitors. The inhibition mechanism was suggested to occur through the formation of a barrier/hydrophobic-type SC and SC+SDS layer irreversibly adsorbed on the CS surface. SC and SDS were found to interact with the CS surface through their carboxylate and sulfonate groups, respectively.

Keywords: Corrosion inhibitors, Carbon steel, Acidic electrolyte, HCl, Adsorption, Caprylate, Sodium dodecyl sulfonate

5.2 Introduction

Carbon steel (CS) is the most used metal alloy as the construction material for pipelines due to its unique mechanical properties, availability, and cost-effectiveness, especially in the oil and gas industry [5]. On the other hand, inorganic acids are used extensively in the oil and gas industry during the production process as scale dissolvers. These acids are also pumped into the oil and gas reservoir formation to stimulate reservoir recovery and enhance production [213, 261]. It is a common practice to use concentrated mineral acids, such as hydrochloric acid (HCl) or hydrofluoric acid (HF) [57].

Carbon steel is highly prone to corrosion due to such an aggressive acidic environment [5]. This could lead to catastrophic damage to the carbon steel surface, resulting in potential equipment failure and substantial economic losses; the annual corrosion-related costs in the oil and gas industry have been estimated to be around 1.4 trillion USD [62].

A typical effective means to control and mitigate internal corrosion is the use of corrosion inhibitors [10]. The most effective inhibitors are mainly organic compounds that adsorb on the carbon steel's surface to form a thin protective barrier layer and impart the metal substrate from the corrosive environment [11, 12]. Majority of the currently-used organic corrosion inhibitors are toxic, non-biodegradable, and have significant bioaccumulation [13]. These concerns have triggered researchers to evaluate the possible application of eco-friendly inhibitors based on natural extracts [125], ionic liquids [126], biological polymers [127], amino acids [262], pharmaceutical products [263], and environmentally heterocyclic compounds [58], to name a few. Some pharmaceutical products showed excellent aqueous solubility and efficient corrosion inhibition [213]. For example, sodium caprylate (SC) is a medium-chain fatty acid found in medium-chain triglycerides and is sometimes used in the food industry and pharmaceutical industry [264, 265]. Carboxylate compounds have shown to be efficient green corrosion inhibitors for different metallic materials in various aqueous solutions. Their corrosion inhibition is prescribed to the availability of the charged carboxylate group (COO^-) for adsorption on the metal surface, and the remaining hydrophobic part of the molecule (e.g., an alkyl chain) to serve as a barrier that impedes transport of corrosive species to the underlaying metal surface. SC was tested as an inhibitor for corrosion of carbon steel in 0.5 M sulfuric acid showing good efficiency, where 30 mM of SC offered a 77% inhibition efficiency [241, 266]. Likewise, sodium palmitate, sodium stearate, and sodium myristate were reported as excellent corrosion inhibitors for magnesium alloys [267], while amino dodecanoic acids were also found to efficiently inhibit corrosion of CS [5, 241, 268, 269].

One approach to boosting the inhibition efficiency of candidate inhibitor molecules is to mix them with other molecules (additives) [270, 271]. These additives increase the interaction between the molecules of the main organic inhibitor and the metal surface [123]. For instance, the optimal corrosion protection efficiency of CS is reported to be 96.9% when mixing 5 mM of potassium iodide and 5 mM of sodium dodecyl sulfonate (SDS) in a HCl solution [271]. It was also reported that mixing 4 mM of SDS with 500 ppm zein increases the inhibition efficiency drastically, reaching more than a 90% protection efficiency of mild steel in sulphuric acid [272].

This led us to investigate the potential use of a mixture consisting of sodium caprylate (SC) and sodium dodecyl sulfonate (SDS), both containing a non-polar hydrophobic alkyl chain and a polar head anion group with vital adsorption characteristics, as a mixed corrosion inhibitor of carbon steel in hydrochloric acid. This mixture has not been studied as a corrosion inhibitor of carbon steel in the given electrolyte, to the best of our knowledge.

5.3 Experimental

5.3.1 Materials

All reagents were of the AR grade and used as received from the suppliers. The corrosive medium (electrolyte) was 0.5 M HCl (except in experiments in which HCl concentration was a parameter of interest) prepared using ultrapure water (18 MΩ cm) and an AR grade of 37% HCl. Sodium caprylate (purity 98%) was purchased from Acros organics (USA) and used as a corrosion inhibitor. Sodium dodecyl sulphate (SDS), denatured ethanol (95% EA), and acetone (Certified ACS) were purchased from Fisher Scientific (USA). G1117 low carbon steel (CS) acquired from McMaster-Carr (USA) with a chemical composition of 0.14-0.20 wt.% carbon, 1.00-1.30 wt.% manganese, up to 0.04 wt.% phosphorus, between 0.08 and 0.13 wt.% sulphur and balance Fe, was used as a metal substrate for corrosion testing.

5.3.2 Instrumentation

Polishing machine MetaServ-3000 and Branson-1510 ultrasonic water bath was used for sample preparation. A conventional three-electrode electrochemical cell, consisting of a conductive graphite rod as the counter electrode, a saturated calomel electrode as reference electrode (SCE), and a carbon steel sample as the working electrode was used in all measurements. An AUTOLAB Potentiostat/Galvanostat/FRA PGSTAT 30 was used for corrosion measurements. This system was interfaced with a computer to control the experiments, and the data were acquired and analyzed using NOVA 2.1 software. The surface morphology of the samples was observed using a field-emission scanning electron microscope (FE-SEM) (Hitachi FE-SEM SU3500). X-ray photoelectron spectroscopy (XPS) was used to evaluate the CS surface chemical compositions using a Thermo Scientific K-alpha XPS system (1486.6 eV photon energy) with an aluminum X-ray source. Goniometer (FSA OCA 15EC)-Data-Physics is an optical contact angle measuring machine employed to evaluate the CS surface wettability in the absence and presence of corrosion inhibitor adsorbed on its surface.

5.3.3 Sample preparation

A carbon steel (CS) metal rod of 1.59 cm in diameter was cut into coins of a thickness of 3.3 mm. A Teflon holder was used to hold the coin sample when immersed in the electrolyte, leaving a metal area of 1.039 cm^2 exposed to the electrolyte (one side of the sample). Before undergoing the corrosion measurements, the samples were adequately pre-treated. Namely, the CS surface was wet-polished using a 600- grit silicon carbide paper for 2 minutes at the rotation speed of 200 rpm. Then, the sample was ultrasonicated in ethanol for 5 minutes to remove the polishing residue. Finally, the substrate was rinsed with acetone to degrease its surface and dried with argon.

5.3.4 Corrosion measurements

Electrochemical/corrosion measurements were carried out in an aqueous 0.5 M HCl (except in experiments in which HCl concentration was a parameter of interest). Electrochemical impedance spectroscopy (EIS), polarization resistance (PR), and Tafel polarization were used to investigate the corrosion rate of the CS samples. Before each corrosion test run, the samples were first conditioned at open-circuit potential (OCP) for 1 hour, unless mentioned otherwise. Then, EIS measurements were performed at OCP in the frequency range between 10 mHz and 50 kHz applying a ±10 mV alternating voltage amplitude. After this, PR measurements were performed in a potential window of ±10 mV with respect to OCP, at a scan rate of 1 mV s^{-1}. Finally, Tafel polarization curves were recorded by anodically polarizing the samples from -200 mV to +200 mV vs. OCP at a scan rate of 1 mV s^{-1}. All the measurements were performed at 22±1° C (except in experiments where temperature was a parameter of interest).

5.3.5 Surface characterization

The CS morphology was evaluated after 3 days of immersion in 0.5 M HCl in the presence and absence of optimum corrosion inhibitor concentration. CS surface topography was studied by field-emission scanning electron microscopy (FE-SEM), while X-ray photoelectron spectroscopy (XPS) was used to evaluate the chemical composition of the CS surface. Water contact angle measurements examined the surface wettability with a drop shape analyzer, in which the image analysis software reported the contact angle (Θ). The contact angles were generated between the CS surface and deionized water drops with a dosing rate of 0.5 μL s^{-1} and a dosing volume of 5 μL.

5.4 Results and discussion

5.4.1 Effect of SC concentration and SDS on corrosion inhibition - Electrochemical Impedance Spectroscopy (EIS) measurements

EIS was initially used to evaluate the electrode/electrolyte interface and corrosion processes occurring on the CS surface in 0.5 M HCl aqueous solution at different SC concentrations in the absence and presence of 5 mM SDS (note that this concentration of SDS is below the critical micelle concentration). The representative Nyquist plots recorded in 40 mM SC in the absence and presence of 5 mM SDS are presented in Fig 5. 1, and the spectrum recorded in the absence of SC and SDS (unprotected surface) is displayed as the inset to the figure. In the first approximation, the diameter of the semi-circle can be taken to be proportional to the corrosion resistance. Thus, first, with the addition of SC into the solution, the spectrum diameter significantly increased (compare the diameter of the blue curve in the main plot to that one in the inset), evidencing that SC increases the CS's corrosion resistance. Then, with the addition of 5 mM SDS into the electrolyte containing 40 mM of SC, the diameter of the EIS spectrum further increased significantly (compare the red and blue curves on the main plot), indicating further improvement in corrosion resistance CS. Consequently, the addition of a small amount of SDS into the SC-containing solution has a significant positive effect on the overall inhibition efficiency of the mixture.

To get quantitative data, all the EIS spectra recorded were modelled employing the electrical equivalent circuits (EECs) presented in Fig 5. 2. The spectra at low frequencies do not show a diffusion behavior (Warburg), suggesting that the CS corrosion mechanism is a process controlled by charge transfer [273]. Consequently, the one-time-constant in Fig 5. 2(a) was used to model the spectrum record in the absence of corrosion inhibitor (control), where R_{el} represents the solution resistance between the reference electrode and the CS working electrode, R_1 is the charge transfer resistance related to the corrosion reactions occurring at OCP, and CPE_1 is the constant phase element associated with the capacitance of the electric double-layer at the electrode/electrolyte interface. However, using this one-time constant EEC to model the EIS data recorded in the presence of the inhibitor resulted in a poor agreement between the model and the experimental data. Consequently, the two-time constant presented in Fig 5. 2(b) was used to model the spectrum record in the presence of the corrosion inhibitor. In this EEC, the outer CPE_1-R_1 time constant has the same meaning as that one in Fig 5. 2(a), and the inner CPE_2-R_2 time constant represents the response of the pseudo-capacitance and resistance of the surface-adsorbed inhibitor layer. Thus, the corrosion resistance of CS in the electrolyte containing the inhibitor is the sum of R_1 and R_2. An excellent agreement between experimental and modelled data in Fig 5. 1 confirms the compatibility of used EECs in explaining the EIS behavior, and the corresponding EEC parameter values are listed in Table 5. 1.

As shown in the table, when SC was added into the electrolyte, the CPE_1 value decreased, and then further dropped upon the addition of SDS into the solution, indicating a reduction in the CS surface area exposed to the electrolyte as a consequence of adsorption of SC/SDS on the CS surface[268]. Also, when SDS was added to the SC-containing solution, the CPE_2 value decreased, related to the increase in the inhibitor layer thickness and/or its compactness.

To estimate the corrosion inhibition efficiency at different SC concentrations and to quantify the synergistic effect upon adding 5 mM SDS into the SC-containing solution, the following equation was used:

$$\eta_{R_{corr}} = \left(1 - \frac{R_{corr,o}}{R_{corr,i}}\right) \times 100\% \quad (5.\ 1)$$

where $R_{corr,o}$ and $R_{corr,i}$ (Ω cm^2) is the corrosion resistance in the absence and presence of the inhibitor, respectively. Fig 5. 3. illustrates the inhibition efficiency at different SC concentrations (note that the blue symbols represent the trend with only SC present in the solution). As we can see, the inhibition efficiency increases with increasing the SC concentration in the bulk solution and levels off into a plateau at 40 mM of SC in the solution, yielding a corrosion inhibition efficiency of 87±5 %. As indicated by the trend in CPE_1 values (Table 1), the increase in corrosion inhibition efficiency in Fig 5. 3 can be linked to the increase in SC surface concentration and thus its surface coverage, resulting in a decreased access of corrosive ions to the CS surface [213, 241, 268, 269]. When the EIS measurements were performed in the solution containing only SDS, there was no change in the corrosion resistance, indicating that SDS alone, although being a known surfactant, cannot be used as a corrosion inhibitor of CS in 0.5 M HCl under the experimental conditions employed (see Fig. 5-S. 1 in the supplemental document). Surprisingly, the resulting corrosion inhibition efficiency increased when 5 mM of SDS was added to the SC-containing electrolyte (red symbol in Fig 5. 3). This increase in the corrosion inhibition efficiency could be attributed to the enhanced adsorption of SC in the presence of SDS due to the presence of long alkyl chains in the SDS [271, 272, 274]. Also, with SDS in the electrolyte, the surface concentration of the inhibitor (SC + SDS) could increase, yielding higher surface coverage by the inhibitor, thicker inhibitor molecular layer, and higher order of the molecules on the CS surface, thus offering a tighter hydrophobic barrier to the transport of corrosive species (ions) to the underlaying CS surface [268].

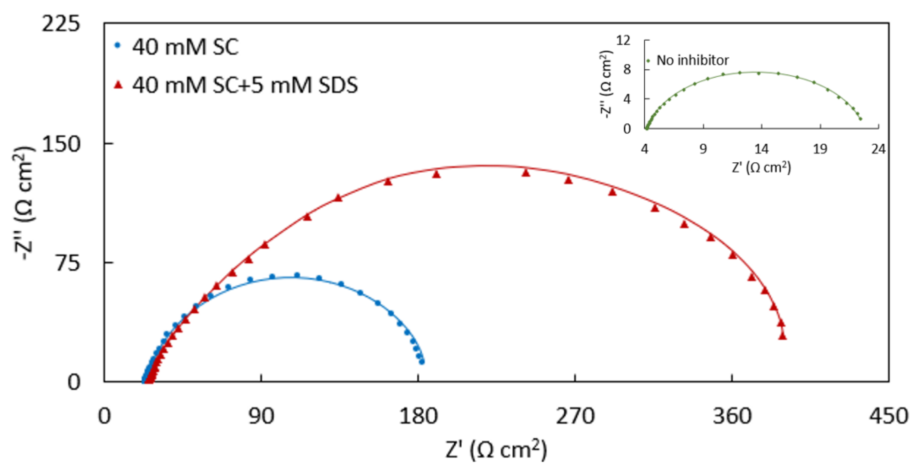

Fig 5. 1 Nyquist plots of CS recorded at OCP in the absence (green symbols, inset plot) and presence of 40 mM of SC (blue circles, main plot) and 40 mM SC + 5 mM SDS (red symbols, main plot) in 0.5 M HCl solution at 295 K. Symbols represent the experimental values, while the solid lines present the simulated spectra.

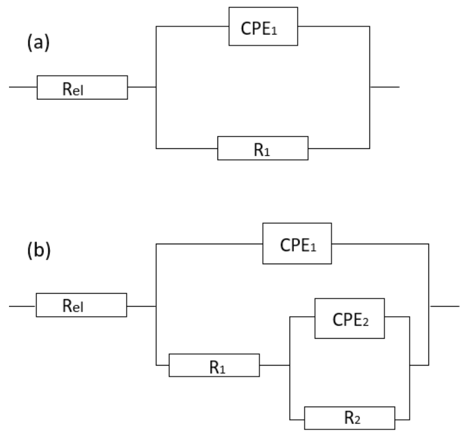

Fig 5. 2 EEC models used to fit EIS spectra of the CS electrode recorded in (a) the inhibitor-free solution (control) and (b) the electrolyte containing SC and SC+ SDS.

Table 5. 1 EEC parameter values obtained by modelling the EIS spectra recorded at OCP on the CS sample immersed in 0.5 HCl at 295 K in the absence and presence of SC and SC+SDS.

	R_{el} (Ω cm^2)	R_{corr}(Ω cm^2)	$CPE_1 \times 10^6$ (Ω^{-1} cm^{-2} s^n)	$CPE_2 \times 10^6$ (Ω^{-1} cm^{-2} s^n)
No inhibitor	4±2	22±4	810±98 (n=0.71±0.09)	
40 mM SC	23±6	182±7	515±53 (n=0.77±0.07)	285±42 (n=0.82±0.05)
40 mM SC+5 mM SDS	25±5	389±3	310±41 (n=0.89±0.04)	192±37 (n=0.91±0.03)

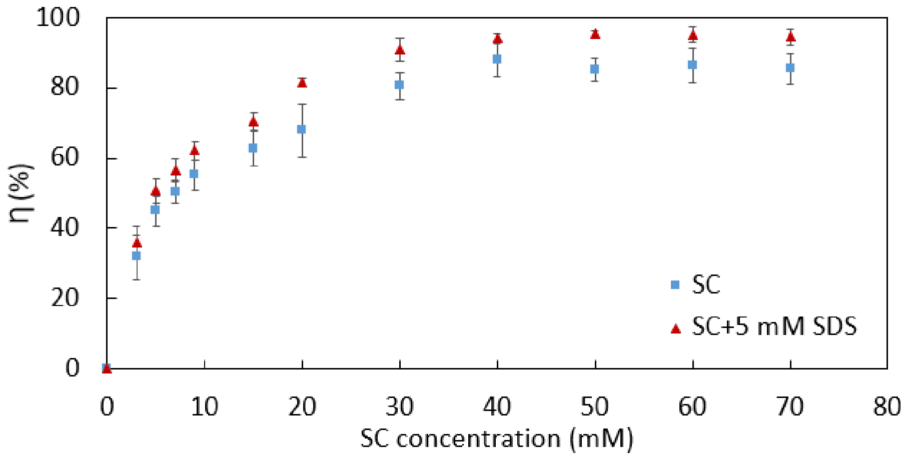

Fig 5. 3 Corrosion inhibition efficiency as a function of SC concentration in 0.5 M HCl obtained from EIS data recorded at 295 K. The red triangle represents the corrosion inhibition efficiency obtained in 0.5 M HCl containing 40 mM SC + 5 mM SDS.

5.4.2 Tafel polarization measurements

Tafel polarization measurements were used to acquire a deeper insight into the systematic aspect of the inhibitor process [275] and to confirm the data obtained from EIS. Fig 5. 4. presents typical potentiodynamic polarization curves for CS recorded in 0.5 M HCl in the absence of the inhibitor (green curve), in the presence of 40 mM of SC in the electrolyte (blue curve), and in the presence of 40 mM SC + 5 mM SDS in the electrolyte. The cathodic branch of the curves is related to the oxygen reduction reaction, while the anodic branch of the curves is related to the CS dissolution reactions. When SC was introduced into the electrolyte, the corrosion potential shifted to more positive values, and the currents decreased, indicating a decrease in corrosion rate due to the interaction of SC with the CS surface. Upon adding SDS into the SC-containing electrolyte, the corrosion potential further shifted to the positive direction, and the currents further decreased, indicating the benefit of SDS presence in the electrolyte on corrosion protection. The corrosion current was determined from the Tafel curves in Fig 5. 4 and the values are presented in Table 5. 2. Thus, with the addition of SC into the electrolyte, the corrosion current decreased by one order of magnitude, evidencing the decrease in corrosion rate in the presence of SC. With the addition of SDS into the SC-containing electrolyte, the corrosion current further decreased, indicating the beneficial effect of SDS on corrosion inhibition. Taking that the current is inversely proportional to resistance, the trend of corrosion current in Table 5. 2 is in accordance with the direction of corrosion resistance in Table 1, and could, thus, be described in the same manner. Similarly, to what was noted with EIS measurements, the presence of only SDS in 0.5 M HCl did not influence the corrosion rate of CS (Fig. 5-S. 2 in the supplemental document), proofing that SDS, when used without SC, cannot act as a CS corrosion inhibitor under the experimental conditions employed.

The percentage of the corrosion inhibition efficiency was calculated from the Tafel measurements by applying the following equation:

$$\eta_{j_{corr}} = \left(1 - \frac{j_{corr,o}}{j_{corr,i}}\right) \times 100\% \tag{5. 2}$$

where $j_{corr,o}$ and $j_{corr,i}$ (A cm^{-2}) is the current density in the absence and presence of the inhibitor, respectively. The corresponding values are presented in Table 5. 2. Similarly to what is seen from EIS measurements, adding 40 mM of SC into the 0.5M HCl resulted in a significant inhibition efficiency (87±5%), while the addition of SDS further increased the inhibition efficiency to 94±2%. Thus, the good agreement between the Tafel and EIS measurements validates the values obtained and the synergistic corrosion inhibition effect achieved by mixing SC and SDS.

In addition to the observed decrease in corrosion current density and increase in corrosion potential upon the addition of SC and then SC+SDS into the electrolyte, Fig 5. 4 also shows that the cathodic Tafel slope decreased while the anodic slope increased, indicating a change in the corrosion mechanism; this will be further discussed in Section 3.5.

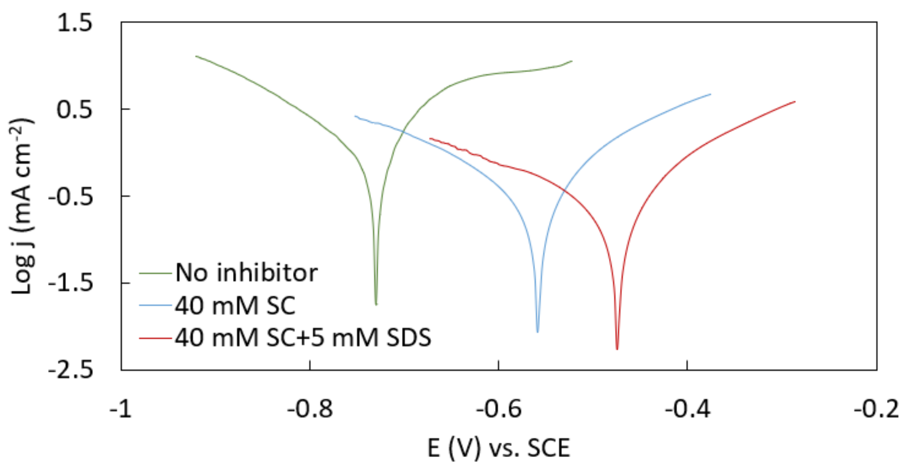

Fig 5. 4 Tafel plots of CS recorded at 295 K in 0.5 M HCl in the absence (green line) and in the presence of 40 mM SC (blue line) and 40 mM SC + 5 mM SDS (red line) in the electrolyte, at a scan rate of 1 mV s^{-1}.

Table 5. 2 Corrosion current density (j_{corr}) obtained from Tafel measurements recorded on the CS sample immersed in 0.5 HCl at 295 K in the absence and presence of SC and SC+SDS in the electrolyte.

	j_{corr} (A cm^{-2})	**η (%)**
No inhibitor	(3.1±0.4) x10^{-3}	
40 mM SC	(3.8±0.5) x10^{-4}	87±5
40 mM SC+5 mM SDS	(1.9±0.3) x10^{-4}	94±2

5.4.3 Adsorption isotherms

To describe the adsorptive interaction of SC and SC-SDS molecules with the CS surface, the surface coverage of the metal by SC and SC+SDS, θ, was taken to be proportional to the inhibition efficiency η. Several adsorption isotherms were tested, and the best agreement between the experimental data and the model was obtained when the linearized Langmuir adsorption isotherm was used [276, 277]:

$$\frac{C}{\theta} = \frac{1}{K_{\text{ads}}} + c \tag{5. 3}$$

where C is the concentration of the inhibitor in the bulk solution (mol cm^{-3}), θ is the surface coverage by the inhibitor layer, K_{ads} represents the equilibrium adsorption constant (cm^3 mol^{-1}). Fig 5. 5 shows a good agreement between the experimental data (symbols) and the adsorption model (lines), confirming the applicability of the Langmuir isotherm in describing the adsorptive interaction of SC and SC+SDS with the CS surface under the experimental conditions employed. The corresponding fitting parameters are listed in Table 5. 3. The data shows that the equilibrium adsorption constant is slightly larger in the presence of SDS in the electrolyte, indicating stronger interaction of the SC+SDS mixture with the CS surface. From the equilibrium adsorption constant values, the corresponding apparent Gibbs free energy of adsorption, ΔG_{ads}, was calculated [278]:

$$\Delta G_{\text{ads}} = -RT \ln (C_{\text{solvent}} K_{\text{ads}}) \tag{5. 4}$$

where R is the gas constant (J mol^{-1} K^{-1}), T is the temperature (K), ΔG_{ads} is the Gibbs free energy of adsorption (kJ mol^{-1}), $C_{solvent}$ is the concentration of solvent used to prepare the solution, which is in the current case water and is equal to 55.5 mol dm^{-1}. The computed values are listed in Table. 3, and the negative values of ΔG_{ads}, imply that the adsorption of SC and SC+SDS on the CS surface is a spontaneous process, being thermodynamically slightly more favourable in the latter mixture.

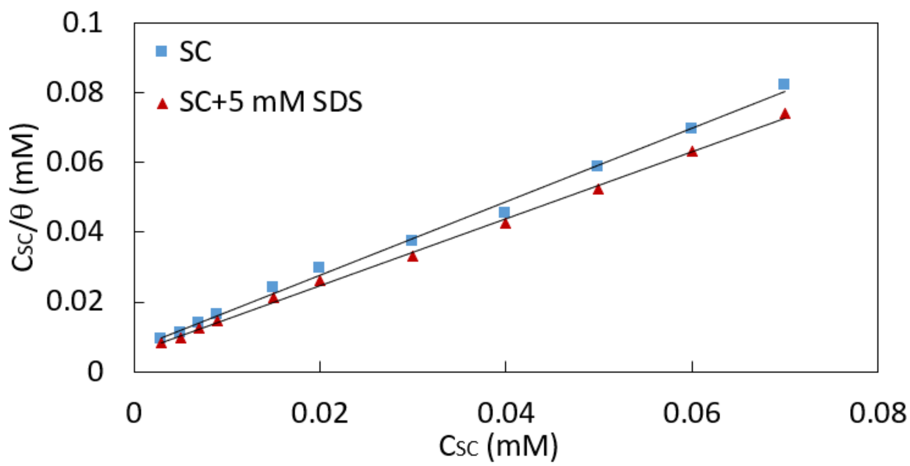

Fig 5. 5 The linearized form of the Langmuir adsorption isotherm for adsorption of SC onto the CS surface in the presence and absence of SDS at 295 K.

Table 5. 3 Thermodynamic parameters for the adsorption of SC and SC+SDS on the CS surface at 298 K in 0.5 M HCl. The parameters were obtained employing the Langmuir adsorption isotherm for fitting the experimental data.

	SC	**SC+SDS**
R^2	0.997	0.998
K_{ads}	153 dm^3 mol^{-1}	179 dm^3 mol^{-1}
ΔG_{ads}	-22.23 kJ mol^{-1}	-22.66 kJ mol^{-1}

5.4.4 Adsorption and desorption kinetics

The kinetic of SC and SC+SDS adsorption on the CS surface is crucial for potential industrial applications of the inhibitor. To study this, the short-duration polarization resistance (PR) technique was employed to evaluate the inhibitor's inhibition efficiency as a function of time. First, the control measurement was performed on the CS sample immersed in 0.5 M HCl (no inhibitors added). In the subsequent experiment, the inhibitor was added into the 0.5 M HCl solution, under vigorous stirring, immediately upon immersion of the CS sample, but at a point far from the CS surface (to avoid high local inhibitor concentration in the vicinity of the CS surface). Eq. (2) was used to compute the time-dependence of inhibition efficiency, and the corresponding data are presented in Fig 5. 6. These results confirm rapid adsorption kinetics, showing a sharp increase in inhibition efficiency to 73% after 15 minutes upon adding SC, while the efficiency reached 88% within the same time in the SC+SDS-containing electrolyte. However, once the adsorption reached its plateau for SC, the inhibition efficiency started to decay slightly. This could be due to the re-orientation of the SC molecule on the CS surface to adopt a more thermodynamically favourable conformation, resulting in a lower degree of corrosion protection. On the other hand, SC+SDS maintained its high inhibition efficiency over the time frame of the experiment, indicating that no structural changes in the mixed molecular layer occurred.

Desorption studies were also performed to evaluate the bond strength between the inhibitor and the CS surface. In these experiments, the inhibitor (SC and SC+SDS) was first adsorbed on the CS surface, and EIS spectra were recorded after one hour of immersion of the sample under OCP conditions. Then, the corrosion resistance was evaluated every hour following the electrolyte dilution. As illustrated in Fig 5. 7, when the SC concentration decreased in the presence of only SC in the solution to 30 mM, the inhibition efficiency slightly dropped. It then continued to minorly decrease with a further reduction in SC concentration in the solution. However, there is no statistical difference in inhibition efficiency in the 30, 20 and 10 mM solutions. This indicates the initial reduction in corrosion resistance at 120 min upon dilution to 30 mM was potentially due to the desorption of weakly-adsorbed SC molecules from the CS surface. However, in the presence of SDS, no change in corrosion efficiency was observed upon multiple electrolyte dilutions, suggesting that the SC+SDS-CS adsorptive bond is relatively strong under the current experimental conditions.

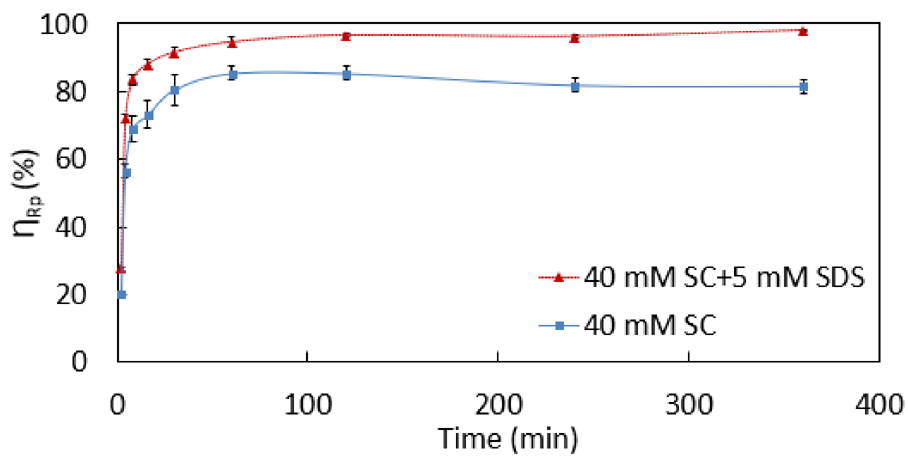

Fig 5. 6 Kinetics of SC and SC+SDS adsorption on the CS surface expressed in terms of inhibition efficiency calculated from polarization resistance measurements. The experiments were performed in 0.5 M HCl at 295 K. The lines are for visual aid only. The first point in the measurements was recorded at 2 minutes.

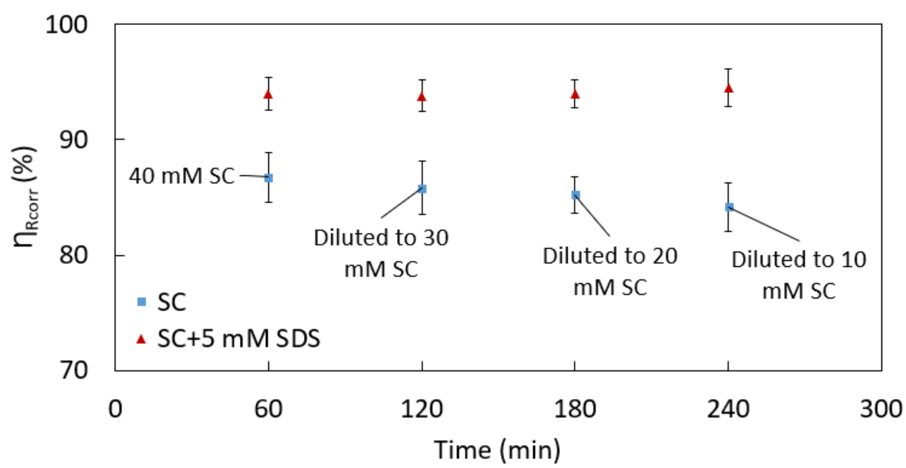

Fig 5. 7 Dependence of corrosion inhibition efficiency of SC and SC+SDS on their concentration in the bulk solution reached by dilution after recording the initial efficiency in 40 mM SC and 40 mM SC + 5 mM SDS in 0.5 M HCl at 295 K. The experiments were performed to evaluate the reversibility of SC and SC+SDS adsorption on the CS surface.

5.4.5 Effect of temperature

The impact of temperature on metal corrosion in an acidic environment is very complex, where etching may occur, leading to new active sites on the CS surface [279]. To assess the influence of temperature on the inhibition efficiency, the resistance of CS to corrosion was examined at temperatures between 303 and 323 K in the absence and presence of the inhibitors. Fig 5. 8 illustrates the corresponding results of inhibition efficiency calculated from EIS experiments. The results show that the corrosion resistance efficiency of SC decreases with increasing temperature. This might be due to the desorption of SC from the CS surface and the resulting shift of SC adsorption equilibrium towards lower surface coverages [280]. However, when SC was combined with SDS, the inhibition efficiency remained statistically constant, indicating that the structure and surface coverage of the adsorbed SC+SDS molecular layer is stable within the temperature range employed. The results confirm that SC+SDS is a promising inhibitor candidate at slightly higher temperatures.

To determine the apparent activation energy of corrosion of CS in the absence and presence of the inhibitor, temperature-dependent corrosion resistance values were examined, and the Arrhenius law was employed:

$$R_{corr}^{-1} \propto \mathrm{A} \exp\left(\frac{-E_{a,app}}{RT}\right) \qquad (5.\ 5)$$

where $E_{a,app}$ represents the corrosion apparent activation energy ($Jmol^{-1}$), A is the pre-exponential Arrhenius constant ($\Omega^{-1}cm^{-2}$), and R is the gas constant (8.314 $Jmol^{-1}K^{-1}$). Fig 5. 9 presents a linearized plot of the Arrhenius equation for the three cases, and the corresponding Arrhenius parameters are shown in Table 5. 4. Surprisingly, the trend of the apparent activation energy values is opposite to what can be expected from the corrosion inhibition efficiency data obtained from EIS and Tafel measurements (Tables 1 and 2); Table 5. 4 shows that the apparent activation energy decreased in when SC was present in the electrolyte, and it then further decreased when SDS was added into the SC-containing electrolyte, suggesting that the corrosion mechanism changed to follow a path of a lower kinetic energy barrier (these paths refer to the corrosion of the CS surface that is free of adsorbed SC and SC+SDS) [281-283]. This decrease in activation energy in the presence of the inhibitor in the electrolyte suggests potential changes in corrosion mechanism to a lower kinetic energy barrier. The change in corrosion mechanism is visible in the Tafel plots in

Fig 5. 4; the cathodic Tafel slope decreased, and the anodic one increased in the SC, and they then further decreased/increased in the SC+SDS containing electrolyte.

While the apparent activation energy (surprisingly) decreased in the presence of SC and SC+SDS in the electrolyte, the corresponding pre-exponential Arrhenius factor values also decreased, but by a significant amount (Table 5. 4); by 7 and 10 orders of magnitude in the presence of SC and SC+SDS, respectively. Referring to the transition-state/activated-complex theory, this significant decrease in the Arrhenius pre-exponential factor can be related to a large decay in the system's entropy [284]. This can be due to the formation of a "rigid and ordered" SC and SC+SDS surface layer, and also due to reduction in the number of surface corrosion reaction sites (*i.e.* the inhibitor-free CS surface area). The latter leads to the decline in the overall number of encounters between the corrosive species present in the electrolyte and the CS surface, which results in a lower overall corrosion rate, *i.e.* higher corrosion resistance (Tables 1 and 2), thus representing the governing corrosion kinetic factor.

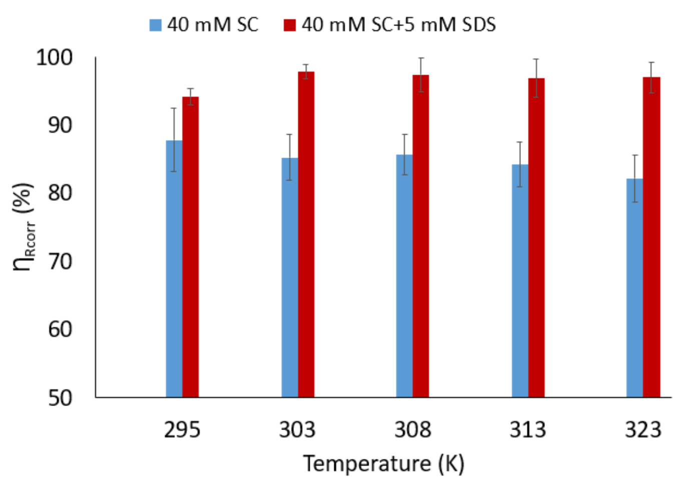

Fig 5. 8 The inhibition efficiency of 40 mM SC and 40 mM SC + 5 mM SDS in protecting the CS surface immersed in 0.5 M HCl at various temperatures. The data was obtained from EIS measurements.

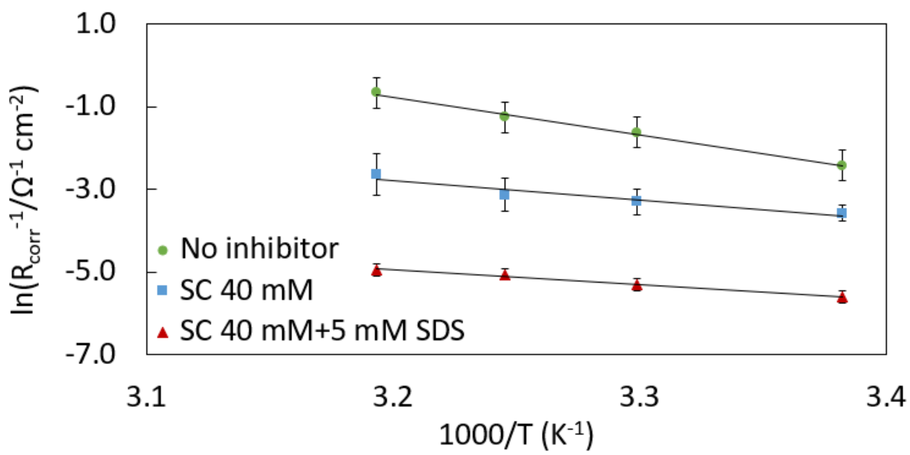

Fig 5. 9 The linearized Arrhenius plot for the CS samples immersed in 0.5 M HCl solution in the absence and presence of 40 mM SC and 40 mM SC + 5 mM SDS. The data were obtained from EIS measurements.

Table 5. 4 Apparent activation energy and Arrhenius pre-exponential factor for corrosion reactions occurring on the CS surface immersed in 0.5 HCl, in the absence and presence of inhibitor.

	No inhibitor	**40 mM SC**	**40 mM SC + 5 mM SDS**
$E_{a,app}$ (kJ mol^{-1})	74.15	38.11	29.04
A (Ω^{-1} cm^{-2})	2.2×10^{12}	2.1×10^{5}	6.5×10^{2}

5.4.6 Effect of HCl concentration

The influence of HCl concentration on the SC and SC+SDS corrosion inhibition efficiency was evaluated, and the results are presented in Fig 5. 10. When only the SC was present in the solution, the corresponding inhibition efficiency slightly decreased with increasing the HCl concentration from 1 M to 2 M and then remained relatively stable with the further increase in HCl concentration. The observed decrease could be either due to pH-induced changes in SC/CS adsorptive type of interactions, causing a lower SC surface concentration/coverage and/or due to the conformational changes in the molecular inhibitor layer [285-287]. However, when SDS was added to the SC-containing electrolyte, the inhibition efficiency did not statistically change with HCl concentration increase. Even in 3 M HCl, 40mM SC + 5 mM SDS offered a very high inhibition efficiency (93.4%). Thus, the data in Fig 5. 10 indicate that SC+SDS is still capable of offering a good protection efficiency of the CS surface regardless of the corrosive severity of the electrolyte under the experimental conditions employed.

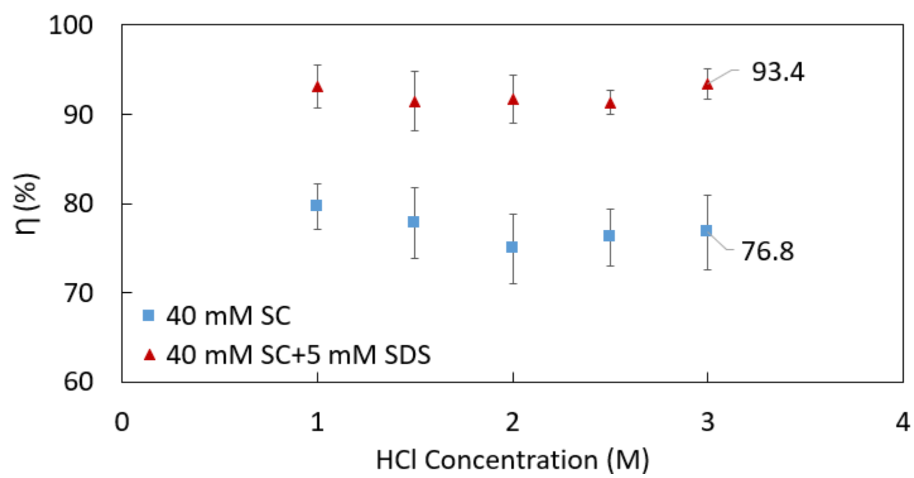

Fig 5. 10 The inhibition efficiency of 40 mM SC and 40 mM SC + 5 mM SDS in protecting the CS surface immersed in HCl solutions of various concentrations. The results were obtained from EIS measurements recorded at 295 K.

5.4.7 The effect of long-term immersion

The performance of the inhibitor over a longer-term immersion of CS in the corrosive electrolyte was studied. EIS measurements in the absence and presence of inhibitor were performed over 48 hours under electrolyte stirring, and the corresponding corrosion inhibition efficiency is presented in Fig 5. 11. In the case of both 40 mM SC and 40 mM SC + 5 mM SDS, the inhibition efficiency increased with immersion time. The initial trend could be related to an increase in surface concentration/coverage by the inhibitor molecules and/or to structural changes in the inhibitor molecular layer, to offer a better barrier against the transport of corrosive species from the electrolyte to the SC surface. After one day, the corrosion inhibition efficiency reached ca. 90% for SC and ca. 96% for SC+SDS. While in the SC+SDS containing solution the efficiency remained constant on the second day of immersion, in the SC-containing solution it slightly decreased, but this decrease was not found to be statistically significant.

SEM images of the CS surface morphology after 3 days of immersion time in the testing electrolytes are presented in Fig 5. 12. The freshly prepared CS surface, Fig 5. 12(a), is characterized by the appearance of scratches produced by mechanical polishing. Fig 5. 12(b) shows the morphology of the CS sample corroded in the absence of the inhibitor, displaying the existence of corrosion products at a larger amount, evidencing its severe corrosion. On the other hand, when the CS sample was immersed in the solution that contained 40 mM SC, the extent of its corrosion was greatly diminished (Fig 5. 12(c)), although some pits/cavities are still noticeable on the surface. The addition of SDS into the SC-containing electrolyte further decreased the extent of CS surface corrosion, as seen in Fig 5. 12(d), confirming the good corrosion inhibition efficiency under the investigated experimental conditions.

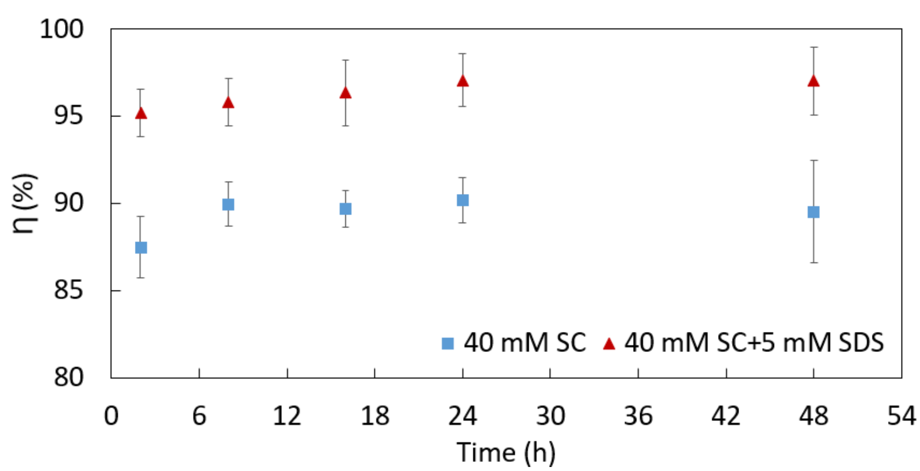

Fig 5. 11 The effect of immersion time on the inhibition efficiency of 40 mM SC and 40 mM SC + 5 mM SDS in protecting a CS surface immersed in 0.5 M HCl. The results were obtained from EIS measurements at 295 K.

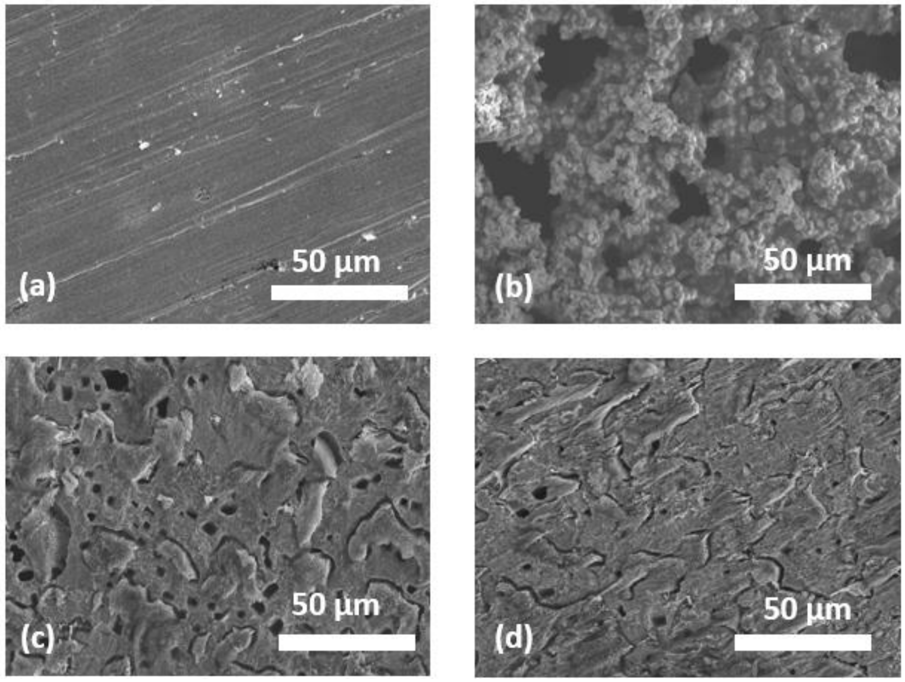

Fig 5. 12 SEM micrographs of the (a) freshly polished CS surface, and the CS surface immersed for 72 hours in 0.5 M HCl solution (b) in the absence of corrosion inhibitor, (c) in the presence of 40 mM SC, and (d) in the presence of 40 mM SC + 5 mM of SDS.

5.4.8 Contact angle measurements

A desired feature of corrosion inhibitors is to enable an increased hydrophobicity of the surfaces that need to be protected. Given that the desorption measurements (Fig 5. 7) showed that both SC and SC+SDS are chemisorbed on the CS surface, the CS samples were first immersed in the electrolyte containing SC and SC+SDS for 1 hour, rinsed well with nano-pure water, argon-dried. Then, the contact angles were determined on these samples and compared to that one done on the freshly polished CS sample. The corresponding results, presented in Fig 5. 13, show that there was an increase in hydrophobicity of the CS surface covered by the SC molecular layer, resulting in a contact angle increase from 49.7±0.2° for the freshly polished CS surface to 78.3±0.9° for the SC-covered surface. This increase in the hydrophobicity of the CS surface also contributes to the good inhibition efficiency of SC, discussed previously in the paper. However, when the SC+SDS molecular layer covered the CS surface, the contact angle further increased to

118.9±2°, rendering the surface relatively hydrophobic, which also explains the enhanced corrosion inhibition efficiency of the SC+SDS inhibitor relative to that one of the SC inhibitors [205].

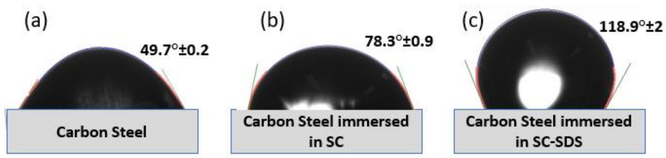

Fig 5. 13 Contact angle values between the deionized water drop and the (a) freshly prepared CS surface, (b) the CS surface that was pre-immersed in an electrolyte containing 40 mM SC, and (c) 40 mM SC + 5 mM SDS. The pre-immersion was done over a period of 1 hour, and the surface was thoroughly rinsed with deionized water and argon-dried before performing the contact angle measurements.

5.4.9 Surface characterization by XPS

X-ray photoelectron spectroscopy (XPS) analysis was performed to examine the surface composition of the CS sample after 24 h of immersion time in 0.5 M HCl in the presence and absence of inhibitors in the solution. After immersion, the CS samples were removed from the electrolyte and then rinsed gently with RO water to eliminate the leftover electrolyte residues and also inhibitor molecules that did not adsorb on the surface. The CS samples were then left overnight to dry under a vacuum to eliminate residual moisture before recording the XPS spectra. Fig 5. 14 shows the corresponding XPS survey spectra. The spectrum of the sample corroded in the absence of an inhibitor in the electrolyte displays the response of Fe 2p, O 1s, and C 1s: Fe 2p arises from the CS, O 1s derives from the surface oxide/hydroxide film, and the C 1s is due to the adventitious carbon. The immersion of CS in 0.5 M HCl containing the inhibitors resulted in significant changes to the corresponding overview spectrum. The tiny peak assigned to the presence of Cl 2p on the SC-protected sample spectrum could be due to the strong interaction of Cl^- ions with the adsorbed SC molecules [288]. In addition, the intensity of the C 1s peak increased when CS was immersed in the SC- and SC+SDS-containing electrolyte, which indicates the presence of the SC and SC+SDS layer on the CS surface. The presence of the small S 2p peak on the spectrum of the SC+SDS protected sample could be related to the response of adsorbed SDS. Moreover, the O 1s core level signal is significantly diminished on the spectra recorded on the samples immersed in the electrolyte containing the inhibitors, indicating a smaller amount of oxides/hydroxides (corrosion products) present on the CS surface.

The obtained high-resolution spectra for C 1s, O s, Fe 2p, S 2p core levels associated with the CS sample kept in the absence and presence of SC and SC+SDS in the electrolyte are presented in Fig 5. 15a-j. The peaks analysis was done by a Gaussian deconvolution fitting of the spectra.

The C 1s spectrum (Fig 5. 15. a, b, c) was deconvoluted into three contributions (see the corresponding designations in Fig 5. 15a). The prominent (large) peak around 285.1 eV can be, for the unprotected sample (figure (a)), due to the adventitious carbon, while for the protected samples (figures (b) and (c)), it can be predominantly related to the C-C/C=C and C-H bonds of the adsorbed inhibitor [289-291]. The peak at 286.2 eV can be prescribed to the C-Cl^-/C-S, due to the strong interaction of Cl^- ions with SC molecules, and to the C-S bond because of the presence of sulfur (S) in SDS [288, 292]. The peak at 288.6 eV may be assigned to the C=O bond formed between the adsorbed adventitious carbon and oxide-covered CS surface (figure (a)), while for the spectra recorded in the presence of SC and SC+SDS it is related to the C=O bond in the molecules (note the large difference in counts between the protected and unprotected samples) [289, 293].

The O 1s spectrum in Fig 5. 15d, where the CS is immersed in the 0.5 mM HCl in the absence of the inhibitor is deconvoluted into three different peaks. The two components at 530.6 eV and 531.1 eV, can be assigned to metal (iron) oxide (O^{2-}) and hydroxide (OH^-) phases, respectively. However, the binding energies at 532.6 eV are likely associated with adsorbed OH (Fe-adsorbed H_2O) and adventitious carbon-oxygen species (O^1 and O^2), as discussed in the previous paragraph in relation to C 1s spectra [294]. Immersion in the electrolyte containing SC and SC-SDS results in complete quenching of the O^{2-} and OH^- components. This indicates that the SC corrosion inhibitors are adsorbed on oxide/hydroxide-free surfaces. (Fig 5. 15e) is deconvoluted into three different peaks at 530.0, 531.5, and 532.1 eV. The peaks at 530.0 and 531.5 eV can be assigned to the oxygen atoms in the coordinate-free carboxylate group in SC adsorbed on the CS surface [295, 296]. Moreover, the observed peak at 532.1 eV can be assigned to the physically/chemically absorbed water within SC on the CS surface [297, 298]. The XPS spectrum recorded on the CS sample immersed in a SC+SDS containing electrolyte (Fig 5. 15f) is deconvoluted into two contributions recorded at 529.2 and 530.5 eV, where the peaks respectively correspond to the presence of sulphate groups in SDS in the form of S=O and $(SO_3)^-$ group [299-302].

The Fe 2p spectrum recorded on the CS surface immersed in the electrolyte that did not contain the inhibitor (Fig 5. 15g) is characterized by two doublets of Fe 2p spin-orbit components (i.e., Fe $2p_{3/2}$ and Fe $2p_{1/2}$). The Fe $2p_{3/2}$ energy at 710.9 eV is ascribed to the response of Fe(II)-oxide/hydroxide, while the peak at 713.9 eV is ascribed to the ferric compounds of Fe^{3+} (resulting from Fe_2O_3) [303-305]. Their corresponding satellites are appearing at 718.1 eV and 721.8 eV, respectively [292, 303-305]. The Fe $2p_{1/2}$ spin exhibits a peak at 724.6 eV, which corresponds to Fe(0) [292]. The peak at 727.8 eV is related to Fe(II), and the peak at 730.4 eV is attributed to Fe(III), and their corresponding satellites are appearing at 733.1 eV, and 735.7 eV, respectively [292, 294, 303-305]. These peaks and their satellites indicate the existence of metal oxides and hydroxides, and agreeing with deconvoluted peaks of O 1s. The peak with lower binding energy at 706.9 eV appeared on the sample immersed in electrolytes containing SC and SC-SDS as can be seen in Fig.15h and 15i is attributed to the presence of metallic iron Fe(0) (uncorroded iron) [292, 303-305]. It should be pointed out that the intensity of Fe-related vibrations recorded on the CS samples that were immersed in the inhibitor-containing solutions (Figs. 15h and 15i) are lower than those recorded in the absence of the inhibitor (Fig 5. 15g), which agrees with the results in Figs. 15d,15 e and 15f, and is due to the presence of SC and SC+SDS on the CS surface.

The existence of SDS adsorbed on the CS surface is also evident from the S 2p spectra presented in Fig 5. 15j. This spectrum could be deconvoluted into two main components centered at the binding energies at 169.1 and 170.4 eV, which can be associated with the existence of sulphates [306]. The O 1s (Fig 5. 15f) and S 2p (Fig 5. 15j) spectra suggest the presence of sulphate groups in the form of S=O and $(SO_3)^-$ [299-301]. In addition, the appearance of these peaks on the S 2p spectrum can be correlated with the formation of the Fe-S complex [307, 308].

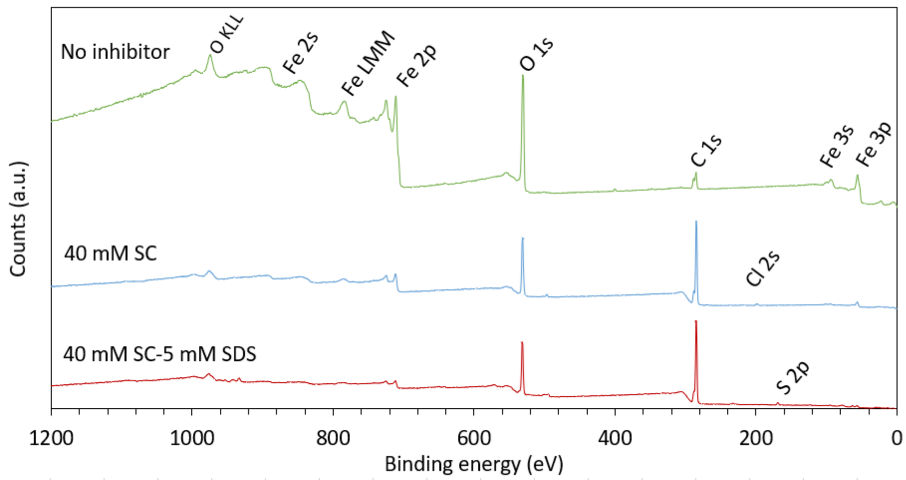

Fig 5. 14 XPS survey spectra of carbon steel samples immersed in 0.5 M HCl solution for 24 h in the absence (top) and presence (bottom) of inhibitor at a concentration of 40 mM SC, and 40 mM SC+5 mM SDS at room temperature.

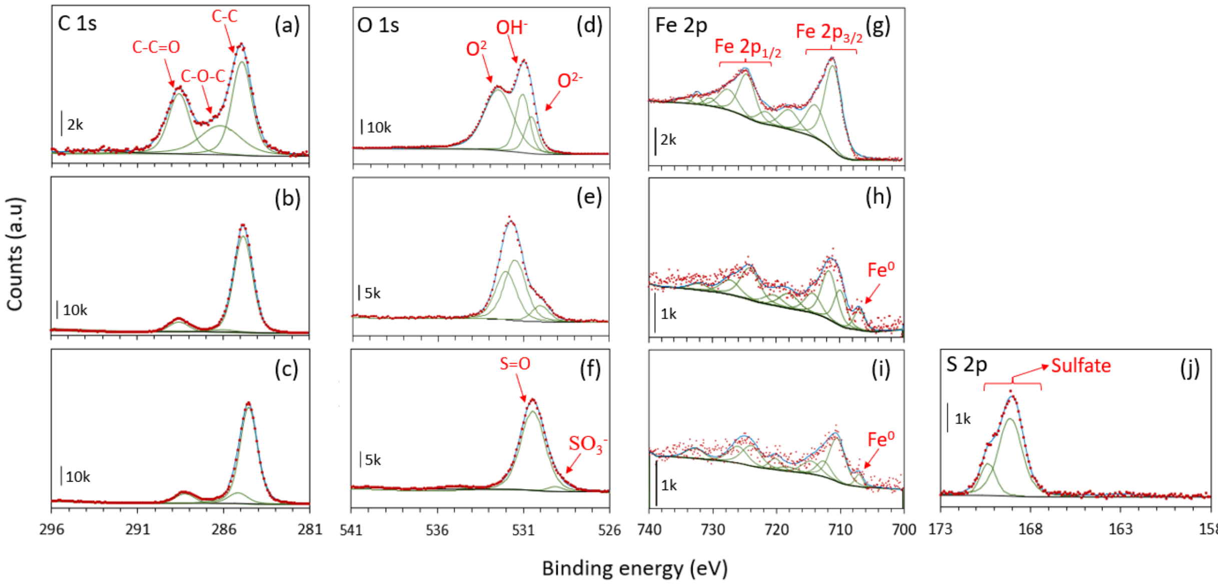

Fig 5. 15 High-resolution deconvoluted XPS spectra of C 1s, O 1s, Fe 2p, and S 2p. Plots (a), (d), and (g) for C 1s, O 1s, Fe 2p, respectively, for CS immersed in 0.5 M HCl solution for 24 h in the absence of inhibitor, Plots (b), (e), and (h) for C 1s, O 1s, Fe 2p, respectively, for CS immersed in 0.5 M HCl solution containing 40 mM SC for 24 h, and plots (c), (f), (i), and (j) for C 1s, O 1s, Fe 2p, S 2p, respectively, for CS immersed in 0.5 M HCl solution containing 40 mM SC+5 mM SDS.

5.5 Conclusions

The potential use of SC and its mixture with SDS as a green molecule for inhibition of CS corrosion in aqueous HCl was investigated using EIS, Tafel polarization, SEM, XPS, and contact angle techniques under different experimental conditions. The following conclusions could summarize the work:

- SC and SC+SDS were found to act as good corrosion inhibitors for CS immersed in aqueous HCl of different concentrations.
- SC and SC-SDS were found to be mixed-type inhibitors.
- The addition of only 5 mM of SDS to the SC-containing electrolyte resulted in a significant increase in the inhibition efficiency.
- After 48 hours of immersion in 0.5M HCl and at 295K, the corrosion inhibition efficiency was ca. 89% for SC and ca. 98% for SC+SDS.
- The corrosion protection mechanism was associated with the spontaneous adsorption of SC and SC-SDS on the CS surface to form a protective physical layer representing a barrier to the transport of corrosive species from the electrolyte to the CS surface.
- The adsorption of both SC and SC-SDS on the CS surface was described by the Langmuir adsorption isotherm.
- The adsorption kinetics of SC and SC-SDS was found to be relatively quick, achieving a maximum inhibition efficiency after ca. 60 min.
- The desorption and temperature-dependent measurements revealed that the adsorptive bond between the CS surface and the inhibitor was relatively strong, and that the molecules offered high corrosion protection even at elevated temperatures.
- XPS suggested that SC is adsorbed on the CS surface through the interaction of its carboxylate group with iron, while the SC+SDS mixture interacted with the CS surface through the SC's carboxylate group and through the thiophenic sulfur in SDS.

- The measured contact angles evidenced that the adsorbed SC and SC+SDS layer rendered the CS surface more hydrophobic, providing a more resistive barrier to the transport of hydrated corrosive species to the CS surface.

Acknowledgements

The authors would like to convey their gratitude to the Qatar National Research Fund (QNRF) under the QRLP postgraduate award granted to Mr. Ahmad Diraki, to the Natural Science and Engineering Council of Canada (NSERC), and to the Chemical Engineering Department at McGill University.

Funding

This work was supported by Qatar National Research Fund (QNRF) under QRLP postgraduate award and by the Natural Science and Engineering Council of Canada (NSERC).

5.6 Supplementary Information

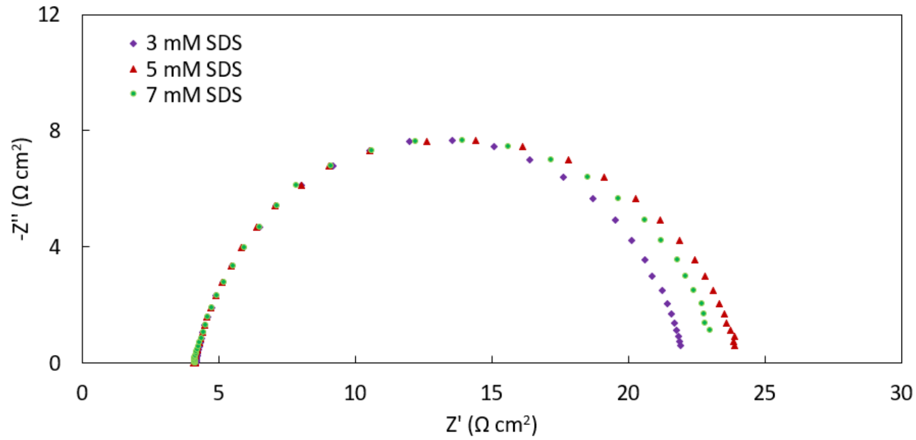

Fig. 5-S. 1 Nyquist plots of CS recorded at OCP and 295 K in the presence of only SDS in 0.5 M HCl solution.

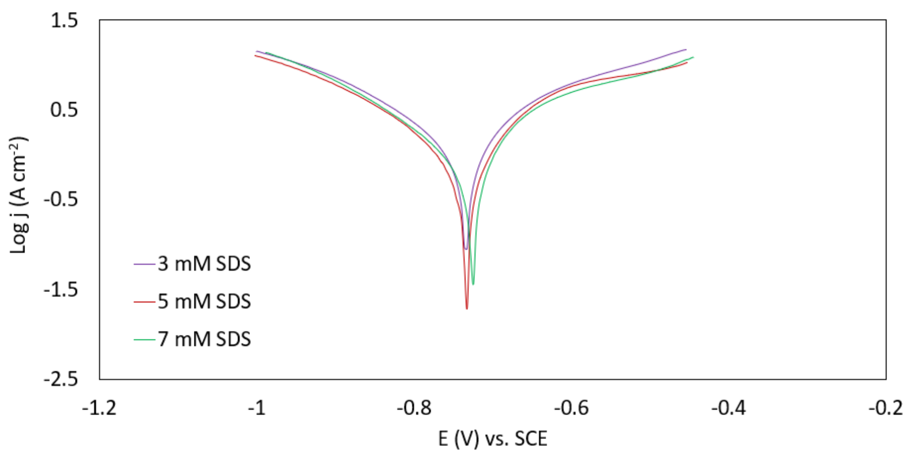

Fig. 5-S. 2 Tafel plots of CS recorded at 295 K in 0.5 M HCl in the presence of only SDS in the solution, and at a scan rate of 1 mV s^{-1}.

Chapter 6

Conclusions

This Ph.D. thesis reports and discusses results

(i) on the development of two types of outer-wall long-term corrosion protection composite/multilayered coatings based on in-house synthesized polyaniline and commercial epoxy for potential use for oil and gas pipelines constructed of CS and immersed in water containing 3.5 wt.% NaCl. To achieve this, a double-layered coating based on the inner electrically conductive polyaniline (PANI) layer doped with graphene oxide (GO) was synthesized electrochemically directly on the CS surface, and the outer commercial epoxy coating was applied on top of the PANI/GO layer. Moreover, a *smart* double-layered coating based on the inner PANI layer, electrochemically formed on the CS surface and doped with sodium caprylate (SC) and sodium dodecyl sulphonate (SDS) as a corrosion inhibitor mixture, and the outer commercial epoxy layer, was also synthesized and characterized.

(ii) on the investigation of an environmentally friendly corrosion inhibitor mix as a possible means for controlling the inner-wall corrosion of CS immersed in HCl.

The work reported throughout this Ph.D. research project in Chapters 3-5 led to the key conclusions summarized in the following sections:

Chapter 3: Anti-corrosive Properties of the Double-layer PANI/graphene-oxide/epoxy Coating in Protecting Carbon Steel in Salt Water

- The optimal GO concentration in the PANI layer was 0.01 wt.%.
- The cross-section SEM images showed the thickness of the layers, 5 μm for PANI/GO, 20 μm for epoxy, and 25 μm for the double layer PANI/GO/epoxy.
- Profilometry measurements also revealed that the thickness of the PANI and PANI/GO coatings was 4.84±0.12 μm, while the epoxy coating was substantially thicker, 20.6±0.2 μm,

and the thickness of the double layer PANI/epoxy and PANI/GO/epoxy coatings was 24.9±0.1 μm.

- The electrochemical results showed that the commercial epoxy coating started gradually failing several days after exposure to the electrolyte. At the same time, it took 37 days for larger pores to appear in the PANI/epoxy coating, which gradually continued to fail.
- On the other hand, the double-layer PANI/GO/epoxy coating offered significantly better long-term anti-corrosive properties, maintaining its structural integrity over 60 days of constant exposure to the corrosive electrolyte.
- EIS showed a 6 order of magnitude higher corrosion resistance for the double-layer PANI/GO/epoxy coated CS in comparison with the unprotected surface.
- The excellent corrosion protection properties of the double-layer coating were prescribed solely to the presence of the underlying PANI/GO layer, which represents a high barrier for the transport of hydrated corrosive ions to the CS surface, through the combined action of charge repulsion and passive oxide film formation, surface energy (hydrophobicity), and blocking mechanisms.
- The FTIR-ATR showed a marked alteration in the characteristic peaks, confirming the formation of new chemical bonds between PANI and graphene oxide (GO), and evidenced the successful incorporation of GO into the PANI coating.

Chapter 4: Smart PANI/epoxy Anti-corrosive Coating for Protection of Carbon Steel in Sea Water

- It was determined that the SC-SDS-doped coating could almost completely recover its anti-corrosive properties within one day upon creating the damage (scratch) in the coating penetrating to the CS surface, sustaining the high level of corrosion protection for the remaining 29 days of constant exposure to the corrosive solution.
- On the other hand, the anti-corrosive properties of the damaged undoped coating deteriorated very quickly (within hours) and continued to deteriorate with time.
- The mechanism of “smart” protection of the doped coating was postulated to be through the release of the dopant (SC-SDS) from the PANI layer at the damaged coating site, driven by a potential difference between the reducing PANI layer and oxidizing (corroding) CS surface.

- This was followed by the adsorption of SC-SDS on the CS surface exposed to the electrolyte and its protection through the formation of a molecular SC-SDS layer offering a barrier for transport of corrosive species to the CS surface.
- The doped coating yielded a hydrophobic surface and good adhesion to CS.
- The FT-IR spectrum of the PANI doped with SC-SDS showed alteration in the characteristic vibrations and appearance of the vibrations due to the incorporation of SC and SDS into the PANI coating

Chapter 5: The influence of the addition of sodium dodecyl sulfonate to sodium caprylate on the corrosion inhibition of carbon steel in aqueous HCl

- The potential use of SC and its mixture with SDS as a green molecule to inhibit CS corrosion in aqueous HCl was investigated using EIS, Tafel polarization, SEM, XPS, and contact angle techniques under different experimental conditions.
- The maximum corrosion inhibition efficiency of 87.9% for SC was achieved within 1 hour of CS immersion in 40 mM SC, while adding only 5 mM to SC boosted the inhibition efficiency to 94.2%.
- After 48 hours of immersion in 0.5M HCl and at 295K, the corrosion inhibition efficiency was maintained, slightly increasing to ca. 89% for SC and ca. 98% for SC+SDS.
- The high inhibition performance was maintained even at higher temperatures.
- The Tafel polarization curves suggested that both SC and SC+SDS act as mixed-type inhibitors.
- The corrosion protection mechanism was associated with the spontaneous adsorption of SC and SC+SDS on the CS surface to form a protective physical layer representing a barrier to the transport of corrosive species from the electrolyte to the CS surface.
- The Langmuir adsorption isotherm described the adsorption of both SC and SC+SDS on the CS surface.
- SC and SC-SDS adsorption kinetics were relatively quick, achieving a maximum inhibition efficiency after ca. 60 min.

- XPS suggested that SC is adsorbed on the CS surface through the interaction of its carboxylate group with iron, while the SC+SDS mixture interacted with the CS surface through the SC's carboxylate group and the thiophenic sulfur in SDS.
- The measured contact angles evidenced that the adsorbed SC and SC+SDS layer rendered the CS surface more hydrophobic, providing a more resistive barrier to transport hydrated corrosive species to the CS surface.

Chapter 7

Original contributions and future work

7.1 Statement of original contributions

The following points present the main original contributions stemming from this work:

- Design, synthesis and characterization of a double-layer coating on carbon steel (CS) surface, composed of polyaniline (PANI) and epoxy, incorporating graphene oxide (GO) as a nanofiller in the PANI layer, and its use for corrosion protection of CS in simulated seawater.

- Design, synthesis and characterization of a smart double-layer coating on a CS surface, composed of an inner PANI and outer epoxy layer, the former incorporating sodium caprylate (SC) and sodium dodecyl sulfonate (SDS) as a corrosion inhibitor mixture that is released upon creating a damage in the coating, to continue protecting the CS surface immersed in simulated seawater.

- Results in this thesis represent the first study of the impact of adding a small amount of SDS to SC to investigate their synergistic effect on corrosion inhibition of CS in an acidic environment containing HCl.

7.2 Future work recommendations

The research work presented in this thesis confirmed the efficient long-term corrosion protection performance of a double-layer coating of PANI/GO-epoxy in protecting CS in simulated seawater, and the smart mechanism action under coating mechanical rupture of the double layer PANI-SC-SDS/epoxy coating in protecting CS in simulated seawater. Moreover, it outlines the investigation of the interactions between SC, SC-SDS as a corrosion inhibitor of CS in acidic aqueous HCl under various experimental conditions. However, the investigated system and the corresponding molecule/ surface interaction phenomena are complex and require more investigation. Hence, future opportunities originated from this research project include:

- Evaluate different graphene-based nanofillers in PANI in more detail, such as multilayer graphene sheets and/or functionalization of nanoparticles on graphene.

- Study the effects of the double layer coating corrosion protection performance by adding graphene into the epoxy layer instead of the PANI layer.

- Produce a double-layer coating composed of an inner PANI/SC-SDS layer and a top (outer) epoxy/GO layer and investigate if the system can act as a smart coating under mechanical rupture.

- Investigate the double layer coating corrosion protection performance in more detail at sample edges and under industrial conditions such as the impact of sea current, shear stress, and sunlight, the influence of temperature on the coating's performance, and the adhesion of epoxy on the PANI layer.

- Evaluate the double-layered coating's long-term performance under accelerated tests such as anodic polarization.

- Examine-in more details the inhibition performance of the mixture of SC and a small amount of SDS as corrosion inhibitors under the influence of the flow rate, high pressure, and in the presence of other factors commonly encountered in the oil and gas industry, such as the existence of dissolved crude oil that could be generated during the acidizing procedure in the petroleum industry.

References

[1] M. G. Fontana, *Corrosion engineering*. Tata McGraw-Hill Education, 2005.

[2] G. H. Koch, M. P. Brongers, N. G. Thompson, Y. P. Virmani, and J. H. Payer, "Corrosion cost and preventive strategies in the United States," 2002.

[3] F. Fragata, R. P. Salai, C. Amorim, and E. Almeida, "Compatibility and incompatibility in anticorrosive painting: The particular case of maintenance painting," *Progress in organic coatings,* vol. 56, no. 4, pp. 257-268, 2006.

[4] M. Pandey and M. Nessim, "Reliability-based inspection of post-tensioned concrete slabs," *Canadian Journal of Civil Engineering,* vol. 23, no. 1, pp. 242-249, 1996.

[5] S. Ghareba and S. Omanovic, "The effect of electrolyte flow on the performance of 12-aminododecanoic acid as a carbon steel corrosion inhibitor in CO2-saturated hydrochloric acid," *Corrosion Science,* vol. 53, no. 11, pp. 3805-3812, 2011.

[6] G. Shen, Y. Chen, and C. Lin, "Corrosion protection of 316 L stainless steel by a TiO 2 nanoparticle coating prepared by sol–gel method," *Thin Solid Films,* vol. 489, no. 1, pp. 130-136, 2005.

[7] L. Cecchetto, D. Delabouglise, and J.-P. Petit, "On the mechanism of the anodic protection of aluminium alloy AA5182 by emeraldine base coatings: Evidences of a galvanic coupling," *Electrochimica acta,* vol. 52, no. 11, pp. 3485-3492, 2007.

[8] G. Moretti, F. Guidi, and G. Grion, "Tryptamine as a green iron corrosion inhibitor in 0.5 M deaerated sulphuric acid," *Corrosion science,* vol. 46, no. 2, pp. 387-403, 2004.

[9] M. Zheludkevich, R. Serra, M. Montemor, I. M. Salvado, and M. Ferreira, "Corrosion protective properties of nanostructured sol–gel hybrid coatings to AA2024-T3," *Surface and Coatings Technology,* vol. 200, no. 9, pp. 3084-3094, 2006.

[10] V. S. Sastri, *Corrosion inhibitors: principles and applications* (no. Sirsi) i9780471976080). Wiley New York, 1998.

[11] N. M. Kaleli, F. Eroğlu, M. Şahin, M. Kalkan, and K. C. Emregül, "Assessment of the inhibitive behavior of a triazole based Schiff base compound in acidic media; an experimental and theoretical approach," *Journal of Molecular Structure,* vol. 1227, p. 129700, 2021.

[12] T. Yan *et al.*, "Investigation of imidazole derivatives as corrosion inhibitors of copper in sulfuric acid: combination of experimental and theoretical researches," *Journal of the Taiwan Institute of Chemical Engineers,* vol. 106, pp. 118-129, 2020.

[13] V. S. Sastri, *Green corrosion inhibitors: theory and practice*. John Wiley & Sons, 2012.

[14] D. K. Chattopadhyay and K. Raju, "Structural engineering of polyurethane coatings for high performance applications," *Progress in polymer science,* vol. 32, no. 3, pp. 352-418, 2007.

[15] G. Gonçalves, A. Baldissera, L. Rodrigues Jr, E. Martini, and C. Ferreira, "Alkyd coatings containing polyanilines for corrosion protection of mild steel," *Synthetic metals,* vol. 161, no. 3-4, pp. 313-323, 2011.

[16] M. Sieber *et al.*, "Corrosion protection of Al/Mg compounds by simultaneous plasma electrolytic oxidation," *Materials Today: Proceedings,* vol. 2, pp. S149-S155, 2015.

[17] D. Merkula, P. Novikov, V. Ivanenkov, V. Sapozhnikov, and Y. Lyakhin, "Utilization of EDN varnish for protection of metal sea-water sampling bottles against corrosion," *OCEANOLOGY-USSR,* vol. 14, no. 2, pp. 299-300, 1974.

[18] M. Stratmann, R. Feser, and A. Leng, "Corrosion protection by organic films," *Electrochimica Acta,* vol. 39, no. 8-9, pp. 1207-1214, 1994.

[19] C.-H. Chang *et al.*, "Novel anticorrosion coatings prepared from polyaniline/graphene composites," *Carbon,* vol. 50, no. 14, pp. 5044-5051, 2012.

[20] D. W. DeBerry, "Modification of the electrochemical and corrosion behavior of stainless steels with an electroactive coating," *Journal of the Electrochemical society,* vol. 132, no. 5, p. 1022, 1985.

[21] V. Mišković-Stanković, J. Zotović, Z. Kačarević-Popović, and M. D. Maksimović, "Corrosion behaviour of epoxy coatings electrodeposited on steel electrochemically modified by Zn–Ni alloy," *Electrochimica acta,* vol. 44, no. 24, pp. 4269-4277, 1999.

[22] Y. Wei, L. Zhang, and W. Ke, "Evaluation of corrosion protection of carbon black filled fusion-bonded epoxy coatings on mild steel during exposure to a quiescent 3% NaCl solution," *Corrosion science,* vol. 49, no. 2, pp. 287-302, 2007.

[23] Y.-X. Lan *et al.*, "Aniline pentamer-modified reduced graphene oxide/epoxy composites as anticorrosion coatings," *Materials Chemistry and Physics,* vol. 264, p. 124446, 2021.

[24] S. Kim *et al.*, "A solution-processable, nanostructured, and conductive graphene/polyaniline hybrid coating for metal-corrosion protection and monitoring," *Scientific reports,* vol. 7, no. 1, pp. 1-9, 2017.

[25] B. Wessling, "Passivation of metals by coating with polyaniline: corrosion potential shift and morphological changes," *Advanced Materials,* vol. 6, no. 3, pp. 226-228, 1994.

[26] N. Ahmad and A. G. MacDiarmid, "Inhibition of corrosion of steels with the exploitation of conducting polymers," *Synthetic Metals,* vol. 78, no. 2, pp. 103-110, 1996.

[27] D. Sazou and C. Georgolios, "Formation of conducting polyaniline coatings on iron surfaces by electropolymerization of aniline in aqueous solutions," *Journal of Electroanalytical Chemistry,* vol. 429, no. 1-2, pp. 81-93, 1997.

[28] S. P. Sitaram, J. O. Stoffer, and T. J. O'Keefe, "Application of conducting polymers in corrosion protection," *Journal of Coatings Technology,* vol. 69, no. 866, pp. 65-69, 1997.

[29] P. Zarras, J. D. Stenger-Smith, and Y. Wei, *Electroactive polymers for corrosion control*. ACS Publications, 2003.

[30] S. Biallozor and A. Kupniewska, "Conducting polymers electrodeposited on active metals," *Synthetic Metals,* vol. 155, no. 3, pp. 443-449, 2005.

[31] M. Khan, A. U. Chaudhry, S. Hashim, M. Zahoor, and M. Iqbal, "Recent developments in intrinsically conductive polymer coatings for corrosion protection," *Chemical Engineering Research Bulletin,* vol. 14, no. 2, pp. 73-86, 2010.

[32] S. De Souza, "Smart coating based on polyaniline acrylic blend for corrosion protection of different metals," *Surface and Coatings Technology,* vol. 201, no. 16-17, pp. 7574-7581, 2007.

[33] P. Kinlen, Y. Ding, and D. Silverman, "Corrosion protection of mild steel using sulfonic and phosphonic acid-doped polyanilines," *Corrosion,* vol. 58, no. 6, pp. 490-497, 2002.

[34] D. W. DeBerry, "Modification of the electrochemical and corrosion behavior of stainless steels with an electroactive coating," *Journal of the Electrochemical society,* vol. 132, no. 5, pp. 1022-1026, 1985.

[35] B. Liao, M. Song, H. Liang, and Y. Pang, "Polymer-layered silicate nanocomposites. 1. A study of poly (ethylene oxide)/Na+-montmorillonite nanocomposites as polyelectrolytes and polyethylene-block-poly (ethylene glycol) copolymer/Na+-montmorillonite nanocomposites as fillers for reinforcement of polyethylene," *Polymer,* vol. 42, no. 25, pp. 10007-10011, 2001.

[36] K. S. Novoselov *et al.*, "Electric field effect in atomically thin carbon films," *science,* vol. 306, no. 5696, pp. 666-669, 2004.

[37] C. Bao *et al.*, "Graphite oxide, graphene, and metal-loaded graphene for fire safety applications of polystyrene," *Journal of Materials Chemistry,* vol. 22, no. 32, pp. 16399-16406, 2012.

[38] J. R. Potts, O. Shankar, L. Du, and R. S. Ruoff, "Processing–morphology–property relationships and composite theory analysis of reduced graphene oxide/natural rubber nanocomposites," *Macromolecules,* vol. 45, no. 15, pp. 6045-6055, 2012.

[39] J. S. Barrett, A. A. Abdala, and F. Srienc, "Poly (hydroxyalkanoate) elastomers and their graphene nanocomposites," *Macromolecules,* vol. 47, no. 12, pp. 3926-3941, 2014.

[40] M. Li, X. Huang, C. Wu, H. Xu, P. Jiang, and T. Tanaka, "Fabrication of two-dimensional hybrid sheets by decorating insulating PANI on reduced graphene oxide for polymer nanocomposites with low dielectric loss and high dielectric constant," *Journal of Materials Chemistry,* vol. 22, no. 44, pp. 23477-23484, 2012.

[41] T. Ramanathan *et al.*, "Functionalized graphene sheets for polymer nanocomposites," *Nature nanotechnology,* vol. 3, no. 6, pp. 327-331, 2008.

[42] C. Macosko, "Graphene/Polymer Nanocomposites," in *APS Meeting Abstracts*, 2010, vol. 1, p. 19007.

[43] R. K. Layek and A. K. Nandi, "A review on synthesis and properties of polymer functionalized graphene," *Polymer,* vol. 54, no. 19, pp. 5087-5103, 2013.

[44] H. Kim *et al.*, "Graphene/polyethylene nanocomposites: effect of polyethylene functionalization and blending methods," *Polymer,* vol. 52, no. 8, pp. 1837-1846, 2011.

[45] K.-H. Liao, Y. T. Park, A. Abdala, and C. Macosko, "Aqueous reduced graphene/thermoplastic polyurethane nanocomposites," *Polymer,* vol. 54, no. 17, pp. 4555-4559, 2013.

[46] D. Chen, H. Zhu, and T. Liu, "In situ thermal preparation of polyimide nanocomposite films containing functionalized graphene sheets," *ACS applied materials & interfaces,* vol. 2, no. 12, pp. 3702-3708, 2010.

[47] Z. Xu and M. J. Buehler, "Geometry controls conformation of graphene sheets: membranes, ribbons, and scrolls," *Acs Nano,* vol. 4, no. 7, pp. 3869-3876, 2010.

[48] D. Prasai, J. C. Tuberquia, R. R. Harl, G. K. Jennings, and K. I. Bolotin, "Graphene: corrosion-inhibiting coating," *ACS nano,* vol. 6, no. 2, pp. 1102-1108, 2012.

[49] K. Chang *et al.*, "Advanced anticorrosive coatings prepared from electroactive polyimide/graphene nanocomposites with synergistic effects of redox catalytic capability and gas barrier properties," *eXPRESS Polym. Lett,* vol. 8, pp. 243-255, 2014.

[50] B. P. Singh, B. K. Jena, S. Bhattacharjee, and L. Besra, "Development of oxidation and corrosion resistance hydrophobic graphene oxide-polymer composite coating on copper," *Surface and Coatings Technology,* vol. 232, pp. 475-481, 2013.

[51] K.-C. Chang *et al.*, "Room-temperature cured hydrophobic epoxy/graphene composites as corrosion inhibitor for cold-rolled steel," *Carbon,* vol. 66, pp. 144-153, 2014.

[52] V. Chaker, *Corrosion forms and control for infrastructure*. ASTM International, 1992.

[53] W. D. Callister Jr and D. G. Rethwisch, *Fundamentals of materials science and engineering: an integrated approach*. John Wiley & Sons, 2020.

[54] S. Harsimran, K. Santosh, and K. Rakesh, "Overview of corrosion and its control: A critical review," *Proceedings on Engineering,* vol. 3, no. 1, pp. 13-24, 2021.

[55] M. Quraishi, D. S. Chauhan, and F. A. Ansari, "Development of environmentally benign corrosion inhibitors for organic acid environments for oil-gas industry," *Journal of Molecular Liquids,* vol. 329, p. 115514, 2021.

[56] L. Pang, Z. Wang, W. Emori, and Y. Zheng, "Under-Deposit Corrosion of Carbon Steel Beneath Full Coverage of CaCO3 Deposit Layer under Different Atmospheres," *Journal of Materials Engineering and Performance,* vol. 30, no. 10, pp. 7552-7563, 2021.

[57] M. S. Kamal, I. Hussein, M. Mahmoud, A. S. Sultan, and M. A. Saad, "Oilfield scale formation and chemical removal: A review," *Journal of petroleum science and engineering,* vol. 171, pp. 127-139, 2018.

[58] M. A. Quraishi, D. S. Chauhan, and V. S. Saji, *Heterocyclic organic corrosion inhibitors: principles and applications*. Elsevier, 2020.

[59] V. S. Saji and S. A. Umoren, *Corrosion inhibitors in the oil and gas industry*. John Wiley & Sons, 2020.

[60] B. J. Usman and S. A. Ali, "Carbon dioxide corrosion inhibitors: a review," *Arabian Journal for Science and Engineering,* vol. 43, no. 1, pp. 1-22, 2018.

[61] G. Koch, J. Varney, N. Thompson, O. Moghissi, M. Gould, and J. Payer, "International measures of prevention, application, and economics of corrosion technologies study," *NACE international,* vol. 216, pp. 2-3, 2016.

[62] T. E. Perez, "Corrosion in the oil and gas industry: an increasing challenge for materials," *Jom,* vol. 65, no. 8, pp. 1033-1042, 2013.

[63] G. Walter, "A critical review of the protection of metals by paints," *Corrosion Science,* vol. 26, no. 1, pp. 27-38, 1986.

[64] P. A. Sørensen, S. Kiil, K. Dam-Johansen, and C. Weinell, "Anticorrosive coatings: a review," *Journal of Coatings Technology and Research,* vol. 6, no. 2, pp. 135-176, 2009.

[65] D. M. Yebra, S. Kiil, and K. Dam-Johansen, "Antifouling technology—past, present and future steps towards efficient and environmentally friendly antifouling coatings," *Progress in organic Coatings,* vol. 50, no. 2, pp. 75-104, 2004.

[66] M. L. Zheludkevich, D. G. Shchukin, K. A. Yasakau, H. Möhwald, and M. G. Ferreira, "Anticorrosion coatings with self-healing effect based on nanocontainers impregnated with corrosion inhibitor," *Chemistry of Materials,* vol. 19, no. 3, pp. 402-411, 2007.

[67] C. G. Munger and L. D. Vincent, "Corrosion prevention by protective coatings," 1999.

[68] D. A. Jones, "Corrosion in selected corrosive environments," *Principles and Prevention of Corrosion, 2nd ed.(Upper Saddle River, NJ: Prentice Hall, 1996),* pp. 387-390, 1992.

[69] D. Gervasio, I. Song, and J. Payer, "Determination of the oxygen reduction products on ASTM A516 steel during cathodic protection," *Journal of applied electrochemistry,* vol. 28, no. 9, pp. 979-992, 1998.

[70] H. Wroblowa, "Intermediate products of atmospheric oxygen reduction and the integrity of metal—organic coating interface," *Journal of Electroanalytical Chemistry,* vol. 339, no. 1-2, pp. 31-40, 1992.

[71] H. Wroblowa and S. Qaderi, "Mechanism and kinetics of oxygen reduction on steel," *Journal of Electroanalytical Chemistry and Interfacial Electrochemistry,* vol. 279, no. 1-2, pp. 231-242, 1990.

[72] G. R. Brubaker and P. B. P. Phipps, *Corrosion chemistry*. ACS Publications, 1979.

[73] M. Finšgar and J. Jackson, "Application of corrosion inhibitors for steels in acidic media for the oil and gas industry: A review," *Corrosion science,* vol. 86, pp. 17-41, 2014.

[74] D. Kjernsmo, K. Kleven, and J. Scheie, *Corrosion Protection: Inspector's Book of Reference*. Hempel, 2003.

[75] D. Kjernsmo, K. Kleven, and J. Scheie, "Corrosion Protection, (2003)," ISBN 87-989694-0-4, HEMPEL A/S.

[76] C. May, *Epoxy resins: chemistry and technology*. Routledge, 2018.

[77] K. Kobayashi and K. Takewaka, "Experimental studies on epoxy coated reinforcing steel for corrosion protection," *International Journal of Cement Composites and Lightweight Concrete,* vol. 6, no. 2, pp. 99-116, 1984.

[78] N. J. Vickers, "Animal communication: when i'm calling you, will you answer too?," *Current biology,* vol. 27, no. 14, pp. R713-R715, 2017.

[79] Z. Yan, W. Liu, N. Gao, H. Wang, and K. Su, "Synthesis and properties of a novel UV-cured fluorinated siloxane graft copolymer for improved surface, dielectric and tribological properties of epoxy acrylate coating," *Applied surface science,* vol. 284, pp. 683-691, 2013.

[80] J. Kim, H. Im, and M. Cho, "Tribological performance of fluorinated polyimide-based nanocomposite coatings reinforced with PMMA-grafted-MWCNT," *Wear,* vol. 271, no. 7-8, pp. 1029-1038, 2011.

[81] Y. Sun *et al.*, "Mechanical and bonding properties of pristine montmorillonite reinforced epoxy asphalt bond coats," *Polymer Composites,* vol. 41, no. 8, pp. 3034-3042, 2020.

[82] W. Jian and D. Lau, "Understanding the effect of functionalization in CNT-epoxy nanocomposite from molecular level," *Composites Science and Technology,* vol. 191, p. 108076, 2020.

[83] R. Aradhana, S. Mohanty, and S. K. Nayak, "Comparison of mechanical, electrical and thermal properties in graphene oxide and reduced graphene oxide filled epoxy nanocomposite adhesives," *Polymer,* vol. 141, pp. 109-123, 2018.

[84] B. Grgur, M. Gvozdenović, V. B. Mišković-Stanković, and Z. Kačarević-Popović, "Corrosion behavior and thermal stability of electrodeposited PANI/epoxy coating system on mild steel in sodium chloride solution," *Progress in Organic Coatings,* vol. 56, no. 2-3, pp. 214-219, 2006.

[85] J. Hou, G. Zhu, J. Xu, and H. Liu, "Anticorrosion performance of epoxy coatings containing small amount of inherently conducting PEDOT/PSS on hull steel in seawater," *Journal of Materials Science & Technology,* vol. 29, no. 7, pp. 678-684, 2013.

[86] A. Zoshki, M. B. Rahmani, F. Masdarolomoor, and S. H. Pilehrood, "Room temperature gas sensing properties of polyaniline/ZnO nanocomposite thin films," *Journal of Nanoelectronics and Optoelectronics,* vol. 12, no. 5, pp. 465-471, 2017.

[87] K. Saravanan, S. Sathiyanarayanan, S. Muralidharan, S. S. Azim, and G. Venkatachari, "Performance evaluation of polyaniline pigmented epoxy coating for corrosion protection of steel in concrete environment," *Progress in Organic Coatings,* vol. 59, no. 2, pp. 160-167, 2007.

[88] A. Kalendová, D. Veselý, and J. Stejskal, "Organic coatings containing polyaniline and inorganic pigments as corrosion inhibitors," *Progress in Organic Coatings,* vol. 62, no. 1, pp. 105-116, 2008.

[89] J. Alam, U. Riaz, and S. Ahmad, "High performance corrosion resistant polyaniline/alkyd ecofriendly coatings," *Current Applied Physics,* vol. 9, no. 1, pp. 80-86, 2009.

[90] A. Sakhri, F. Perrin, E. Aragon, S. Lamouric, and A. Benaboura, "Chlorinated rubber paints for corrosion prevention of mild steel: A comparison between zinc phosphate and polyaniline pigments," *Corrosion Science,* vol. 52, no. 3, pp. 901-909, 2010.

[91] U. Riaz, S. Ahmad, and S. Ashraf, "Comparison of corrosion protective performance of nanostructured polyaniline and poly (1-naphthylamine)-based alkyd coatings on mild steel," *Materials and corrosion,* vol. 60, no. 4, pp. 280-286, 2009.

[92] R. Patil and S. Radhakrishnan, "Conducting polymer based hybrid nano-composites for enhanced corrosion protective coatings," *Progress in Organic Coatings,* vol. 57, no. 4, pp. 332-336, 2006.

[93] C.-W. Peng *et al.*, "Nano-casting technique to prepare polyaniline surface with biomimetic superhydrophobic structures for anticorrosion application," *Electrochimica Acta,* vol. 95, pp. 192-199, 2013.

[94] G. Kousik, S. Pitchumani, and N. Renganathan, "Electrochemical characterization of polythiophene-coated steel," *Progress in organic coatings,* vol. 43, no. 4, pp. 286-291, 2001.

[95] U. Rammelt, P. Nguyen, and W. Plieth, "Protection of mild steel by modification with thin films of polymethylthiophene," *Electrochimica Acta,* vol. 46, no. 26, pp. 4251-4257, 2001.

[96] C. Ocampo, E. Armelin, F. Liesa, C. Alemán, X. Ramis, and J. I. Iribarren, "Application of a polythiophene derivative as anticorrosive additive for paints," *Progress in organic coatings,* vol. 53, no. 3, pp. 217-224, 2005.

[97] D. Kowalski, M. Ueda, and T. Ohtsuka, "Corrosion protection of steel by bi-layered polypyrrole doped with molybdophosphate and naphthalenedisulfonate anions," *Corrosion science,* vol. 49, no. 3, pp. 1635-1644, 2007.

[98] P. Herrasti, A. Del Rio, and J. Recio, "Electrodeposition of homogeneous and adherent polypyrrole on copper for corrosion protection," *Electrochimica acta,* vol. 52, no. 23, pp. 6496-6501, 2007.

[99] G. Bereket and E. Hür, "The corrosion protection of mild steel by single layered polypyrrole and multilayered polypyrrole/poly (5-amino-1-naphthol) coatings," *Progress in Organic Coatings,* vol. 65, no. 1, pp. 116-124, 2009.

[100] W. Su and J. O. Iroh, "Electrodeposition mechanism, adhesion and corrosion performance of polypyrrole and poly (N-methylpyrrole) coatings on steel substrates," *Synthetic metals,* vol. 114, no. 3, pp. 225-234, 2000.

[101] M. Hosseini, M. Raghibi-Boroujeni, I. Ahadzadeh, R. Najjar, and M. S. Dorraji, "Effect of polypyrrole–montmorillonite nanocomposites powder addition on corrosion performance of epoxy coatings on Al 5000," *Progress in Organic Coatings,* vol. 66, no. 3, pp. 321-327, 2009.

[102] D. E. Tallman, K. L. Levine, C. Siripirom, V. G. Gelling, G. P. Bierwagen, and S. G. Croll, "Nanocomposite of polypyrrole and alumina nanoparticles as a coating filler for the corrosion protection of aluminium alloy 2024-T3," *Applied Surface Science,* vol. 254, no. 17, pp. 5452-5459, 2008.

[103] G. S. Akundy, R. Rajagopalan, and J. O. Iroh, "Electrochemical deposition of polyaniline–polypyrrole composite coatings on aluminum," *Journal of applied polymer science,* vol. 83, no. 9, pp. 1970-1977, 2002.

[104] R. Rajagopalan and J. Iroh, "Corrosion performance of polyaniline–polypyrrole composite coatings applied to low carbon steel," *Surface engineering,* vol. 18, no. 1, pp. 59-63, 2002.

[105] B. Wessling, "Corrosion prevention with an organic metal (polyaniline): surface ennobling, passivation, corrosion test results," *Materials and Corrosion,* vol. 47, no. 8, pp. 439-445, 1996.

[106] B. Wessling, "Corrosion prevention with an organic metal (polyaniline): Surface ennobling, passivation, corrosion tests results," *Paintindia,* vol. 52, no. 1, pp. 53-60, 2002.

[107] P. P. Deshpande, N. G. Jadhav, V. J. Gelling, and D. Sazou, "Conducting polymers for corrosion protection: a review," *Journal of Coatings Technology and Research,* vol. 11, no. 4, pp. 473-494, 2014.

[108] R. Gašparac and C. R. Martin, "Investigations of the mechanism of corrosion inhibition by polyaniline. Polyaniline-coated stainless steel in sulfuric acid solution," *Journal of The Electrochemical Society,* vol. 148, no. 4, pp. B138-B145, 2001.

[109] R. Hasanov and S. Bilgiç, "Monolayer and bilayer conducting polymer coatings for corrosion protection of steel in 1M H 2 SO 4 solution," *Progress in Organic Coatings,* vol. 64, no. 4, pp. 435-445, 2009.

[110] P. Chandrasekhar, *Conducting polymers, fundamentals and applications: a practical approach*. Springer Science & Business Media, 2013.

[111] R. M. Powell, R. W. Puls, S. K. Hightower, and D. A. Sabatini, "Coupled iron corrosion and chromate reduction: mechanisms for subsurface remediation," *Environmental Science & Technology,* vol. 29, no. 8, pp. 1913-1922, 1995.

[112] R. W. Revie, "Uhlig's corrosion handbook, John Wiley & Sons," *Inc., New York, USA,* pp. 1227-1238, 2000.

[113] H. Jafari, K. Akbarzade, and I. Danaee, "Corrosion inhibition of carbon steel immersed in a 1 M HCl solution using benzothiazole derivatives," *Arabian journal of chemistry,* vol. 12, no. 7, pp. 1387-1394, 2019.

[114] H. Saifi, S. Ouchenane, R. Bourenane, S. Boukerche, S. Joiret, and H. Takenouti, "Electrochemical behavior investigation of cysteine on nickel corrosion in acidic medium," *Journal of Failure Analysis and Prevention,* vol. 19, no. 6, pp. 1597-1606, 2019.

[115] J. Cui, R. Shi, and Y. Pei, "Novel inorganic solid controlled-release inhibitor for Q235-b anticorrosion treatment in 1 M HCl," *Applied Surface Science,* vol. 416, pp. 213-224, 2017.

[116] M. Saadawy, "Effect of inorganic anions on the pitting behaviour of austenitic stainless steel 304 in H2SO4 solution containing chloride ion," *International Journal of Electrochemical Science,* vol. 11, pp. 2345-2359, 2016.

[117] M. Mouanga, F. Andreatta, M.-E. Druart, E. Marin, L. Fedrizzi, and M.-G. Olivier, "A localized approach to study the effect of cerium salts as cathodic inhibitor on iron/aluminum galvanic coupling," *Corrosion Science,* vol. 90, pp. 491-502, 2015.

[118] T. V. Kulakovskaya, V. M. Vagabov, and I. S. Kulaev, "Inorganic polyphosphate in industry, agriculture and medicine: Modern state and outlook," *Process Biochemistry,* vol. 47, no. 1, pp. 1-10, 2012.

[119] A.-E. A. Hermas, A. M. Elnady, and R. M. Ali, "Corrosion inhibition of stainless steel in sulfuric acid solution containing sulfide ions," *Anti-Corrosion Methods and Materials,* 2019.

[120] L. Yohai, W. Schreiner, M. Vázquez, and M. Valcarce, "Phosphate ions as effective inhibitors for carbon steel in carbonated solutions contaminated with chloride ions," *Electrochimica Acta,* vol. 202, pp. 231-242, 2016.

[121] L. Yohai, M. Valcarce, and M. Vázquez, "Testing phosphate ions as corrosion inhibitors for construction steel in mortars," *Electrochimica Acta,* vol. 202, pp. 316-324, 2016.

[122] T. Harvey, F. Walsh, and A. Nahlé, "A review of inhibitors for the corrosion of transition metals in aqueous acids," *Journal of Molecular Liquids,* vol. 266, pp. 160-175, 2018.

[123] C. Verma, E. E. Ebenso, and M. Quraishi, "Corrosion inhibitors for ferrous and non-ferrous metals and alloys in ionic sodium chloride solutions: A review," *Journal of Molecular Liquids,* vol. 248, pp. 927-942, 2017.

[124] S. Marzorati, L. Verotta, and S. P. Trasatti, "Green corrosion inhibitors from natural sources and biomass wastes," *Molecules,* vol. 24, no. 1, p. 48, 2018.

[125] C. Verma, E. E. Ebenso, I. Bahadur, and M. Quraishi, "An overview on plant extracts as environmental sustainable and green corrosion inhibitors for metals and alloys in aggressive corrosive media," *Journal of molecular liquids,* vol. 266, pp. 577-590, 2018.

[126] C. Verma, E. E. Ebenso, and M. Quraishi, "Ionic liquids as green and sustainable corrosion inhibitors for metals and alloys: an overview," *Journal of Molecular Liquids,* vol. 233, pp. 403-414, 2017.

[127] S. A. Umoren and U. M. Eduok, "Application of carbohydrate polymers as corrosion inhibitors for metal substrates in different media: a review," *Carbohydrate polymers,* vol. 140, pp. 314-341, 2016.

[128] U. CEFAS, "Guidelines for the UK Revised Offshore Chemical Notification Scheme," *Burnham-on-Crouch, Essex, UK,* 2001.

[129] U. Osha, "Globally harmonized system of classification and labelling of chemicals (GHS)," *UN Econ. Comm. Eur,* vol. 224, 2013.

[130] Y.-Z. Long *et al.*, "Recent advances in synthesis, physical properties and applications of conducting polymer nanotubes and nanofibers," *Progress in Polymer Science,* vol. 36, no. 10, pp. 1415-1442, 2011.

[131] M. Woodson and J. Liu, "Guided growth of nanoscale conducting polymer structures on surface-functionalized nanopatterns," *Journal of the American Chemical Society,* vol. 128, no. 11, pp. 3760-3763, 2006.

[132] J. Stejskal, I. Sapurina, and M. Trchová, "Polyaniline nanostructures and the role of aniline oligomers in their formation," *Progress in Polymer Science,* vol. 35, no. 12, pp. 1420-1481, 2010.

[133] B. Yao, G. Wang, J. Ye, and X. Li, "Corrosion inhibition of carbon steel by polyaniline nanofibers," *Materials Letters,* vol. 62, no. 12, pp. 1775-1778, 2008.

[134] J. Stejskal, M. Exnerová, Z. Morávková, M. Trchová, J. Hromádková, and J. Prokeš, "Oxidative stability of polyaniline," *Polymer Degradation and Stability,* vol. 97, no. 6, pp. 1026-1033, 2012.

[135] X. Yang, B. Li, H. Wang, and B. Hou, "Anticorrosion performance of polyaniline nanostructures on mild steel," *Progress in Organic Coatings,* vol. 69, no. 3, pp. 267-271, 2010.

[136] G. Ćirić-Marjanović, "Recent advances in polyaniline composites with metals, metalloids and nonmetals," *Synthetic Metals,* vol. 170, pp. 31-56, 2013.

[137] H. Bhandari, S. A. Kumar, and S. Dhawan, "Conducting polymer nanocomposites for anticorrosive and antistatic applications," in *Nanocomposites-New Trends and Developments*: InTech, 2012.

[138] M. Ioniţă and A. Prună, "Polypyrrole/carbon nanotube composites: molecular modeling and experimental investigation as anti-corrosive coating," *Progress in Organic Coatings,* vol. 72, no. 4, pp. 647-652, 2011.

[139] M. Hosseini, R. Bagheri, and R. Najjar, "Electropolymerization of polypyrrole and polypyrrole-ZnO nanocomposites on mild steel and its corrosion protection performance," *Journal of Applied Polymer Science,* vol. 121, no. 6, pp. 3159-3166, 2011.

[140] C. Lee, X. Wei, J. W. Kysar, and J. Hone, "Measurement of the elastic properties and intrinsic strength of monolayer graphene," *science,* vol. 321, no. 5887, pp. 385-388, 2008.

[141] E. Stolyarova *et al.*, "Observation of graphene bubbles and effective mass transport under graphene films," *Nano letters,* vol. 9, no. 1, pp. 332-337, 2008.

[142] Y. Hu and X. Sun, "Chemically functionalized graphene and their applications in electrochemical energy conversion and storage," in *Advances in Graphene Science*: InTech, 2013.

[143] N. Kirkland, T. Schiller, N. Medhekar, and N. Birbilis, "Exploring graphene as a corrosion protection barrier," *Corrosion Science,* vol. 56, pp. 1-4, 2012.

[144] R. S. Raman *et al.*, "Protecting copper from electrochemical degradation by graphene coating," *Carbon,* vol. 50, no. 11, pp. 4040-4045, 2012.

[145] Y. Dong, Q. Liu, and Q. Zhou, "Corrosion behavior of Cu during graphene growth by CVD," *Corrosion science,* vol. 89, pp. 214-219, 2014.

[146] Y. Zhang *et al.*, "The distribution of wrinkles and their effects on the oxidation resistance of chemical vapor deposition graphene," *Carbon,* vol. 70, pp. 81-86, 2014.

[147] F. Hui, Y. Shi, Y. Ji, M. Lanza, and H. Duan, "Mechanical properties of locally oxidized graphene electrodes," *Archive of Applied Mechanics,* vol. 85, no. 3, pp. 339-345, 2015.

[148] K. Qi, Y. Sun, H. Duan, and X. Guo, "A corrosion-protective coating based on a solution-processable polymer-grafted graphene oxide nanocomposite," *Corrosion Science,* vol. 98, pp. 500-506, 2015.

[149] H. Zheng, Y. Shao, Y. Wang, G. Meng, and B. Liu, "Reinforcing the corrosion protection property of epoxy coating by using graphene oxide–poly (urea–formaldehyde) composites," *Corrosion Science,* 2017.

[150] V. A. Mooss, A. A. Bhopale, P. P. Deshpande, and A. A. Athawale, "Graphene oxide-modified polyaniline pigment for epoxy based anti-corrosion coatings," *Chemical Papers,* vol. 71, no. 8, pp. 1515-1528, 2017.

[151] B. Ramezanzadeh, M. M. Moghadam, N. Shohani, and M. Mahdavian, "Effects of highly crystalline and conductive polyaniline/graphene oxide composites on the corrosion protection performance of a zinc-rich epoxy coating," *Chemical Engineering Journal,* vol. 320, pp. 363-375, 2017.

[152] B. Ramezanzadeh, Z. Haeri, and M. Ramezanzadeh, "A facile route of making silica nanoparticles-covered graphene oxide nanohybrids (SiO 2-GO); fabrication of SiO 2-GO/epoxy composite coating with superior barrier and corrosion protection performance," *Chemical Engineering Journal,* vol. 303, pp. 511-528, 2016.

[153] N. Parhizkar, T. Shahrabi, and B. Ramezanzadeh, "A new approach for enhancement of the corrosion protection properties and interfacial adhesion bonds between the epoxy coating and steel substrate through surface treatment by covalently modified amino functionalized graphene oxide film," *Corrosion Science,* 2017.

[154] J. Mondal, A. Marques, L. Aarik, J. Kozlova, A. Simões, and V. Sammelselg, "Development of a thin ceramic-graphene nanolaminate coating for corrosion protection of stainless steel," *Corrosion Science,* vol. 105, pp. 161-169, 2016.

[155] B. Ramezanzadeh, A. Ahmadi, and M. Mahdavian, "Enhancement of the corrosion protection performance and cathodic delamination resistance of epoxy coating through treatment of steel substrate by a novel nanometric sol-gel based silane composite film filled with functionalized graphene oxide nanosheets," *Corrosion Science,* vol. 109, pp. 182-205, 2016.

[156] K. S. Aneja, H. M. Böhm, A. Khanna, and S. Böhm, "Functionalised graphene as a barrier against corrosion," *FlatChem,* vol. 1, pp. 11-19, 2017.

[157] S. Pourhashem, A. Rashidi, M. R. Vaezi, and M. R. Bagherzadeh, "Excellent corrosion protection performance of epoxy composite coatings filled with amino-silane functionalized graphene oxide," *Surface and Coatings Technology,* vol. 317, pp. 1-9, 2017.

[158] C. Glover, C. Richards, J. Baker, G. Williams, and H. McMurray, "In-coating graphene nano-platelets for environmentally-friendly corrosion protection of iron," *Corrosion Science,* vol. 114, pp. 169-172, 2017.

[159] Y. Jafari, S. Ghoreishi, and M. Shabani-Nooshabadi, "Polyaniline/graphene nanocomposite coatings on copper: electropolymerization, characterization, and evaluation of corrosion protection performance," *Synthetic Metals,* vol. 217, pp. 220-230, 2016.

[160] K. S. Aneja, S. Bohm, A. Khanna, and H. M. Bohm, "Graphene based anticorrosive coatings for Cr (VI) replacement," *Nanoscale,* vol. 7, no. 42, pp. 17879-17888, 2015.

[161] K. Cai *et al.*, "Preparation of polyaniline/graphene composites with excellent anti-corrosion properties and their application in waterborne polyurethane anticorrosive coatings," *RSC advances,* vol. 6, no. 98, pp. 95965-95972, 2016.

[162] A. Ambrosi and M. Pumera, "The structural stability of graphene anticorrosion coating materials is compromised at low potentials," *Chemistry–A European Journal,* vol. 21, no. 21, pp. 7896-7901, 2015.

[163] C. Qiu, D. Liu, K. Jin, L. Fang, G. Xie, and J. Robertson, "Electrochemical functionalization of 316 stainless steel with polyaniline-graphene oxide: Corrosion resistance study," *Materials Chemistry and Physics,* vol. 198, pp. 90-98, 2017.

[164] N. Wilds, "Corrosion under insulation," *Trends in oil and gas corrosion research and technologies,* pp. 409-429, 2017.

[165] S. Abd El Wanees, A. B. Radwan, M. Alsharif, and S. Abd El Haleem, "Initiation and inhibition of pitting corrosion on reinforcing steel under natural corrosion conditions," *Materials chemistry and physics,* vol. 190, pp. 79-95, 2017.

[166] E. Ituen, A. James, O. Akaranta, and S. Sun, "Eco-friendly corrosion inhibitor from Pennisetum purpureum biomass and synergistic intensifiers for mild steel," *Chinese Journal of Chemical Engineering,* vol. 24, no. 10, pp. 1442-1447, 2016.

[167] H. Kaur, J. Sharma, D. Jindal, R. K. Arya, S. K. Ahuja, and S. B. Arya, "Crosslinked polymer doped binary coatings for corrosion protection," *Progress in Organic Coatings,* vol. 125, pp. 32-39, 2018.

[168] P. Pradeepa, S. Edwinraj, and M. R. Prabhu, "Effects of ceramic filler in poly (vinyl chloride)/poly (ethyl methacrylate) based polymer blend electrolytes," *Chinese Chemical Letters,* vol. 26, no. 9, pp. 1191-1196, 2015.

[169] W. R. Wu *et al.*, "Surface Layering and Supersaturation for Top-Down Nanostructural Development during Spin Coating of Polymer/Fullerene Thin Films," *Advanced Energy Materials,* vol. 7, no. 14, p. 1601842, 2017.

[170] W. Chen *et al.*, "Compositionally modulated microstructure in nano-layered Ni-P metallic glass composite coating prepared by electrodeposition," *Surface and Coatings Technology,* vol. 389, p. 125636, 2020.

[171] Y. Zhou, A. E. Hartemink, Z. Shi, Z. Liang, and Y. Lu, "Land use and climate change effects on soil organic carbon in North and Northeast China," *Science of the Total Environment,* vol. 647, pp. 1230-1238, 2019.

[172] J.-M. Yeh, H.-Y. Huang, C.-L. Chen, W.-F. Su, and Y.-H. Yu, "Siloxane-modified epoxy resin–clay nanocomposite coatings with advanced anticorrosive properties prepared by a solution dispersion approach," *Surface and Coatings Technology,* vol. 200, no. 8, pp. 2753-2763, 2006.

[173] W.-F. Ji, M. M. Ahmed, K.-H. Luo, K.-Y. Chen, Y.-C. Lee, and J.-M. Yeh, "Epoxy thermoset coatings with fine controllable hierarchical structures prepared from bio-inspired photo-/colloidal lithography technique for anticorrosion application," *Progress in Organic Coatings,* vol. 152, p. 106132, 2021.

[174] M. Calovi, S. Rossi, F. Deflorian, S. Dire, and R. Ceccato, "Effect of functionalized graphene oxide concentration on the corrosion resistance properties provided by cataphoretic acrylic coatings," *Materials Chemistry and Physics,* vol. 239, p. 121984, 2020.

[175] M. Ascencio and S. Omanovic, "Investigation of the Corrosion Mechanism of WE43 Mg-Alloy in a Simulated Body Fluid: The Effect of Electrolyte Renewal," in *ECS Meeting Abstracts*, 2013, no. 14: IOP Publishing, p. 652.

[176] M. A. A. Pinedo, *Investigation of the Corrosion Behaviour of Bare and Polypyrrole-coated WE43 Magnesium Alloy for the Development of Biodegradable Implants*. McGill University (Canada), 2016.

[177] K.-C. Chang *et al.*, "Corrigendum to "Room-temperature cured hydrophobic epoxy/graphene composites as corrosion inhibitor for cold-rolled steel"[Carbon 66 (2014) 144–153]," *Carbon,* vol. 100, no. 82, p. 611, 2015.

[178] D. Nguyen *et al.*, "Synthesis of ethanol-soluble few-layer graphene nanosheets for flexible and transparent conducting composite films," *Nanotechnology,* vol. 22, no. 29, p. 295606, 2011.

[179] M. M. Ahmed and T. Imae, "Electrochemical properties of a thermally expanded magnetic graphene composite with a conductive polymer," *Physical Chemistry Chemical Physics,* vol. 18, no. 15, pp. 10400-10410, 2016.

[180] M. M. Ahmed and T. Imae, "Effect of external magnetic field on cyclic voltammetry of exfoliated graphene-based magnetic composites with conductive polymer and carbon dots," *Journal of Magnetism and Magnetic Materials,* vol. 491, p. 165604, 2019.

[181] K.-C. Chang *et al.*, "Advanced anticorrosive coatings prepared from electroactive polyimide/graphene nanocomposites with synergistic effects of redox catalytic capability and gas barrier properties," *Express Polymer Letters,* vol. 8, no. 4, 2014.

[182] M. d. F. Montemor, "Functional and smart coatings for corrosion protection: A review of recent advances," *Surface and Coatings Technology,* vol. 258, pp. 17-37, 2014.

[183] G. Eda and M. Chhowalla, "Chemically derived graphene oxide: towards large-area thin-film electronics and optoelectronics," *Advanced materials,* vol. 22, no. 22, pp. 2392-2415, 2010.

[184] S. P. Koenig, N. G. Boddeti, M. L. Dunn, and J. S. Bunch, "Ultrastrong adhesion of graphene membranes," *Nature nanotechnology,* vol. 6, no. 9, pp. 543-546, 2011.

[185] R. Berlia, M. P. Kumar, and C. Srivastava, "Electrochemical behavior of Sn–graphene composite coating," *RSC advances,* vol. 5, no. 87, pp. 71413-71418, 2015.

[186] A. A. Balandin *et al.*, "Superior thermal conductivity of single-layer graphene," *Nano letters,* vol. 8, no. 3, pp. 902-907, 2008.

[187] K. Rajitha and K. N. Mohana, "Application of modified graphene oxide–Polycaprolactone nanocomposite coating for corrosion control of mild steel in saline medium," *Materials Chemistry and Physics,* vol. 241, p. 122050, 2020.

[188] M. Selvam, K. Saminathan, P. Siva, P. Saha, and V. Rajendran, "Corrosion behavior of Mg/graphene composite in aqueous electrolyte," *Materials chemistry and physics,* vol. 172, pp. 129-136, 2016.

[189] A. Nautiyal and S. Parida, "Comparison of polyaniline electrodeposition on carbon steel from oxalic acid and salicylate medium," *Progress in Organic Coatings,* vol. 94, pp. 28-33, 2016.

[190] J. Camalet, J. Lacroix, S. Aeiyach, K. Chane-Ching, and P. Lacaze, "Electrosynthesis of adherent polyaniline films on iron and mild steel in aqueous oxalic acid medium," *Synthetic Metals,* vol. 93, no. 2, pp. 133-142, 1998.

[191] Y. Jafari, S. M. Ghoreishi, and M. Shabani-Nooshabadi, "Electrochemical deposition and characterization of polyaniline-graphene nanocomposite films and its corrosion protection properties," *Journal of Polymer Research,* vol. 23, no. 5, p. 91, 2016.

[192] D. Astm, "D3359-Standard test method for measuring adhesion by tape test," *Tool and Tape,* 2002.

[193] L. R. Vargas, A. K. Poli, R. d. C. L. Dutra, C. B. d. Souza, M. R. Baldan, and E. S. Gonçalves, "Formation of composite polyaniline and graphene oxide by physical mixture method," *Journal of Aerospace Technology and Management,* vol. 9, pp. 29-38, 2017.

[194] S. Yang, S. Zhu, and R. Hong, "Graphene oxide/polyaniline nanocomposites used in anticorrosive coatings for environmental protection," *Coatings,* vol. 10, no. 12, p. 1215, 2020.

[195] X. Zhao, S. Liu, and B. R. Hou, "A Comparative Study of Neat Epoxy Coating and NanoZrO2/Epoxy Coating for Corrosion Protection on Carbon Steel," in *Applied Mechanics and Materials*, 2014, vol. 599: Trans Tech Publ, pp. 3-6.

[196] S. Palaniappan, "Chemical and electrochemical polymerization of aniline using tartaric acid," *European polymer journal,* vol. 37, no. 5, pp. 975-981, 2001.

[197] K. Kamaraj, S. Sathiyanarayanan, S. Muthukrishnan, and G. Venkatachari, "Corrosion protection of iron by benzoate doped polyaniline containing coatings," *Progress in Organic Coatings,* vol. 64, no. 4, pp. 460-465, 2009.

[198] Y. Zhang *et al.*, "A study on corrosion protection of different polyaniline coatings for mild steel," *Progress in Organic Coatings,* vol. 111, pp. 240-247, 2017.

[199] A. Mirmohseni, M. Azizi, and M. S. S. Dorraji, "Cationic graphene oxide nanosheets intercalated with polyaniline nanofibers: A promising candidate for simultaneous anticorrosion, antistatic, and antibacterial applications," *Progress in Organic Coatings,* vol. 139, p. 105419, 2020.

[200] N. Ö. Pekmez, E. Abacı, K. Cınkıllı, and A. Yağan, "Polybithiophene and its bilayers with polyaniline coatings on stainless steel by electropolymerization in aqueous medium," *Progress in Organic Coatings,* vol. 65, no. 4, pp. 462-468, 2009.

[201] F. S. Omar, A. Numan, N. Duraisamy, M. M. Ramly, K. Ramesh, and S. Ramesh, "Binary composite of polyaniline/copper cobaltite for high performance asymmetric supercapacitor application," *Electrochimica Acta,* vol. 227, pp. 41-48, 2017.

[202] P. Manivel, M. Dhakshnamoorthy, A. Balamurugan, N. Ponpandian, D. Mangalaraj, and C. Viswanathan, "Conducting polyaniline-graphene oxide fibrous nanocomposites: preparation, characterization and simultaneous electrochemical detection of ascorbic acid, dopamine and uric acid," *Rsc Advances,* vol. 3, no. 34, pp. 14428-14437, 2013.

[203] T. N. A. B. T. A. Mutalib, S. J. Tan, K. L. Foo, Y. M. Liew, C. Y. Heah, and M. M. A. B. Abdullah, "Properties of polyaniline/graphene oxide (PANI/GO) composites: effect of GO loading," *Polymer Bulletin,* vol. 78, no. 9, pp. 4835-4847, 2021.

[204] K.-C. Chang *et al.*, "Synergistic effects of hydrophobicity and gas barrier properties on the anticorrosion property of PMMA nanocomposite coatings embedded with graphene nanosheets," *Polymer Chemistry,* vol. 5, no. 3, pp. 1049-1056, 2013.

[205] N. H. Othman, M. C. Ismail, M. Mustapha, N. Sallih, K. E. Kee, and R. A. Jaal, "Graphene-based polymer nanocomposites as barrier coatings for corrosion protection," *Progress in Organic Coatings,* vol. 135, pp. 82-99, 2019.

[206] M. Sababi, H. Terryn, and J. Mol, "The influence of a Zr-based conversion treatment on interfacial bonding strength and stability of epoxy coated carbon steel," *Progress in Organic Coatings,* vol. 105, pp. 29-36, 2017.

[207] J. Bajat, V. Mišković-Stanković, J. P. Popić, and D. M. Dražić, "Adhesion characteristics and corrosion stability of epoxy coatings electrodeposited on phosphated hot-dip galvanized steel," *Progress in organic coatings,* vol. 63, no. 2, pp. 201-208, 2008.

[208] E. McCafferty, "Validation of corrosion rates measured by the Tafel extrapolation method," *Corrosion science,* vol. 47, no. 12, pp. 3202-3215, 2005.

[209] Z. Hu *et al.*, "Superior anti-corrosion performance on Cu substrate achieved by dense polypropylene coating with ultrahigh inhibition efficiency deposited via the environmental-friendly method," *Corrosion Science,* p. 109783, 2021.

[210] T.-H. Le, Y. Kim, and H. Yoon, "Electrical and electrochemical properties of conducting polymers," *Polymers,* vol. 9, no. 4, p. 150, 2017.

[211] T. Ohtsuka, "Corrosion protection of steels by conducting polymer coating," *International Journal of Corrosion,* vol. 2012, 2012.

[212] Y. Wei, J. Wang, X. Jia, J.-M. Yeh, and P. Spellane, "Polyaniline as corrosion protection coatings on cold rolled steel," *Polymer,* vol. 36, no. 23, pp. 4535-4537, 1995.

[213] A. Alrebh, M. B. Rammal, and S. Omanovic, "A pyridine derivative 2-(2-Methylaminoethyl) pyridine (MAEP) as a ‘green’corrosion inhibitor for low-carbon steel in hydrochloric acid media," *Journal of Molecular Structure,* vol. 1238, p. 130333, 2021.

[214] W. Fan, H. Wang, C. Wang, Z. Liu, K. Li, and Y. Zhu, "A sustainable dynamic redox reaction passive film for long-term anti-corrosion of carbon steel surface," *Journal of Colloid and Interface Science,* vol. 580, pp. 146-159, 2020.

[215] A. Damian and S. Omanovic, "Electrochemical reduction of NAD+ on a polycrystalline gold electrode," *Journal of Molecular Catalysis A: Chemical,* vol. 253, no. 1-2, pp. 222-233, 2006.

[216] T. Rout, G. Jha, A. Singh, N. Bandyopadhyay, and O. Mohanty, "Development of conducting polyaniline coating: a novel approach to superior corrosion resistance," *Surface and Coatings Technology,* vol. 167, no. 1, pp. 16-24, 2003.

[217] N.-T. Nguyen, S.-S. Ho, and C. L.-N. Low, "A polymeric microgripper with integrated thermal actuators," *Journal of Micromechanics and Microengineering,* vol. 14, no. 7, p. 969, 2004.

[218] R. Maurya, A. R. Siddiqui, P. K. Katiyar, and K. Balani, "Mechanical, tribological and anti-corrosive properties of polyaniline/graphene coated Mg-9Li-7Al-1Sn and Mg-9Li-5Al-3Sn-1Zn alloys," *Journal of Materials Science & Technology,* vol. 35, no. 8, pp. 1767-1778, 2019.

[219] S. Zhou, Y. Wu, W. Zhao, J. Yu, F. Jiang, and L. Ma, "Comparative corrosion resistance of graphene sheets with different structures in waterborne epoxy coatings," *Colloids and Surfaces A: Physicochemical and Engineering Aspects,* vol. 556, pp. 273-283, 2018.

[220] J.-H. Ding, H.-R. Zhao, Y. Zheng, X. Zhao, and H.-B. Yu, "A long-term anticorrsive coating through graphene passivation," *Carbon,* vol. 138, pp. 197-206, 2018.

[221] B. Ramezanzadeh, S. Niroumandrad, A. Ahmadi, M. Mahdavian, and M. M. Moghadam, "Enhancement of barrier and corrosion protection performance of an epoxy coating through wet transfer of amino functionalized graphene oxide," *Corrosion Science,* vol. 103, pp. 283-304, 2016.

[222] H. Lu, S. Zhang, W. Li, Y. Cui, and T. Yang, "Synthesis of graphene oxide-based sulfonated oligoanilines coatings for synergistically enhanced corrosion protection in 3.5% NaCl solution," *ACS applied materials & interfaces,* vol. 9, no. 4, pp. 4034-4043, 2017.

[223] F. Cheng, "Monitor safety of aged fuel pipelines," *Nature,* vol. 529, no. 7585, pp. 156-156, 2016.

[224] C. Liu, S. Qiu, P. Du, H. Zhao, and L. Wang, "An ionic liquid–graphene oxide hybrid nanomaterial: synthesis and anticorrosive applications," *Nanoscale,* vol. 10, no. 17, pp. 8115-8124, 2018.

[225] A. Ghazi, E. Ghasemi, M. Mahdavian, B. Ramezanzadeh, and M. Rostami, "The application of benzimidazole and zinc cations intercalated sodium montmorillonite as smart ion exchange inhibiting pigments in the epoxy ester coating," *Corrosion Science,* vol. 94, pp. 207-217, 2015.

[226] J. Dong, W. Pan, J. Luo, and R. Liu, "Synthesis of inhibitor-loaded polyaniline microcapsules with dual anti-corrosion functions for protection of carbon steel," *Electrochimica Acta,* vol. 364, p. 137299, 2020.

[227] P. B. Raja and M. G. Sethuraman, "Natural products as corrosion inhibitor for metals in corrosive media—a review," *Materials letters,* vol. 62, no. 1, pp. 113-116, 2008.

[228] M. Kendig, A. Davenport, and H. Isaacs, "The mechanism of corrosion inhibition by chromate conversion coatings from X-ray absorption near edge spectroscopy (XANES)," *Corrosion Science,* vol. 34, no. 1, pp. 41-49, 1993.

[229] X. Shi and N. Dalal, "Generation of hydroxyl radical by chromate in biologically relevant systems: role of Cr (V) complexes versus tetraperoxochromate (V)," *Environmental health perspectives,* vol. 102, no. suppl 3, pp. 231-236, 1994.

[230] V. Dalmoro, S. Cedron, D. S. Azambuja, and K. R. L. Castagno, "Polypyrrole film doped with corrosion-inhibitors electropolymerized on AA 1100," *Materials Research,* vol. 22, 2019.

[231] Z. Hu *et al.*, "Superior anti-corrosion performance on Cu substrate achieved by dense polypropylene coating with ultrahigh inhibition efficiency deposited via the environmental-friendly method," *Corrosion Science,* vol. 191, p. 109783, 2021.

[232] P. Sambyal, G. Ruhi, R. Dhawan, and S. K. Dhawan, "Designing of smart coatings of conducting polymer poly (aniline-co-phenetidine)/SiO2 composites for corrosion protection in marine environment," *Surface and Coatings Technology,* vol. 303, pp. 362-371, 2016.

[233] A. Kalendová, D. Veselý, M. Kohl, and J. Stejskal, "Effect of surface treatment of pigment particles with polypyrrole and polyaniline phosphate on their corrosion inhibiting properties in organic coatings," *Progress in Organic Coatings,* vol. 77, no. 9, pp. 1465-1483, 2014.

[234] L. Zhang, W. Du, A. Nautiyal, Z. Liu, and X. Zhang, "Recent progress on nanostructured conducting polymers and composites: synthesis, application and future aspects," *Science China Materials,* vol. 61, no. 3, pp. 303-352, 2018.

[235] X.-Z. Gao, H.-J. Liu, F. Cheng, and Y. Chen, "Thermoresponsive polyaniline nanoparticles: Preparation, characterization, and their potential application in waterborne anticorrosion coatings," *Chemical Engineering Journal,* vol. 283, pp. 682-691, 2016.

[236] Y. Feng and Y. F. Cheng, "An intelligent coating doped with inhibitor-encapsulated nanocontainers for corrosion protection of pipeline steel," *Chemical Engineering Journal,* vol. 315, pp. 537-551, 2017.

[237] Z. Chen, W. Yang, Y. Chen, X. Yin, and Y. Liu, "Smart coatings embedded with polydopamine-decorated layer-by-layer assembled SnO2 nanocontainers for the corrosion protection of 304 stainless steels," *Journal of Colloid and Interface Science,* vol. 579, pp. 741-753, 2020.

[238] S. Khasim and A. Pasha, "Enhanced corrosion protection of A-36 steel using epoxy-reinforced CSA-doped polyaniline-SnO 2 nanocomposite smart coatings," *Journal of Bio-and Tribo-Corrosion,* vol. 7, no. 1, pp. 1-11, 2021.

[239] X. Zhu, J. Zhao, and C. Wang, "Acid and base dual-controlled cargo molecule release from polyaniline gated-hollow mesoporous silica nanoparticles," *Polymer Chemistry,* vol. 7, no. 42, pp. 6467-6474, 2016.

[240] A.Diraki and S. Omanovic, "Anti-corrosive Properties of the Double-layer PANI/graphene-oxide/epoxy Coating in Protecting Carbon Steel in Salt Water," *Progress in Organic Coatings,* vol. submitted, no. submitted, p. submitted, March (2022).

[241] S. Ghareba and S. Omanovic, "Corrosion inhibition of carbon steel in sulfuric acid by sodium caprylate," *Balance,* vol. 100, pp. 74-84, 2016.

[242] H. Zhao, S. Li, R. Lin, B. Yang, and L. Zhang, "Effect of curing agent content on properties of zinc-rich epoxy primer nano-coating," in *IOP Conference Series: Earth and Environmental Science*, 2019, vol. 252, no. 2: IOP Publishing, p. 022047.

[243] Y. Negishi, T. Sakai, H. Sembokuya, M. Kubouchi, and K. Tsuda, "The effect of amount of hardener on degradation behavior of epoxy resin in liquids," in *Durability Analysis of Composite Systems 2001*: CRC Press, 2020, pp. 333-337.

[244] C. Hu, T. Li, H. Yin, L. Hu, J. Tang, and K. Ren, "Preparation and corrosion protection of three different acids doped polyaniline/epoxy resin composite coatings on carbon steel," *Colloids and Surfaces A: Physicochemical and Engineering Aspects,* vol. 612, p. 126069, 2021.

[245] J. Wang, J. Wang, Z. Yang, Z. Wang, F. Zhang, and S. Wang, "A novel strategy for the synthesis of polyaniline nanostructures with controlled morphology," *Reactive and Functional Polymers,* vol. 68, no. 10, pp. 1435-1440, 2008.

[246] W. Shao, R. Jamal, F. Xu, A. Ubul, and T. Abdiryim, "The effect of a small amount of water on the structure and electrochemical properties of solid-state synthesized polyaniline," *Materials,* vol. 5, no. 10, pp. 1811-1825, 2012.

[247] J. Carneiro, P. M. Döll-Boscardin, B. C. Fiorin, J. M. Nadal, P. V. Farago, and J. P. d. Paula, "Development and characterization of hyaluronic acid-lysine nanoparticles with potential as innovative dermal filling," *Brazilian Journal of Pharmaceutical Sciences,* vol. 52, pp. 645-651, 2016.

[248] M. Buchholz *et al.*, "Interaction of carboxylic acids with rutile TiO2 (110): IR-investigations of terephthalic and benzoic acid adsorbed on a single crystal substrate," *Surface Science,* vol. 643, pp. 117-123, 2016.

[249] Q. Wang *et al.*, "A highly selective electrochemical sensor for nifedipine based on layer-by-layer assembly films from polyaniline and multiwalled carbon nanotube," *Journal of Applied Polymer Science,* vol. 133, no. 21, 2016.

[250] B. Rivas and C. Sanchez, "Poly (2-) and (3-aminobenzoic acids) and their copolymers with aniline: Synthesis, characterization, and properties," *Journal of applied polymer science,* vol. 89, no. 10, pp. 2641-2648, 2003.

[251] S. Bhadra and D. Khastgir, "Extrinsic and intrinsic structural change during heat treatment of polyaniline," *Polymer degradation and stability,* vol. 93, no. 6, pp. 1094-1099, 2008.

[252] E. B. Caldona, D. W. Smith Jr, and D. O. Wipf, "Surface electroanalytical approaches to organic polymeric coatings," *Polymer International,* vol. 70, no. 7, pp. 927-937, 2021.

[253] B. Hirschorn, M. E. Orazem, B. Tribollet, V. Vivier, I. Frateur, and M. Musiani, "Determination of effective capacitance and film thickness from constant-phase-element parameters," *Electrochimica acta,* vol. 55, no. 21, pp. 6218-6227, 2010.

[254] F. Cotting and I. V. Aoki, "Smart protection provided by epoxy clear coating doped with polystyrene microcapsules containing silanol and Ce (III) ions as corrosion inhibitors," *Surface and Coatings Technology,* vol. 303, pp. 310-318, 2016.

[255] Z. Tian *et al.*, "Recent progress in the preparation of polyaniline nanostructures and their applications in anticorrosive coatings," *RSC advances,* vol. 4, no. 54, pp. 28195-28208, 2014.

[256] A. Nautiyal, J. E. Cook, and X. Zhang, "Tunable electrochemical performance of polyaniline coating via facile ion exchanges," *Progress in Organic Coatings,* vol. 136, p. 105309, 2019.

[257] J.-M. Pernaut and J. R. Reynolds, "Use of conducting electroactive polymers for drug delivery and sensing of bioactive molecules. A redox chemistry approach," *The Journal of Physical Chemistry B,* vol. 104, no. 17, pp. 4080-4090, 2000.

[258] M. Rohwerder and A. Michalik, "Conducting polymers for corrosion protection: What makes the difference between failure and success?," *Electrochimica Acta,* vol. 53, no. 3, pp. 1300-1313, 2007.

[259] S. Ortaboy, "Electropolymerization of aniline in phosphonium-based ionic liquids and their application as protective films against corrosion," *Journal of Applied Polymer Science,* vol. 133, no. 38, 2016.

[260] J. Nicholls, N. J. Simms, W. Chan, and H. Evans, "Smart overlay coatings—concept and practice," *Surface and Coatings Technology,* vol. 149, no. 2-3, pp. 236-244, 2002.

[261] S. Portier, L. André, and F.-D. Vuataz, "Review on chemical stimulation techniques in oil industry and applications to geothermal systems," *Engine, work package,* vol. 4, p. 32, 2007.

[262] D. S. Chauhan, M. Quraishi, V. Srivastava, and J. Haque, "Virgin and chemically functionalized amino acids as green corrosion inhibitors: Influence of molecular structure through experimental and in silico studies," *Journal of Molecular Structure,* vol. 1226, p. 129259, 2021.

[263] G. Gece, "Drugs: A review of promising novel corrosion inhibitors," *Corrosion Science,* vol. 53, no. 12, pp. 3873-3898, 2011.

[264] J. Zhao, J. Hu, and X. Ma, "Sodium caprylate improves intestinal mucosal barrier function and antioxidant capacity by altering gut microbial metabolism," *Food & Function,* vol. 12, no. 20, pp. 9750-9762, 2021.

[265] L. Hu, J. Tang, X. Zhang, and Y. Li, "Sodium caprylate wash during Protein A chromatography as an effective means for removing protease (s) responsible for target antibody fragmentation," *Protein Expression and Purification,* vol. 186, p. 105907, 2021.

[266] A. Diraki and S. Omanovic, "Smart PANI/epoxy anti-corrosive coating for protection of carbon steel in sea water," *Progress in Organic Coatings,* vol. 168, p. 106835, 2022.

[267] N. Dinodi and A. N. Shetty, "Alkyl carboxylates as efficient and green inhibitors of magnesium alloy ZE41 corrosion in aqueous salt solution," *Corrosion Science,* vol. 85, pp. 411-427, 2014.

[268] S. Ghareba and S. Omanovic, "Interaction of 12-aminododecanoic acid with a carbon steel surface: towards the development of 'green'corrosion inhibitors," *Corrosion Science,* vol. 52, no. 6, pp. 2104-2113, 2010.

[269] S. Ghareba and S. Omanovic, "12-Aminododecanoic acid as a corrosion inhibitor for carbon steel," *Electrochimica acta,* vol. 56, no. 11, pp. 3890-3898, 2011.

[270] M. Ramezanzadeh, G. Bahlakeh, B. Ramezanzadeh, and Z. Sanaei, "Adsorption mechanism and synergistic corrosion-inhibiting effect between the green Nettle leaves extract and Zn2+ cations on carbon steel," *Journal of Industrial and Engineering Chemistry,* vol. 77, pp. 323-343, 2019.

[271] J. Tan, L. Guo, H. Yang, F. Zhang, and Y. El Bakri, "Synergistic effect of potassium iodide and sodium dodecyl sulfonate on the corrosion inhibition of carbon steel in HCl medium: a combined experimental and theoretical investigation," *RSC Advances,* vol. 10, no. 26, pp. 15163-15170, 2020.

[272] P. Roy and D. Sukul, "Protein–surfactant aggregate as a potential corrosion inhibitor for mild steel in sulphuric acid: zein–SDS system," *RSC Advances,* vol. 5, no. 2, pp. 1359-1365, 2015.

[273] A. Yurt, B. Duran, and H. Dal, "An experimental and theoretical investigation on adsorption properties of some diphenolic Schiff bases as corrosion inhibitors at acidic solution/mild steel interface," *Arabian Journal of Chemistry,* vol. 7, no. 5, pp. 732-740, 2014.

[274] A. Yousefi, S. A. Aslanzadeh, and J. Akbari, "Experimental and DFT studies of 1-methylimidazolium trinitrophenoxide as modifier for corrosion inhibition of SDS for mild steel in hydrochloric acid," *Anti-Corrosion Methods and Materials,* 2018.

[275] M. Deyab, S. Abd El-Rehim, and S. Keera, "Study of the effect of association between anionic surfactant and neutral copolymer on the corrosion behaviour of carbon steel in cyclohexane propionic acid," *Colloids and Surfaces A: Physicochemical and Engineering Aspects,* vol. 348, no. 1-3, pp. 170-176, 2009.

[276] A. Diraki, H. R. Mackey, G. McKay, and A. Abdala, "Removal of emulsified and dissolved diesel oil from high salinity wastewater by adsorption onto graphene oxide," *Journal of Environmental Chemical Engineering,* vol. 7, no. 3, p. 103106, 2019.

[277] A. Diraki, H. Mackey, G. McKay, and A. A. Abdala, "Removal of oil from oil–water emulsions using thermally reduced graphene and graphene nanoplatelets," *Chemical Engineering Research and Design,* vol. 137, pp. 47-59, 2018.

[278] L. Guo, J. Tan, S. Kaya, S. Leng, Q. Li, and F. Zhang, "Multidimensional insights into the corrosion inhibition of 3, 3-dithiodipropionic acid on Q235 steel in H2SO4 medium: A combined experimental and in silico investigation," *Journal of colloid and interface science,* vol. 570, pp. 116-124, 2020.

[279] F. Bentiss, M. Lebrini, and M. Lagrenee, "Thermodynamic characterization of metal dissolution and inhibitor adsorption processes in mild steel/2, 5-bis (n-thienyl)-1, 3, 4-thiadiazoles/hydrochloric acid system," *Corrosion science,* vol. 47, no. 12, pp. 2915-2931, 2005.

[280] A. Popova, M. Christov, and A. Vasilev, "Inhibitive properties of quaternary ammonium bromides of N-containing heterocycles on acid mild steel corrosion. Part II: EIS results," *Corrosion Science,* vol. 49, no. 8, pp. 3290-3302, 2007.

[281] A. Popova, E. Sokolova, S. Raicheva, and M. Christov, "AC and DC study of the temperature effect on mild steel corrosion in acid media in the presence of benzimidazole derivatives," *Corrosion science,* vol. 45, no. 1, pp. 33-58, 2003.

[282] E. A. Noor and A. H. Al-Moubaraki, "Thermodynamic study of metal corrosion and inhibitor adsorption processes in mild steel/1-methyl-4 [4′(-X)-styryl pyridinium iodides/hydrochloric acid systems," *Materials Chemistry and Physics,* vol. 110, no. 1, pp. 145-154, 2008.

[283] M. Hegazy and M. Zaky, "Inhibition effect of novel nonionic surfactants on the corrosion of carbon steel in acidic medium," *Corrosion science,* vol. 52, no. 4, pp. 1333-1341, 2010.

[284] P. Atkins and J. De Paula, *Elements of physical chemistry*. Oxford University Press, USA, 2013.

[285] R. Solmaz, G. Kardaş, M. Çulha, B. Yazıcı, and M. Erbil, "Investigation of adsorption and inhibitive effect of 2-mercaptothiazoline on corrosion of mild steel in hydrochloric acid media," *Electrochimica Acta,* vol. 53, no. 20, pp. 5941-5952, 2008.

[286] M. A. Amin, S. S. Abd EI-Rehim, E. E. El-Sherbini, O. A. Hazzazi, and M. N. Abbas, "Polyacrylic acid as a corrosion inhibitor for aluminium in weakly alkaline solutions. Part I: Weight loss, polarization, impedance EFM and EDX studies," *Corrosion Science,* vol. 51, no. 3, pp. 658-667, 2009.

[287] Y. Liu *et al.*, "Inhibition effect of sparteine isomers with different stereochemical conformations on the corrosion of mild steel in hydrochloric acid solution," *Journal of Molecular Liquids,* vol. 345, p. 117833, 2022.

[288] J. Flieger, J. Feder-Kubis, and M. Tatarczak-Michalewska, "Chiral ionic liquids: Structural diversity, properties and applications in selected separation techniques," *International journal of molecular sciences,* vol. 21, no. 12, p. 4253, 2020.

[289] W. Zhang *et al.*, "Tetrahydroacridines as corrosion inhibitor for X80 steel corrosion in simulated acidic oilfield water," *Journal of Molecular Liquids,* vol. 293, p. 111478, 2019.

[290] Y. Meng *et al.*, "Inhibition of mild steel corrosion in hydrochloric acid using two novel pyridine Schiff base derivatives: a comparative study of experimental and theoretical results," *Rsc Advances,* vol. 7, no. 68, pp. 43014-43029, 2017.

[291] W. Zhang, H.-J. Li, Y. Wang, Y. Liu, Q.-Z. Gu, and Y.-C. Wu, "Gravimetric, electrochemical and surface studies on the anticorrosive properties of 1-(2-pyridyl)-2-thiourea and 2-(imidazol-2-yl)-pyridine for mild steel in hydrochloric acid," *New Journal of Chemistry,* vol. 42, no. 15, pp. 12649-12665, 2018.

[292] N. Z. N. Hashim, K. Kassim, H. M. Zaki, A. I. Alharthi, and Z. Embong, "XPS and DFT investigations of corrosion inhibition of substituted benzylidene Schiff bases on mild steel in hydrochloric acid," *Applied Surface Science,* vol. 476, pp. 861-877, 2019.

[293] S. Kelemen, M. Afeworki, M. Gorbaty, and A. Cohen, "Characterization of organically bound oxygen forms in lignites, peats, and pyrolyzed peats by X-ray photoelectron spectroscopy (XPS) and solid-state 13C NMR methods," *Energy & fuels,* vol. 16, no. 6, pp. 1450-1462, 2002.

[294] A. Al-Refaie, J. Walton, R. Cottis, and R. Lindsay, "Photoelectron spectroscopy study of the inhibition of mild steel corrosion by molybdate and nitrite anions," *Corrosion Science,* vol. 52, no. 2, pp. 422-428, 2010.

[295] L. Shen, R. Liang, M. Luo, F. Jing, and L. Wu, "Electronic effects of ligand substitution on metal–organic framework photocatalysts: the case study of UiO-66," *Physical chemistry chemical physics,* vol. 17, no. 1, pp. 117-121, 2015.

[296] Y. Wang *et al.*, "Missing-node directed synthesis of hierarchical pores on a zirconium metal–organic framework with tunable porosity and enhanced surface acidity via a microdroplet flow reaction," *Journal of Materials Chemistry A,* vol. 5, no. 42, pp. 22372-22379, 2017.

[297] M. Kohantorabi, S. Giannakis, G. Moussavi, M. Bensimon, M. R. Gholami, and C. Pulgarin, "An innovative, highly stable Ag/ZIF-67@ GO nanocomposite with exceptional peroxymonosulfate (PMS) activation efficacy, for the destruction of chemical and microbiological contaminants under visible light," *Journal of Hazardous Materials,* vol. 413, p. 125308, 2021.

[298] S. Rezaee and S. Shahrokhian, "Facile synthesis of petal-like NiCo/NiO-CoO/nanoporous carbon composite based on mixed-metallic MOFs and their application for electrocatalytic oxidation of methanol," *Applied Catalysis B: Environmental,* vol. 244, pp. 802-813, 2019.

[299] X.-L. Wei, M. Fahlman, and A. Epstein, "XPS study of highly sulfonated polyaniline," *Macromolecules,* vol. 32, no. 9, pp. 3114-3117, 1999.

[300] P. Siril, N. Shiju, D. Brown, and K. Wilson, "Optimising catalytic properties of supported sulfonic acid catalysts," *Applied Catalysis A: General,* vol. 364, no. 1-2, pp. 95-100, 2009.

[301] S.-A. Wohlgemuth, F. Vilela, M.-M. Titirici, and M. Antonietti, "A one-pot hydrothermal synthesis of tunable dual heteroatom-doped carbon microspheres," *Green Chemistry,* vol. 14, no. 3, pp. 741-749, 2012.

[302] M. Tourabi, K. Nohair, M. Traisnel, C. Jama, and F. Bentiss, "Electrochemical and XPS studies of the corrosion inhibition of carbon steel in hydrochloric acid pickling solutions by 3, 5-bis (2-thienylmethyl)-4-amino-1, 2, 4-triazole," *Corrosion Science,* vol. 75, pp. 123-133, 2013.

[303] S. Roosendaal, B. Van Asselen, J. Elsenaar, A. Vredenberg, and F. Habraken, "The oxidation state of Fe (100) after initial oxidation in O2," *Surface Science,* vol. 442, no. 3, pp. 329-337, 1999.

[304] P. C. Graat and M. A. Somers, "Simultaneous determination of composition and thickness of thin iron-oxide films from XPS Fe 2p spectra," *Applied Surface Science,* vol. 100, pp. 36-40, 1996.

[305] T. Yamashita and P. Hayes, "Analysis of XPS spectra of Fe2+ and Fe3+ ions in oxide materials," *Applied surface science,* vol. 254, no. 8, pp. 2441-2449, 2008.

[306] M. Lebrini, M. Lagrenee, H. Vezin, L. Gengembre, and F. Bentiss, "Electrochemical and quantum chemical studies of new thiadiazole derivatives adsorption on mild steel in normal hydrochloric acid medium," *Corrosion Science,* vol. 47, no. 2, pp. 485-505, 2005.

[307] M. Belghiti *et al.*, "Piperine derivatives as green corrosion inhibitors on iron surface; DFT, Monte Carlo dynamics study and complexation modes," *Journal of Molecular Liquids,* vol. 261, pp. 62-75, 2018.

[308] M. Mousavi, M. Mohammadalizadeh, and A. Khosravan, "Theoretical investigation of corrosion inhibition effect of imidazole and its derivatives on mild steel using cluster model," *Corrosion science,* vol. 53, no. 10, pp. 3086-3091, 2011.